Doctoral Dissertation

CMOS-based Optical Power-Transfer System

for Implantable and Wearable Medical Devices

CMOS 制御光電力伝送システムによる生体埋め込み

・ウェアラブルデバイスに関する研究

Nattakarn Wuthibenjaphonchai

September 2020

Graduate School of Materials Science

Nara Institute of Science and Technology

Abstract

Over the decades, the demand for wireless portable devices has been increased rapidly. They become more involving in our daily life and use in various fields. Including medical devices, wireless mobile devices provide comfort and convenience for both patients and healthcare providers. The most common power source for wireless devices is the battery. However, the battery still has limitations in terms of design and safety. It requires a large volume in the device and periodic maintenance due to its lifetime.

This thesis proposes a CMOS-base optical power-transfer system to solve the battery limitations. The proposed system utilizes an energy harvesting technology and CMOS technology for minimizing power system size, reducing maintenance, and still providing sufficient power for the target circuit or device. The system was designed to accumulate power converting from a serially connected, ultra-small photodiodes, and intermittently delivers the power to a target circuit. To demonstrate the power-transfer system, two medical applications were designed and introduced the system as their power supply system.

The first application is a bio-implantable device with the concept of IoT. An optical ID circuit was designed to generate an ID for supporting the IoT technology. The power system was developed to supply continuous power and a clock signal for operating sensor and IoT support system. The second application is a wearable device for non-invasive glucose monitoring. The device is designed to measure glucose from sweat using amperometric measurement. This device utilizes the pulse power supply from the proposed system for transferring the detected data as a PWM signal.

The proposed system was designed and demonstrated using the two designed devices. The result shows that the optical power-transfer system provides sufficient power for the target circuit, and the designed device works as expected in both applications.

Acknowledgment

This thesis becomes a reality with the kind support and help of many individuals. I would like to express my sincere gratitude to all of them for their active guidance, cooperation, and encouragement. Without these following people, this thesis would never have been possible.

First and foremost, I would like to thank Professor Jun Ohta for giving me a chance and continued support to pursue a doctoral degree at Nara Institute of Science and Technology. Because of his wisdom and his personality, he is one of the reasons why I decided to study master degree and continue my doctoral degree here at NAIST. Without a doubt, I have never regretted making this decision. He does not only give me academic-related advice, but he also supports me on other matters and always hands me great life advice. For me, he is like a family member here in Japan.

I also would like to thank Professor Takashi Tokuda for his guidance, motivation, and immense knowledge. The door to his office was always open whenever I ran into trouble or had a question. Even after he transferred to Tokyo Institute of Technology, he still continuously supports my work. It is an absolute pleasure working with a high maintenance researcher like him. I could not have imagined having a better advisor than him.

My sincere thanks also go to the rest of my thesis committees: Professor Masakazu Nakamura and Associate Professor Takuya Nakashima. I am gratefully indebted to them for their precious wisdom and guidance on my work along these three years.

I wish to thank Associate Professor Kiyotaka Sasagawa, Associate Professor Toshihiko Noda, Associate Professor Hiroyuki Tashiro, Assistant Professor Makito Haruta, and Assistant Professor Hironari Takehara for their helpful feedback and discussion. I would also like to

Dedication

To my beloved parents.

Contents

List of Figures

List of Tables

Chapter 1

Introduction

Since the past decade, portable wireless devices have been progressively developed and became more necessary in our day-to-day life. The obvious examples are smartphones, smartwatches, and even medical devices. The development of these devices involves several advances in technologies. Therefore, developers must face technical challenges in various fields. One of the main technology in portable wireless devices is the power supply system.

1.1 Problem Statement

The most familiar for the power supply system is a battery. Even though battery technology has been developed in many years, the battery still has limitations in terms of design and safety for some applications, especially medical applications. For the design, the volume and weight of the battery occupy a large percentage of the total device. Consequently, the minimum size of the device is limited by the size of the battery. For safety, the toxicity of the battery affects both humans and the environment. In the medical application, the size and safety of the device is a significant matter to provide comfort and reduce risk/harm for patients and healthcare providers; the battery technology is not the best answer for the power supply system.

1.2 Thesis Purpose

This thesis proposes a CMOS-based optical power-transfer system. The proposed system aims to solve the limitations of the battery and maintain sufficient power supply for the

devices. The system utilizes an energy harvesting technology and a CMOS technology for providing safety, convenience, design flexibility, and easily integrating with a micro-size electronic circuit. By using the photovoltaic effect, the optical power-transfer system accumulates and supplies sufficient power to the connected circuit. Therefore, the system only requires a light source to operate its system.

In addition, two medical devices were also designed and merged with the optical power transfer system as their power system. These two devices demonstrate the operation and exemplify the applications of the proposed system.

1.3 Thesis Overview

In this section, a brief overview of the thesis was provided. Figure 1 outlines the scope and structure of this thesis. There are six chapters in this thesis, and they are shortly explained below.

Chapter 1: *Introduction*

This chapter provides an overview of this thesis. A brief background is given. Then, the problem of the recent power supply system and the purpose of this research are described.

Chapter 2: *Power Supply System for Portable Wireless Devices*

A review of battery technology is described. The limitation of battery technology is discussed in detail in this chapter. Then, the alternative power supply technology, which is an energy harvesting technology, is presented. The state-of-art and

advantages of energy harvesting are explained. Lastly, the optical energy harvesting technology is defined.

Chapter 3: *CMOS-based Optical Power-Transfer System*

Due to the demand of portable wireless devices and the limitation of the battery, a CMOS-based optical power-transfer system was designed and developed. The system converts light to electrical power. Then, the power is accumulated and supplied to the target circuit. This system was simulated and evaluated. The detail of the design and evaluation results will be explained in this chapter.

Chapter 4: *Bio-implantable Device with Concept of Internet of Things*

The first example of the optical power-transfer system utilization is implantable and IoT applications. An implantable and IoT device requires a continuous power supply and a clock signal for operation. The proposed optical power-transfer system was adapted to match the needs of this implantable and IoT device. Moreover, an optical ID circuit that was used to support IoT application was also designed and presented in this chapter.

Chapter 5: *CMOS-based Wearable Device for Non-invasive Glucose Monitoring*

In this chapter, the second application of the optical power-transfer circuit is presented. A CMOS-based wearable device for non-invasive glucose monitoring operated by optical power transfer was designed. The device aims to attach to human skin and detect glucose from sweat. The detection uses an amperometric measurement with a three-electrode electrochemical sensor. Moreover, the

designed device utilizes the advantage of the pulse power supply from the proposed

system for its data transmission.

Chapter 6: *Conclusion*

The last chapter summarizes all the research results in this thesis and concludes the

outcomes of the thesis. Then, future research opportunities are presented.
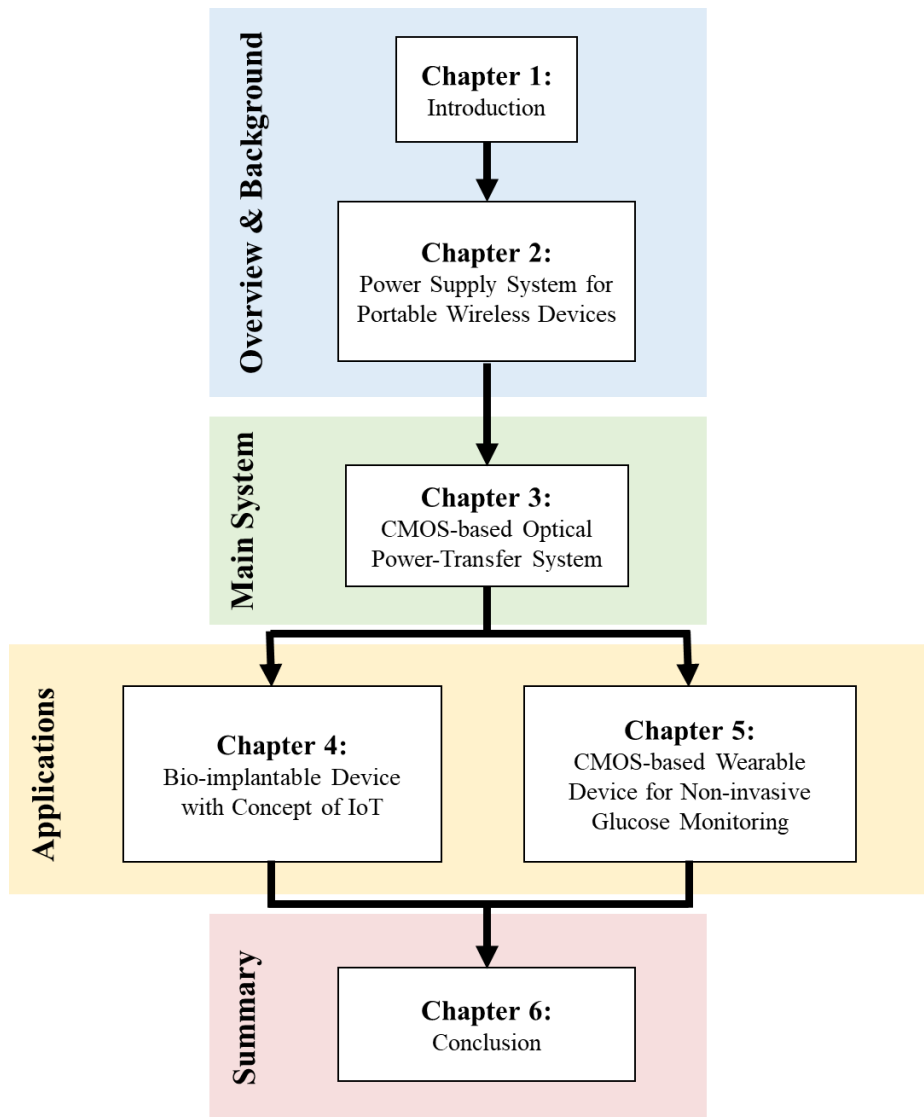
Figure 1 An overview of the content of the thesis.

1.4 Thesis Organization

The remaining chapters in this thesis are organized as follows. Chapter 2 provides background information and reviews technologies of the power supply system in small devices. Chapter 3 presents the design and evaluation results of the proposed optical power-transfer system. Chapter 4 and Chapter 5 present the applications of the proposed system. Finally, Chapter 6 draws conclusions, presents a summary of the main outcomes in this thesis, and presents future opportunities.

Chapter 2

Power Supply System for Portable Wireless Devices

Living with no electricity might not be easy as many items in your home count on it to function. Since the discovery of electricity, humanity relies on it. Many technological advancements, including electronic devices, have been developed based on electricity. With the increased need for mobility, portable electronic devices have become ubiquitous in modern society. The recent rapid expansion in the use of portable computers, personal data assistants, cellular phones, camcorders, and power tools creates a strong demand for fast deployment of portable power storage technologies at an unprecedented rate. First, the power supply technology was only for wheeled applications, then for portable and finally nowadays wearable use [1].

In this chapter, two types of portable power supply technologies will be explained and discussed. The first one is a battery, which is a common power supply/storage technology in portable devices. The second one is an energy harvesting technology, which is an alternative way to supply/storage technology in portable devices.

2.1 Common Power Supply in Portable Wireless Devices

2.1.1 Electric Battery

Batteries have been around for a long time. In 1800, Volta discovered that a continuous flow of electrical force was generated when using certain fluids as conductors to promote an electrochemical reaction between two metals or electrodes [1-2]. This led to the invention of

the first voltaic cell, better known as the battery. Until now, many types of batteries have been discovered. Batteries generally can be classified into two major battery types; primary batteries and secondary batteries.

Primary batteries are batteries that cannot be recharged once depleted. This means the electrochemical reaction of the electrochemical cells in the primary batteries cannot be reversed. They are available in various sizes according to the applications. The most popular among the primary batteries are alkaline batteries. However, the downside of alkaline batteries is the low load current, which limits their application. Therefore, the alkaline batteries can use with only devices that require low current like remote controls, flashlights, and portable entertainment devices. Moreover, the kind of batteries is not reusable. From this limitation, the secondary batteries were developed [3-4].

Secondary batteries, also known as rechargeable batteries, are batteries that can be recharged once depleted. The electrochemical reaction of their electrochemical cells can be reversed by applying a specific voltage to the battery in the reversed direction. The secondary batteries can be further classified into several other types based on their combination of electrode and electrolyte materials. The commonly used are Lithium-ion (Li-ion), Lead-acid, Nickel–Cadmium (NiCd), and Nickel–Metal Hydride (NiMH). The difference in chemistry affects the property of the batteries. The general application of the secondary that is easily seen in our daily life is in smartphone and other gadgets [3-4].

Due to the advance and option of battery technology, more and more products today are battery operated. The battery provides a stable power supply and portable ability to the installed devices. Subsequently, batteries have become ubiquitous in modern society. They are in various products, including electronic devices, vehicles, and medical devices. Especially for medical applications, the advantages of a battery such as portable and convenient are the main

factor that the medical device manufacturers are seeking. The battery implementation allows the medical device to become smaller, easier to carry, and more ergonomic. However, the risk of using batteries must be considered because batteries are based on chemical reactions, and the medical application needs close contact with the human body.

2.1.2 Bottle Neck of Electric Battery in Medical Devices

Despite the numerous advantages of batteries, hazards associated with the failure of these batteries can be catastrophic. Multiple viral videos have demonstrated the dangers of products with rechargeable batteries, which have the potential to overheat, explode, and catch fire. While the dangers must be considered no matter what the product, the stakes are even higher when a medical device is affected [5]. The potential hazards also include the electrolyte leakage causing toxic exposure, and malfunction of the device due to battery capacity depletion. Although these hazards can cause much harm to users in any situation, the danger is intensified with medical devices, which contact directly to human skin or implant inside the human body.

Besides the mentioned issues, the minimum weight and size that batteries provide also limits the medical device design. Particularly in the implantable and wearable application, the device design should be comfortable for the user. The weight and size limitation of the battery forces increasing system heaviness and volume. Moreover, even the battery manufacturers have significantly improved battery life, the medical device with batteries requires periodic maintenance due to battery life. Especially the implanted device, their maintenance is unhandy and difficult, if not impossible, for patients and healthcare providers to remove [6].

From an environmental perspective, defective batteries are also considered hazardous waste due to their toxicity. To manufacture batteries, the needed energy is about 50 times greater than the energy it contains [4]. Due to their high pollutant content compared to their small energy content, the batteries, specifically, the primary one is considered a wasteful, environmentally unfriendly technology.

To solve the limitation of battery, an alternative power supply system was introduced. The alternative system adopts an energy harvesting technology for converting and accumulating an ambient energy source, which is also called renewable energy.

2.2 Energy Harvesting Technology in Portable Wireless Devices

2.2.1 Energy Harvesting Technology

Wireless portable electronic devices are increasingly popular as they do not require connection to the mains power grid. Most of these wireless devices are solely powered by a battery that limits system lifetime, increases system volume, needs high maintenance, and harms the environment [7–10]. To fulfill these gaps, portable electronic devices must face several technical and ecological challenges. That is where the increasing demand for energy harvesters have become an efficient and green alternative for gathering energy from the environment and offer an answer to some of the challenges above [11-13].

Over centuries, macro-energy harvesting technology has been developed and widely uses in many power plants. Energy conversion/harvesting technologies mainly aim to convert from an ambient energy source into electrical power and accumulate the power for later use [9, 11, 15-22]. This available ambient energy source has many forms, such as solar power,

thermal energy, wind energy, and vibrations. The usually seen form of this huge-sized energy harvesting is windmills, watermills, and passive solar power systems [23]. Even though they make a lot of difference in the powered industrial filed, they are not game-changers for electronic designers. The key design for portable electronic devices is less wiring and size. A micro- energy harvesting technology has been developed to meet those needs.

Due to the availability of the micro-energy harvesting technology, there is growing demand and expectation for the alternative power system. This technology is, without any doubt, a very attractive technique for a wide variety of self-powered, micro-sized electronic devices and systems. Examples of such systems are wireless sensors, environmental monitoring networks, military devices, watches, and Bluetooth headsets, including medical devices [9, 14, 23-31]. Table 1 shows current energy harvesting techniques that broadly use in small electronic devices [13, 32-33].

Table 1 Comparison of different energy harvesting technologies.

Harvesting technique	Ambient energy source	Harvesting method	Harvesting device	Factor
Optical energy harvesting	Light	Photovoltaic effect	Solar cell/ Photodiode	Light intensity
Thermoelectric energy harvesting	Temperature	Thermoelectric (Seebeck effect)	Thermoelectric generator (TEG)	Thermal difference
Mechanical energy harvesting	Vibration	Piezoelectric effect, Electromagnetic, Electrostatic	Piezoelectric material	Vibration frequency
Electromagnetic wave harvesting	Radio frequency	Ubiquitous radio transmitter	RF coil, Antennas	Distance and RF harmonic
Acoustic energy harvesting	Noise	Helmholtz effect	Artificial lithium niobate	Sound decibel

2.2.2 Advantages of Energy Harvesting for Medical application

The energy harvesting technology allows the device to eliminate batteries, which causes many concerns in medical applications. It remains the portable ability of the battery with the additional advantage of fewer wires. The devices powered by harvested energy also have a longer lifetime. Therefore, the devices require less maintenance routine, which is more cost-effective and convenient for both patients and healthcare providers. As mentioned before, the size and weight are very important for designing medical devices. To consider these two factors, some of the energy harvesting techniques can integrate into the micro-sized device. Thus, the medical devices powered by energy harvesting technology is more comfortable by reducing the device size and weight. Unlike batteries, energy harvesting technology is considered a green technology. The fact that this technology utilizes ambient power and gives devices longer lifetime, it reduces waste and pollution regarding the environment.

2.2.3 Optical Energy Harvesting Technology

Among many energy harvesting techniques, the optical energy harvesting offers the highest power density. It is also available in a micro-sized photodiode. The photodiode can wire in series connection to provide larger power. The connection does not need to be on a single solid substrate, which means it gets the flexibility to design the device. Compared with the electromagnetic technique, which uses in many wireless technologies, the optical energy harvesting has the merits of remote power transfer and applicability for ultra-small wireless devices with small size [34].

Light, including solar energy, is one of the most common sources for miniaturized energy conversion/harvesting technology and can be directly converted into electric energy by

the photovoltaic effect [35-41]. The photovoltaic effect refers to photons of exciting electrons into a higher state of energy, allowing them to act as charge carriers for the generated electric current. Although this form of power production is not steady and is much less effective than batteries, it can be significantly useful in low-power sensor applications. Therefore, there is a great need for power-controlling circuits to accumulate and transmit the harvested energy into usable steady voltage levels successfully.

Chapter 3

CMOS-based Optical Power-Transfer System

3.1 Introduction

As mentioned in Chapter 2.2.2,　the main concern of the optical energy harvesting technology is that a generated power by photovoltaic effect is not steady because it depends on the intensity of light source and size of photovoltaic cells or photodiodes. Therefore, a power-controlling part to accumulate and transfer the power into usable steady voltage levels successfully is required. To design the power-controlling in a wireless powering circuit, one of the commonly accepted ideas is to drive a system in two-phase intermittent operation of "charge and operation (discharge)" [42]. The wireless powering circuit also needs a voltage boosting-circuit to provide an appropriate supply voltage for a load circuit [43-44]. Therefore, the circuits have a complex design.

To reduce the complication of the power system, this research proposed a single-stage optical power-transfer circuit. The single-state circuit was designed base on CMOS technology to use as the main power-controlling circuit for small-sized devices. The circuit accumulates small amounts of energy from the optical power converter and delivers power to a target circuit intermittently. Since the design is a very simple "charge and operation" circuit, this approach allowed the powering circuit to omit the voltage-boosting circuit. Therefore, the single-stage optical power-transfer circuit has a more simple design, and easily match between the powering system and the load circuit. The operation flow chart of the designed single-state optical power-transfer circuit was shown in Fig. 2.
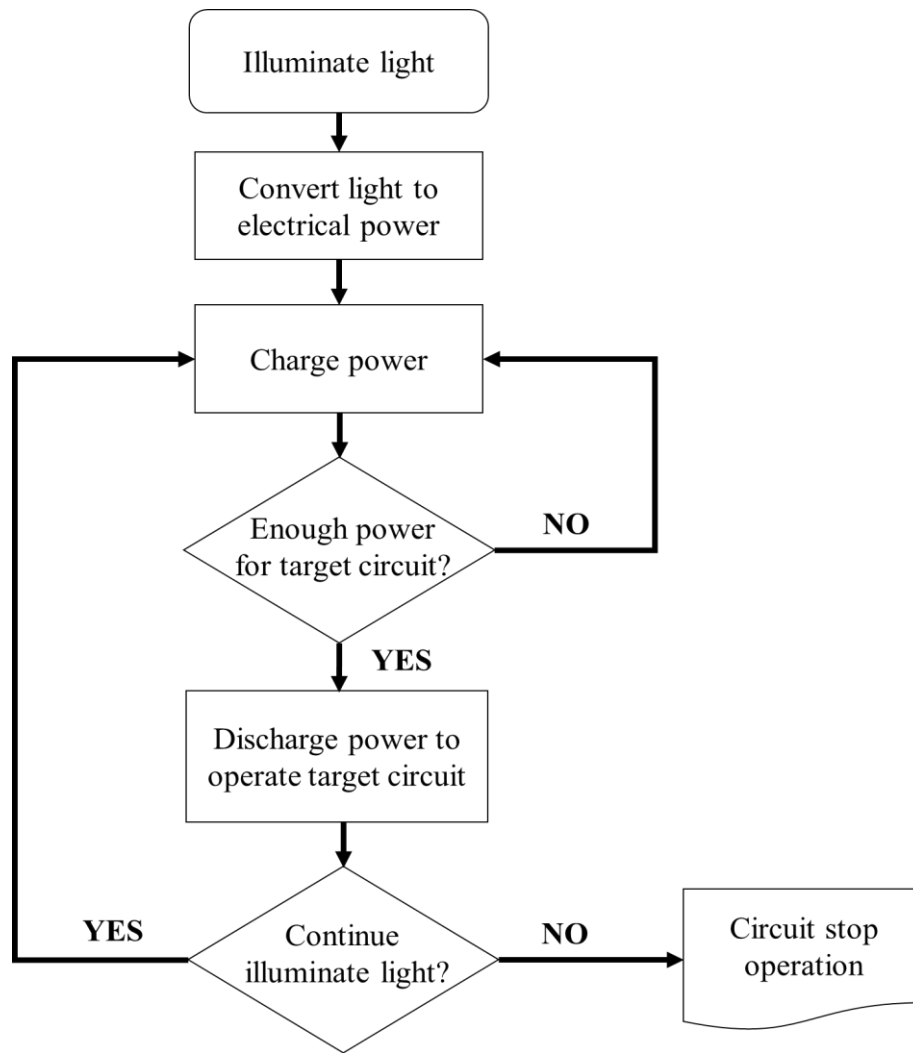
Figure 2 Flow chart of charge and operation in the single-state optical power-transfer circuit.

For optical power converter, a bare chip type of ultra-small silicon photodiode in Fig. 3 was used to convert light to electrical power. The size of the photodiode is 0.8 mm x 0.9 mm, and the typical voltage generated by this photodiode is approximately 0.4 V. Due to the typically generated voltage, it is reasonable to use serially connected photodiodes as a power receiver to provide "sufficient voltage and limited current."
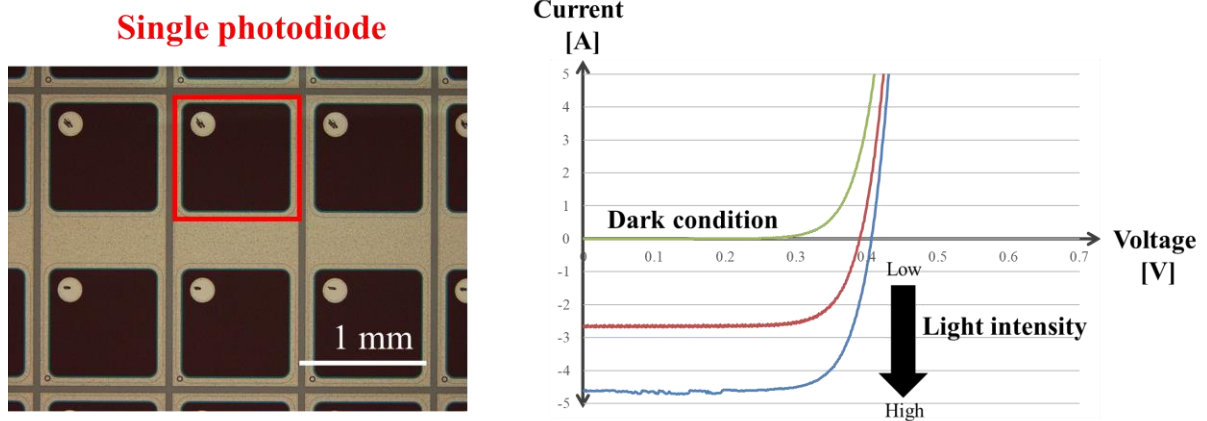
Figure 3 Microphotography and V-I characteristic of the ultra-small silicon photodiode.

In Chapter 3, the design and evaluation of the single-state optical power-transfer were explained. To give examples of its applications, the optical power-transfer circuit with the series-connected photodiodes were applied in two applications. These two applications are implantable and IoT devices, and wearable glucose monitoring device applications. Both applications basically have the proposed circuit as their power system. The details of both devices are in Chapters 4 and 5.

3.2 Circuit Design

3.2.1 Circuit Overview

A single-stage optical power-transfer circuit is the core of the proposed optical energy harvesting technology for small wireless devices [34, 45-46]. The function of the single-stage circuit is energy accumulation and intermittent load operation. Figure 4 provides a block diagram of the single-stage optical power-transfer circuit, while Table 2 shows the function of each component presented in Fig. 4. In the figure, the single-stage circuit consists of two external components and three internal chip components. The external components are a power

converter and an external capacitor. Another three internal components inside the CMOS chip are a CMOS voltage detector, a bias voltage source, and a CMOS switch. The power converter consists of 10 series connected photodiodes to obtain sufficient voltage. The number of solar cells is determined based on the supply voltage of the circuit to be operated. The bias voltage source is also the series-connected photodiodes. The bias voltage source supplies two fixed bias voltages (V_{bn} and V_{bp}) that are required for operation. These two bias voltages have an important role in controlling a charge/discharge operation of the voltage detector.
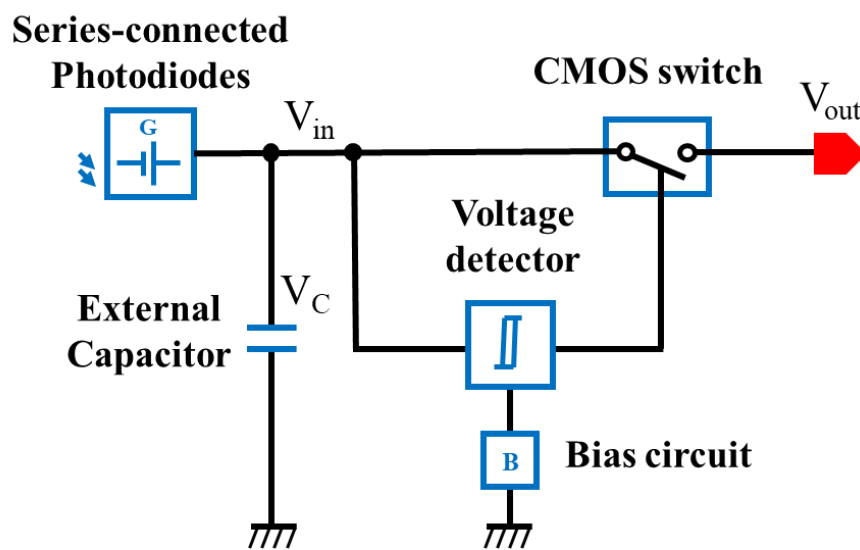
Figure 4 Block diagram of the single-stage optical power-transfer circuit.

Table 2 Functions of the single-stage optical power-transfer components.

Component	Function
1. Power converter (Photodiodes)	Converts light into DC electrical power
2. Capacitor	Accumulates power from solar cell
3. Voltage detector	Self-powered Schmitt trigger that controls charge/discharge operation
4. Bias voltage source	Controls operation of voltage detector
5. CMOS switch	Supplies or holds output power

The single-stage optical power-transfer circuit operation begins when starting to emit light to the photodiodes. The photodiodes convert optical power to electrical power and supply the generated power to charge the external capacitor. When the stored voltage at the capacitor reaches V_{TH} (i.e., V_{on}), the voltage detector turns on the CMOS switch. The capacitor then consequently discharges to supply power to the target circuit. Following the discharge phase, when the stored voltage at the capacitor drops to V_{TL} (i.e., V_{off}), the voltage detector turns off the CMOS switch. Then, the capacitor stops supplying power, as illustrated in Fig. 5. Therefore, the capacitor is recharged while no load is present, which is called a charge phase. This operation loop will repeat the charge and discharge phase until stop emitting the light.
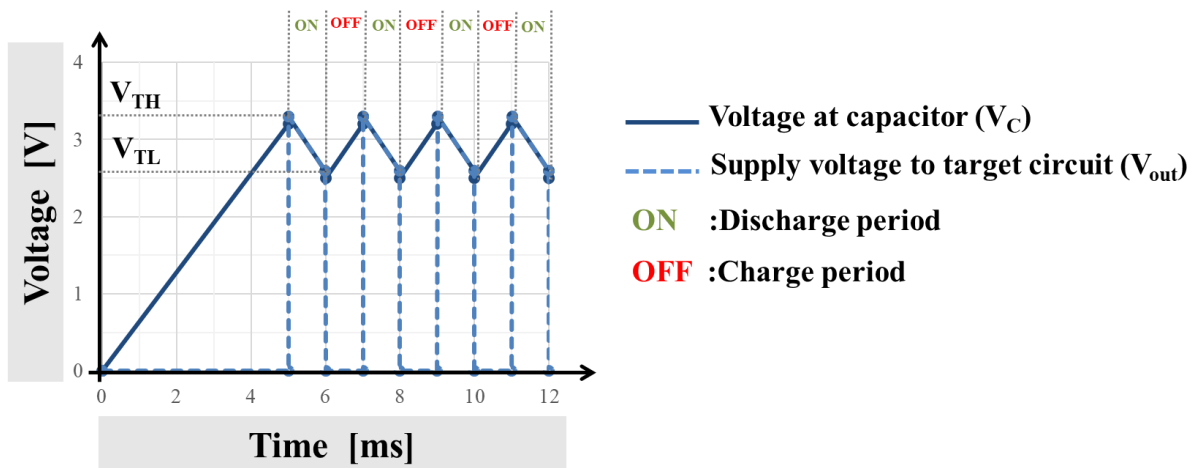
Figure 5 Simulated operation of the single-stage optical power-transfer circuit.

3.2.2 Voltage Detector

The voltage detector is an important part in the designed single-state optical power-transfer circuit. Its role is to monitor the accumulated voltage at the capacitor and to send a signal for turning on and off the CMOS switch when the voltage at the capacitor is enough or too low for the target circuit. The appropriate voltage level for the target circuit can be set by choosing the bias voltages from the bias circuit.
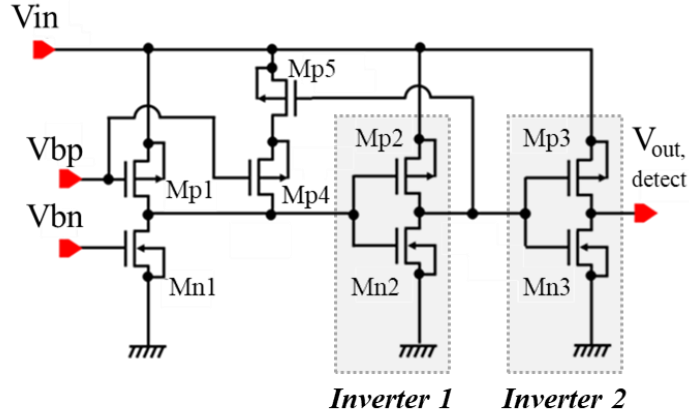
Transistor	Width	Length
Mn1	$0.4 \, \mu$m	$4 \, \mu$m
Mn2	$1 \, \mu$m	$4 \, \mu$m
Mn3	$1 \, \mu$m	$4 \, \mu$m
Mp1	$8 \, \mu$m	$4 \, \mu$m
Mp2	$1 \, \mu$m	$4 \, \mu$m
Mp3	$1 \, \mu$m	$4 \, \mu$m
Mp4	$10 \, \mu$m	$4 \, \mu$m
Mp5	$10 \, \mu$m	$4 \, \mu$m

Figure 6 MOS-level schematic and transistor sizes of the voltage detector circuit.

The voltage detector comprises of five PMOS and three NMOS. Two pairs of PMOS and PMOS are used as two CMOS inverters. Figure 6 shows the schematic of the voltage detector and the size of each NMOS and PMOS. Figure 7 is the operation mode of the voltage detector (LOW means voltage equals zero, and HIGH means voltage equals V_{in}). The voltage detector operation has two conditions. The first condition (Fig. 7(a)) is 'LOW' output voltage. When input voltage (V_{in}) is lower than the high threshold voltage (V_{TH}), the resistance of PMOS1 (Mp1) is larger than NMOS1 (Mn1). An output voltage 1 (V_{out1}) equals ground (GND, V= 0 V). This Vout1 is an input voltage of the inverter1. Therefore, an output of inverter1 (V_{out2}) equals Vin. This Vout2 is an input signal of PMOS switch (Mp5) and an input voltage of the inverter2. Therefore, the PMOS4 (Mp4) does not operate because the Mp5 turns off, and the output voltage of the inverter2, which is the final output voltage of the voltage detector

($V_{out, detect}$) is zero. On the other hand, the second condition (Fig. 7(b)) is 'HIGH' output voltage. When Vin is higher than V_{TH} of Mp1, the resistance of Mp1 is smaller than Mn1. The V_{out1} is equal to V_{in}. Therefore, a Vout2 is equal to zero. Therefore, the Mp5 turns on, and the final output voltage of the voltage detector is equal to Vin. When the Mp5 turns on, the size of PMOS changes from only Mp1 to the Mp1 combined with Mp4. The threshold voltage also consequently changes from high threshold voltage (V_{TH}) to low threshold voltage (V_{TL}) due to the PMOS size changed. Finally, when V_{in} decreases lower than V_{TL}, the voltage detector operation will switch back to the fist condition. By using the on-off Mp5 and the loop, the voltage detector operates as a hysteresis. The DC analysis in Fig. 8 shows the simulation result of the hysteresis operation of the voltage detector at $V_{bn} = 0.5$ V, $V_{bp} = 2.5$ V when varying V_{in} from 0 to 5 V and 5 to 0 V.
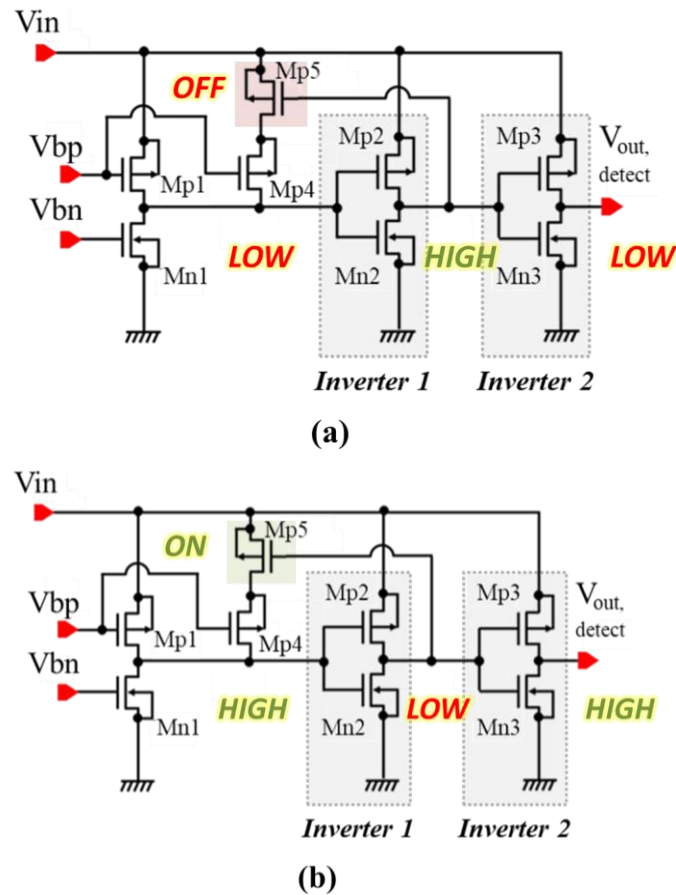
Figure 7 Operation mode of voltage detector:

(a) LOW output voltage, and (b) HIGH output voltage
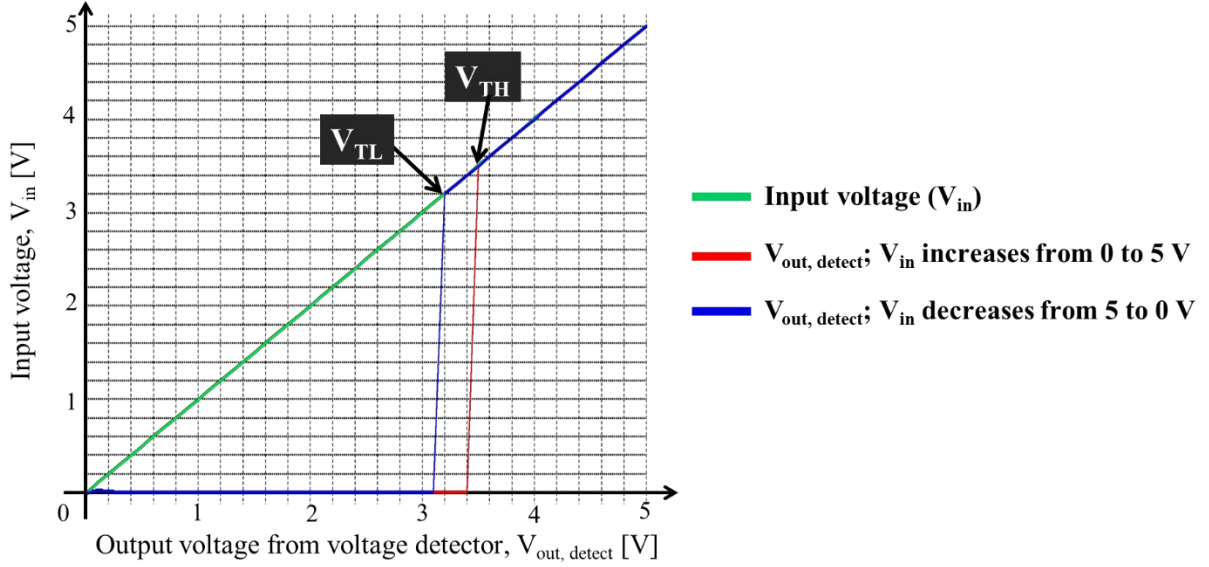
Figure 8 DC analysis simulation result of the voltage detector operation.

The output voltage from the voltage detector ($V_{out,detect}$) is an input signal of the CMOS switch. The switch turns on when $V_{out,detect}$ is high (b), and turns off when $V_{out,detect}$ is low (a). When switching on, the voltage that supplies the target circuit is equal to the voltage at the capacitor (Vin). When switching on, the voltage that supply to the target circuit is stopped means the voltage is equal to zero.

According to the circuit operation, the threshold voltages (V_{TH} and V_{TL}) is the range of the output voltage that supplies to the target circuit. The maximum output voltage level is V_{TH}, and the minimum output voltage level is V_{TL}. These threshold voltage levels must be controlled to match the sufficient operating voltage of the target circuit. In Figure 6, the gate voltage of the Mp1 is V_{bp}, and the gate voltage of the Mn1 is V_{bn}. The V_{TH} and V_{TL} levels depend on the V_{bn} and V_{bp} voltages from the bias circuit [47]. Therefore, the on-off period of the single-state optical power-transfer circuit is adjustable by changing V_{bn} and V_{bp}.

3.3 Evaluation

3.3.1 Operation of Controllable Voltage Detector

As mentioned in Chapter 3.2, the threshold voltages in the voltage detector can be controlled using the bias circuit. To evaluate the voltage detector circuit, a 4 V_{p-p} ramp voltage was applied to the circuit as an input voltage, V_{in}. A resister was connected to the output line as a load to discharge the accumulated power. The relationship between the threshold voltages (V_{TH} and V_{TL}) and bias voltages (V_{bn} and V_{bp}) in Fig. 9 is assessed by applying a matrix of bias voltages from 0.4 to 2.8 V and measuring the corresponding threshold voltages. The results indicate that the threshold voltages can be adjusted by changing the bias voltages, as designed. However, the bias voltage must be set within the operation range of the voltage detector. If not so, the circuit will not operate.
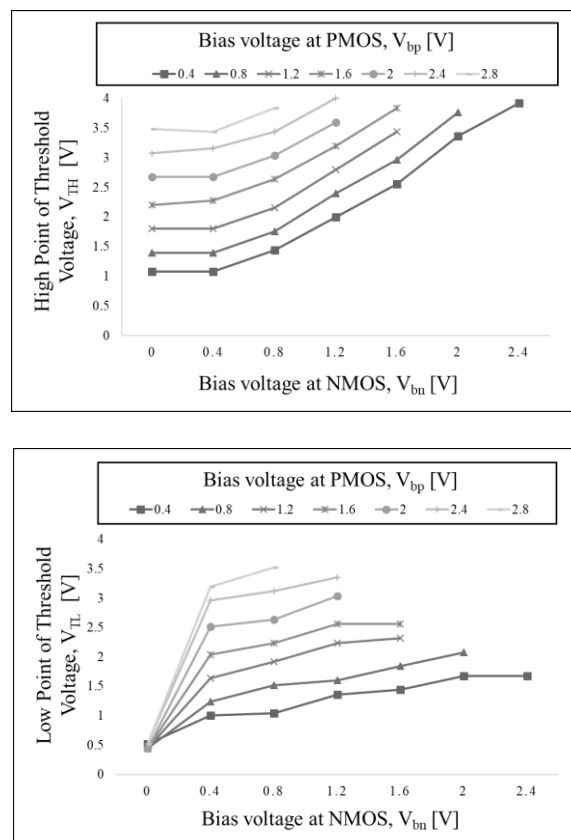
Figure 9 Relationship between threshold voltages and bias voltages.

To confirm the signal transmission from the voltage detector to the CMOS switch, the same 4 V_{p-p} ramp voltage and resister were used as input voltage and load. Figure 10 is an example of the output signal from the optical power-transfer circuit at V_{bn} = 0.8 V, and V_{bp} = 2.8 V. The switch turns on when Vin higher than 3.8 V and turns off when Vin lower than 3.6 which are the high and low threshold voltage (V_{TH}, V_{TL}). The signals confirm that the signal from the voltage detector turns on-off the CMOS switch properly.
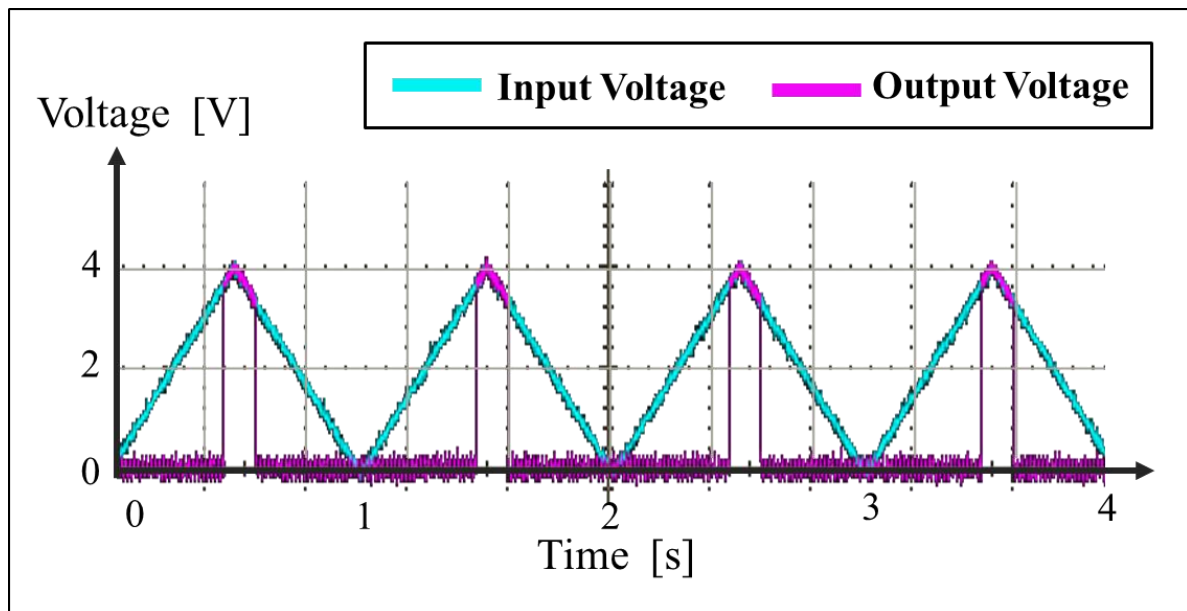
Figure 10 Voltage signals of the single-state optical power-transfer circuit

with 4 Vp-p ramp input voltage.

In practical devices, I use series-connected photodiodes to supply bias voltages. Therefore, the variations of V_{bn} and V_{bp} from light intensity may cause some shifts in threshold values. By changing the light intensity, the threshold values become low in low illumination and high in high illumination. It might slightly change the voltage level but not completely stop the operation. On the other hand, the circuit operation is limited by the illumination for the powering PDs, not the biasing PDs.

3.3.2 Initial Time Requirement and Intermittent Operation

In actual applications, the circuit is operated by current from serially connected photodiodes (PDs unit). The capacitor voltage is zero at the initial operation stage, and increases as the PDs unit generates photocurrent. It is reasonable to use a current source to emulate the PDs unit. The characteristic of the optical power-transfer operation when the circuit operates correctly is as follows. The capacitor voltage increases to up to V_{TH}, the CMOS switch is turned on to operate the target circuit, and the operation is stopped at V_{TL} for recharging. Following the first operation, the capacitor is charged and discharged between V_{TH} and V_{TL}, which provides a shorter charging time than the initial charge. If the photocurrent is lower than a specific current consumed by the power-transfer circuit, the first turn-on at V_{TH} will not occur. To evaluate the initial time requirement of the optical power-transfer circuit, I measured the relationship between the input current and the initial capacitor charging time. I used a constant-current source to supply input current and set $V_{bn} = 0.8$ V and $V_{bp} = 1.6$ V as a typical operating condition for this evaluation. Figure 11 shows the graph of the measurement results. At a higher input current, the capacitor is charged quickly, so the initial charging time is shorter; however, lower current result in a longer initial charging time. In this experiment, I stepped down the current value until it cannot operate the circuit. The last and smallest current that can operate the circuit is 2.4 μA. Therefore, the minimum operating current of the optical power-transfer circuit is 2.4 μA, and the initial time depends on the intensity of the light source. In theory, the relation between capacitor charging time and input current is exponential. Due to the current consumption in the optical power-transfer system itself, the experimental charging time is slightly different from the theoretical graph.
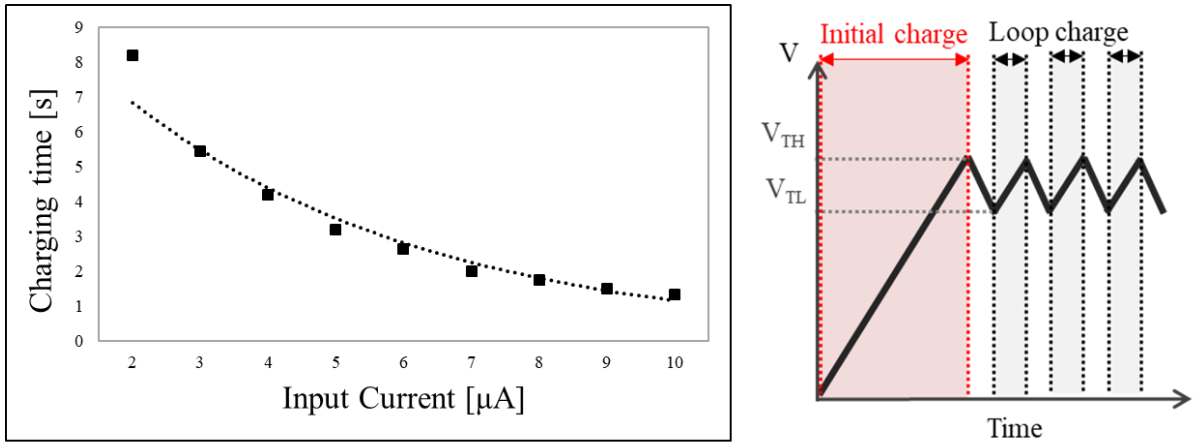
Figure 11 Relationship between initial charging time and input current.

By forwarding to the actual applications, the operation of the optical power-transfer circuit was evaluated. The series-connected external photodiodes and resister are utilized as a source of input voltage (V_{in}) and load. At enough input from the photodiodes and appropriate settings of the bias voltages, the circuit works the same as the simulation shown in Fig. 5. The result of these evaluations indicates that the designed optical power-transfer circuit works as expected. Figure 12 shows the typical operation of the optical power-transfer circuit, which can charge capacitors and supply voltage to the target circuit.
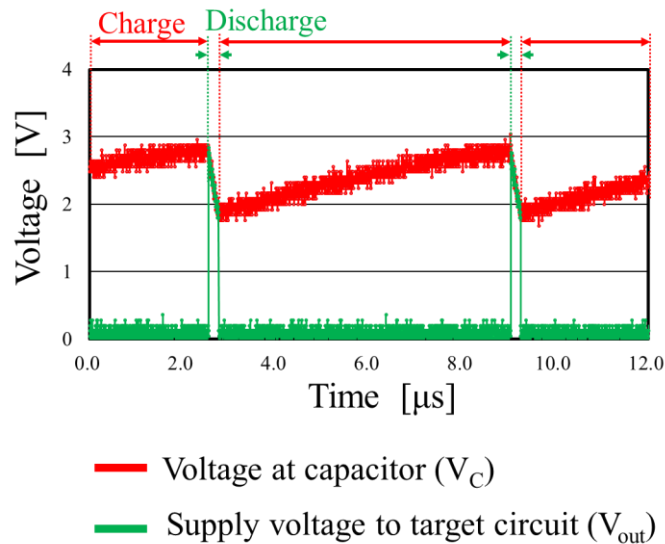
Figure 12 Voltage signals of the single-state optical power-transfer circuit

with completely optical input power (photodiodes).

3.4 Summary & Discussion

The optical power-transfer circuit was designed to be an alternative power source for the wireless micro-sized electronic devices and systems. The design of this circuit is less complicated compared with the common wireless circuit that requires a voltage boosting circuit. The optical power-transfer circuit was successfully designed and evaluated. The results show that the circuit charges power and then operates the target circuit/load as expected. Moreover, the supply voltage level from the power-transfer circuit is controllable by changing the bias voltage to match the operation voltage of the target circuit. The required initial time to operate the power-transfer circuit depends on the intensity of the light source. The minimum operating current is 2.4 μA. To exemplify the function of the single-state optical power-transfer circuit, the optical power-transfer circuit was applied for optogenetic application [34]. Moreover, the circuit also applied for another two wireless small medical device applications as their power supply system. The detail of both applications, which are implantable with IoT application, and wearable glucose monitoring application, will be explained in the following Chapters 4 and 5.

Chapter 4

First Application:

Bio-implantable Device with Concept of Internet of Things

4.1 Overview

The first application for examining the operation of the optical power-transfer circuit is bio-implantable and Internet-of-Things (IoT) devices [48-52]. In this chapter, a CMOS-based optical power-transfer system for bio-implantable and Internet of Things (IoT) devices was presented. The device was designed based on the needs of the power system in bio-implantable devices. The power system of this device was adapted from the basic single-state optical power-transfer circuit in Chapter 3 to accumulates a small amount of photoelectrically converted energy in an external capacitor and intermittently supplies this power to a target sensor. Furthermore, a photoelectrically powered optical identification (ID) circuit that is suitable for IoT technology applications was also developed and include in the designed device. The purpose, design, and evaluation of the CMOS-based optical power-transfer system for bio-implantable and Internet of Things (IoT) devices will be explained in detail in this Chapter.

4.1.1 Power System for Implantable Devices

The demand for wireless implantable devices has increased, especially in medical applications. From the viewpoint of the implantable device, the size and maintenance process of the device are the key design. The primary design of this bio-implantable device constraint is the battery. As mentioned in Chapter 1, the battery limits the lifetime of the electronic system and increases the volume of the device. Therefore, the proposed single-state optical power-

transfer circuit was applied to fill the gap of the needs in the implantable device's power system. It is also reasonable to design the proposed power transfer to be as small as possible for the application to implantable microelectronic devices in deep parts of the body.

Moreover, most of the medical devices require a continuous power supply. Hence, the proposed single-state optical power-transfer circuit must be adapted to match this need. One thigh that must be considered when applied to the photodiodes in the bio-implantable devices is the light source.

Considering the bio-implantable application, red and infrared (IR) light (wavelength: 800 to 1000 nm) was used as the light source. The advantage of red and IR light is they can penetrate soft tissue, bone, and brain parenchyma [53]. Therefore, the IR light can pass through human tissue and illuminate the Si-cell photodiodes on the device. However, it does not mean that the wavelength region is limited in the red/NIR region for this system. Since the conventional Si photodiodes/solar cells were used, the device can operate in the visible to NIR region. Even the location of the device in the body still slightly affects the light transmission from the light source to the device, the efficiency of the power transfer primarily depends on the performance of the photodiodes.

4.1.2 Internet of Things (IoT) for Biomedical Applications

Internet of Things (IoT) is simply described as the network of interconnected things or devices which are embedded with sensors, necessary electronics, and network connectivity. The network connectivity enables IoT devices to exchange their data. IoT has come a long way in recent years and is well integrated within multiple industries, including the healthcare space. Nowadays, there is a growing number of IoT uses in the medical industry. Due to the continued implementation of IoT within healthcare, the medical IoT will become more and more involved

on our daily basis and will lead to a drastic increase in productivity and analysis of data for better healthcare. For example, if a patient has more than one medical device in his/her body, the IoT system can identify the status of each device and also show their data in a single portable display.

To support the IoT system, I designed the device to provide a powerful and unique solution for realizing the IoT system consisting of very small distributed identification (ID) and sensing nodes that can be operated by intentional and environmental illumination. The generated ID of this device is displayed and transmitted by two LEDs.

4.2 Purpose

The purpose of this work is to design and evaluate a CMOS-based optical power-transfer circuit for bio-implantable and Internet of Things (IoT) devices by using an optical ID circuit as a target circuit and external photodiodes as a power supply source. This device also presents as one of the example applications of the single-state optical power-transfer circuit in Chapter 3. The CMOS-based optical power-transfer circuit was designed to be a power supply system of the bio-implantable device instead of the battery. The designed device also includes an optical ID circuit to generate an optical ID for supporting IoT application. The optical ID of the device was displayed using two LEDs (blue and green LED). The device provides a steady, continuous power supply for the implantable device and a clock signal for the IoT system by using a dual-stage configuration. Figure 13 shows a conceptual illustration of a CMOS-based optical power-transfer system for bio-implantable and Internet of Things (IoT) devices.
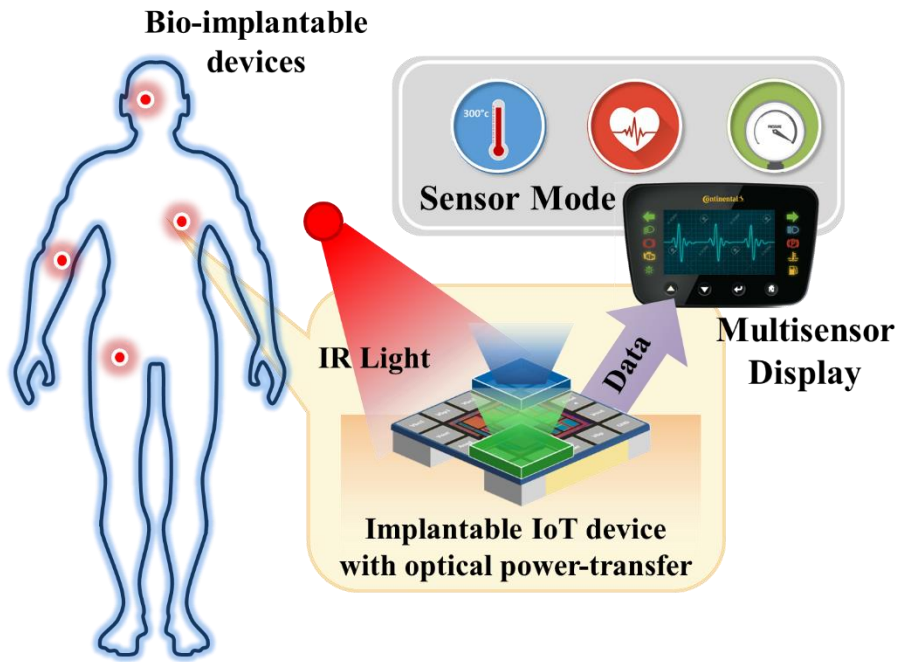
Figure 13 Concept of IoT system for an implantable device

based on proposed optical power-transfer technology.

4.3 Circuit Design

4.3.1 Device Overview

The optical power-transfer system with IoT for implantable device requires a clock signal and a continuous power supply. The single-state optical power-transfer circuit presented in Chapter 3 can be applied to operate a target circuit intermittently [45]. The target circuit should be designed to be able to complete its function within a single powering pulse. If a small amount of power is available independently of the main powering pulses, various controlling circuits can be implemented, and the target circuit functionality can be extended. For the clock signal, the on-off digital signal resulting from the operation of the single-state optical power-transfer circuit can be directly used as an optional clock signal. However, in order to continuously supply power, a dual-stage power-transfer circuit was developed by serially

connecting two optical power-transfer circuits with a different set of bias voltages. Means, the first stage provides a clock signal, and the second stage provides a continuous supply voltage. As mentioned before, this device also provides an optical ID circuit to support IoT application. The optical ID circuit was included with the dual-stage optical power-transfer circuit to generate and send/display the ID of the connected implantable device. In this work, the optical ID circuit was also used as a target load circuit for demonstration.

The operation starts when emitting IR light to the device. The photodiodes convert light to electrical power. The power is accumulated in the capacitor of the dual-state optical power-transfer circuit. At the appropriate amount of accumulated power, the dual-state circuit supplies continuous power and a clock signal to both the optical ID circuit and the implantable device. Then, the optical ID circuit generates the ID of the device. Figure 14 shows the operation flow chart of the designed optical power-transfer for bio-implantable and IoT devices.
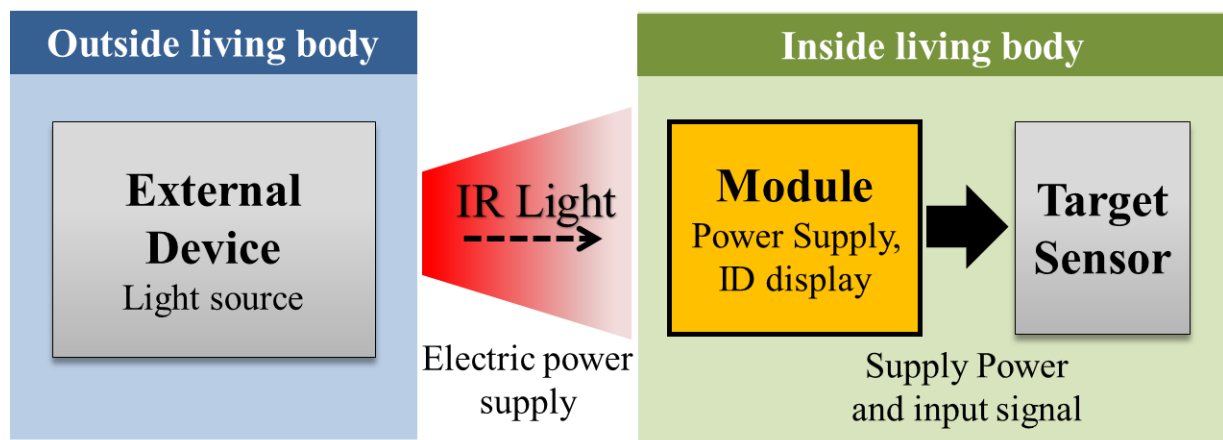
Figure 14 Operation flow chart of optical power-transfer

for bio-implantable and IoT devices.

4.3.2 Dual-stage Optical Power-Transfer Circuit

A dual-stage optical power-transfer circuit was originally designed by developing from

the single-stage optical power-transfer circuit to continuously supply a small amount of power for sequential operation. Two single-stage optical power-transfer circuits with differing V_{bn} and V_{bp} values were serially connected. The first optical power-transfer circuit generates powering pulses for a load such as an LED, also providing a clock signal to inform the target circuit that C_1 is providing a current. The second circuit operates as an active rectifier to provide a small amount of power from C_2 to the target circuit. This architecture allows for the implementation of sequential operations in the target circuit.

From the basic design, the second optical power-transfer circuit can start to accumulate power at its capacitor only when the first circuit turns on. This consequence produces a delay in the initial start time of the operation. To decrease the initial start time, a bypass NMOS switch was introduced. The switch was connected between V_{in} and V_2 line. Therefore, the dual-state circuit can charge the capacitor at the second optical power-transfer circuit (C_2) when the first optical power-transfer circuit still turns on. To simulate the operation of the dual-state circuit, the photodiode model was designed to use as a power supply. The actual schematic and the parameter setting of the simulation from the CAD program shows in Fig. 15 and Fig. 16.
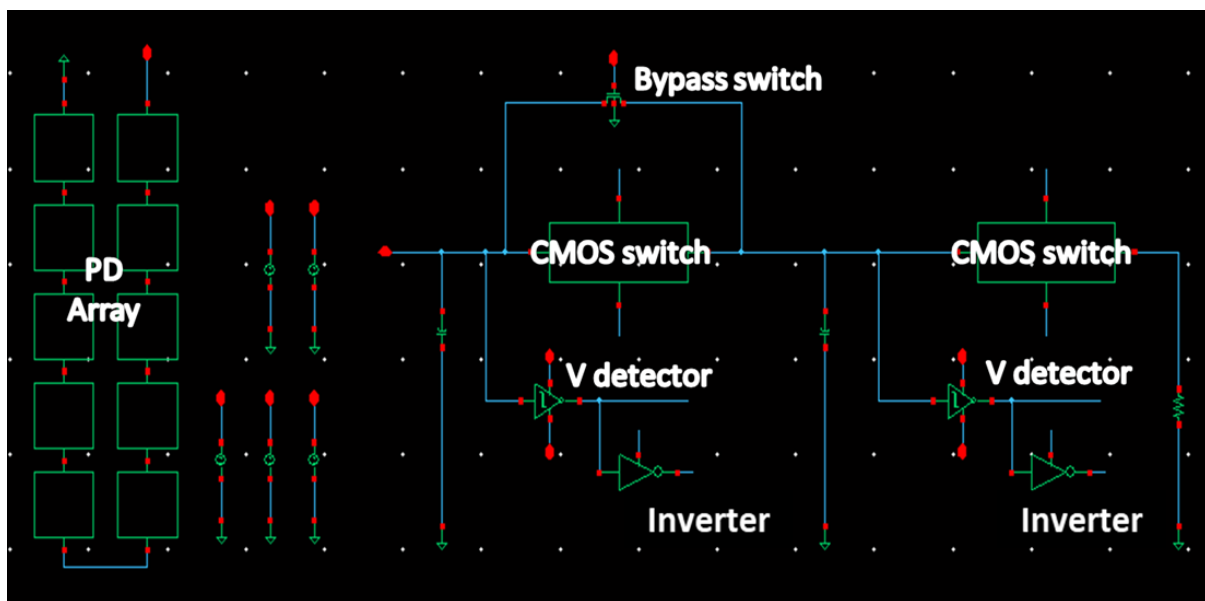
Figure 15 Schematic of the dual-state optical power-transfer circuit.

Parameter	Value
Capacitor	100 nF
I photodiode	100 uA
Vbn1	0.3 V
Vbn2	0.18 V
Vbp1	2.5 V
Vbp2	1.25 V
Vbypass	2 V
Load	30 kOhm
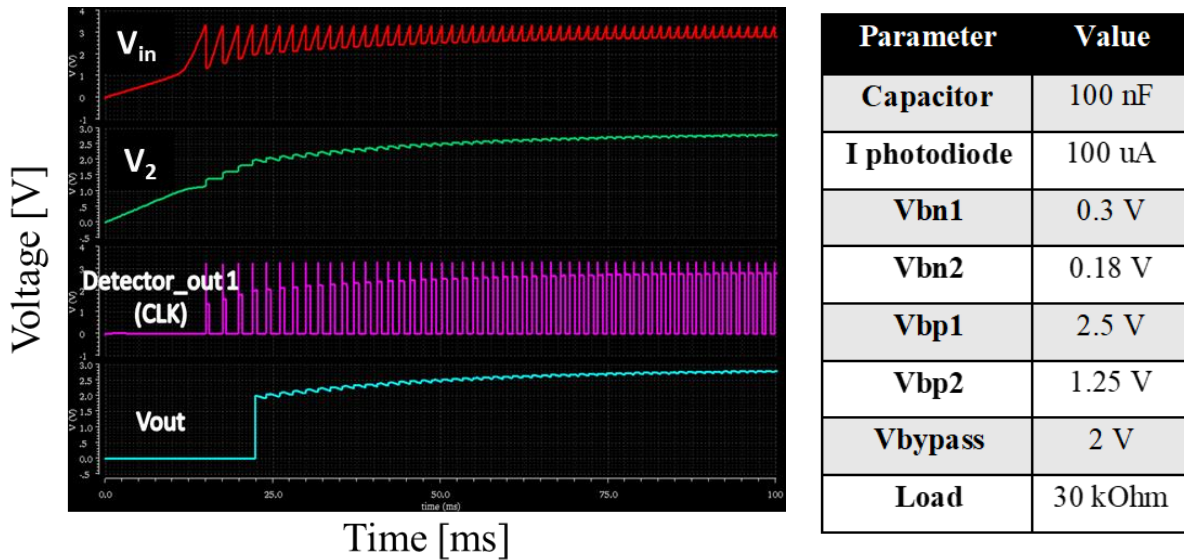
Figure 16 Simulation result of the dual-state optical power-transfer operation.

The outputs of the designed dual-stage circuit are the continuous power (Vout) and the clock signal (CLK). The outputs are supplied to the optical ID circuit and the target implantable device/sensor. The block diagram of the dual-state optical power-transfer with an optical ID circuit for the implantable device was presented in Fig. 17. The target sensor represents the bio-implantable device, which is supplied power by the optical power-transfer circuit.
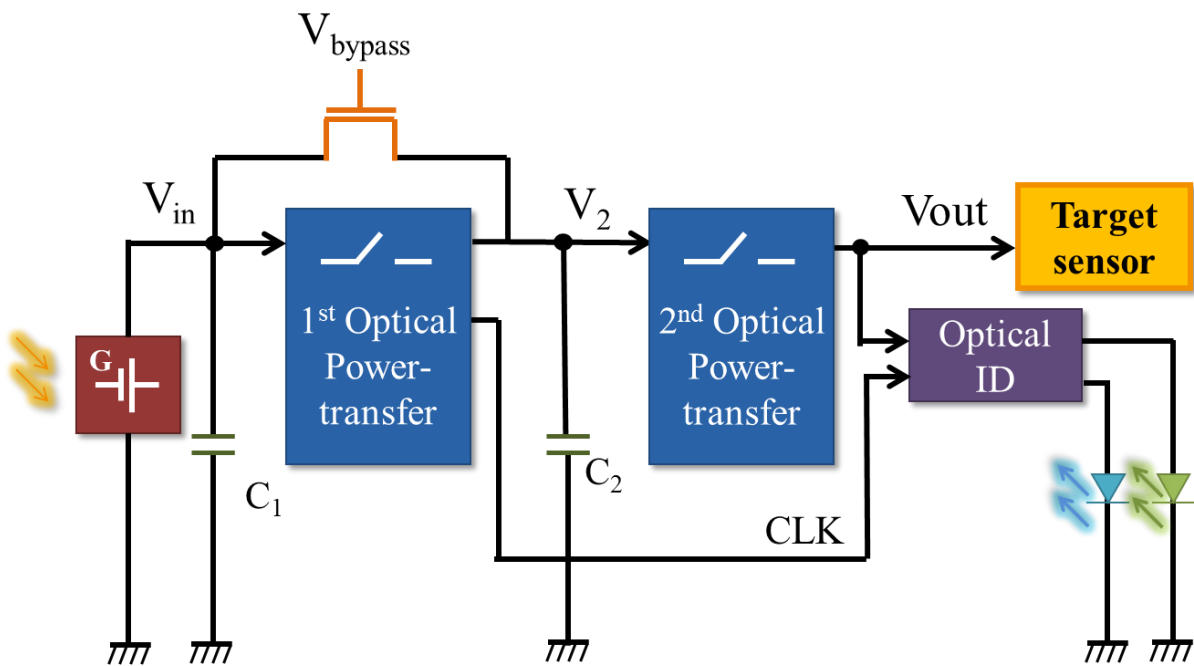
Figure 17 Block diagram of the dual-state optical power-transfer with optical ID circuit.

4.3.3 Optical ID circuit

To demonstrate the operation of the proposed optical energy harvesting technology, we developed a photoelectrically powered optical ID transmission device, which also serves as the prototype for the IoT application. The optical ID circuit can generate an ID for each device and then display the ID via two LEDs. Figure 18 shows a block diagram of the optical ID circuit. The optical ID circuit contains three main components, namely the power-on-reset (POR), which is used for starting up the circuit, a scanner-based sequencer, and LED drivers.
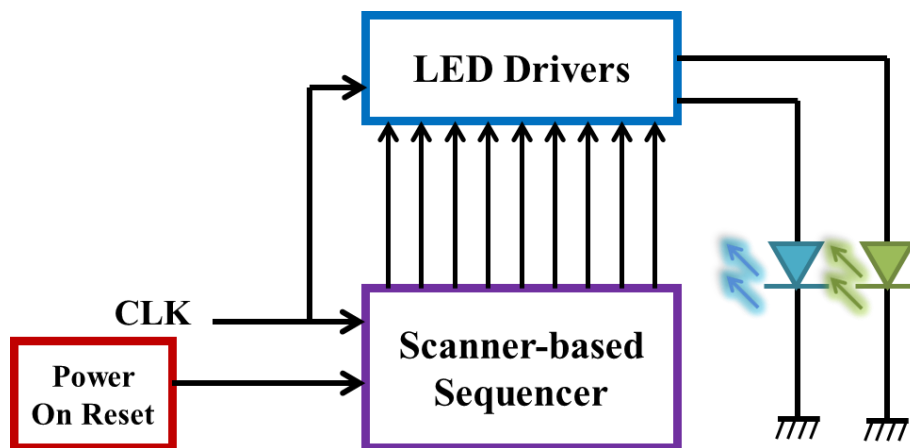
Figure 18 Block diagram of optical ID circuit.

When it is powered, the scanner sequencer (Fig. 19), which mainly consists of nine D-flip flops, one D-latch, and logic gates, provides nine pulses for one set of one starting bit and eight ID bits (S1-S8) from nine D-flip flops as shown in Fig. 20. Due to the D-flip flop works at the rising edge of the clock signal, each generated pulse width from the scanner (working period) two times longer than the period of the clock signal when the clock signal coefficient is 0.5. Other components are used to restart and generate repetitive signals. Therefore, the scanner operates as an ID bit sequence generator and sends the generated bit sequence to the LED driver.
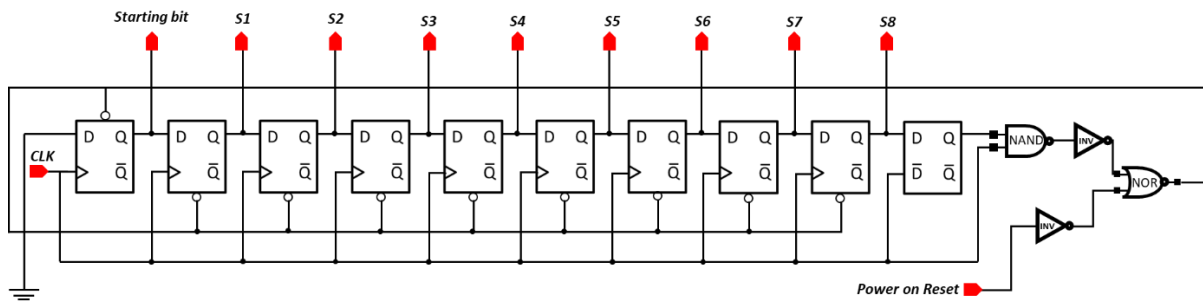
Figure 19 Schematic of scanner sequencer.
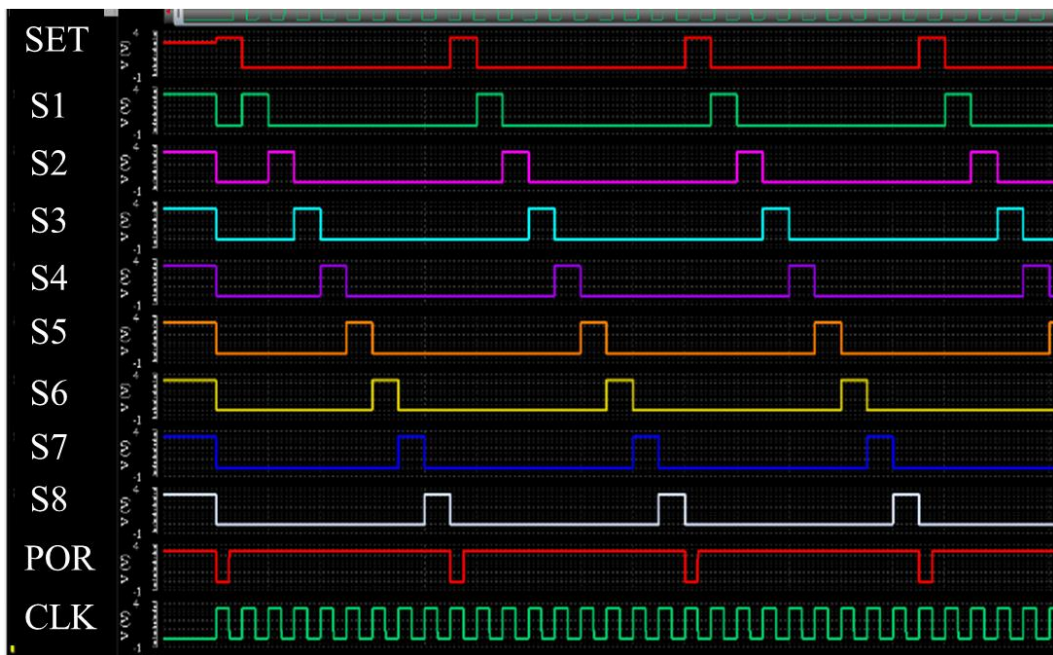
SET	S1	S2	S3	S4	S5	S6	S7	S8
1	0	0	0	0	0	0	0	0
0	1	0	0	0	0	0	0	0
0	0	1	0	0	0	0	0	0
...	...	...	...	...	...	...	...	...
0	0	0	0	0	0	0	0	1
1	0	0	0	0	0	0	0	0

Restart

Figure 20 Simulation result and output table of scanner sequencer.

Then, the ID generator part in the LED driver (Fig. 21) creates the ID using logic gates. Then, the signal separator part divides the signal for blue and green LED. In Figure 22, the created ID is "SBGBBGBGG" as an example design ID for the operation. S is a starting bit that both blue and green LED blink at the same time, B is for a blue LED, and G is for a green LED. Following this, the circuit automatically transmits a two-color ID signal to the two LEDs to display the ID. The LEDs show the sensor ID, which consists of one starting bit for identifying the ID starting point and another eight bits for showing the device's ID.
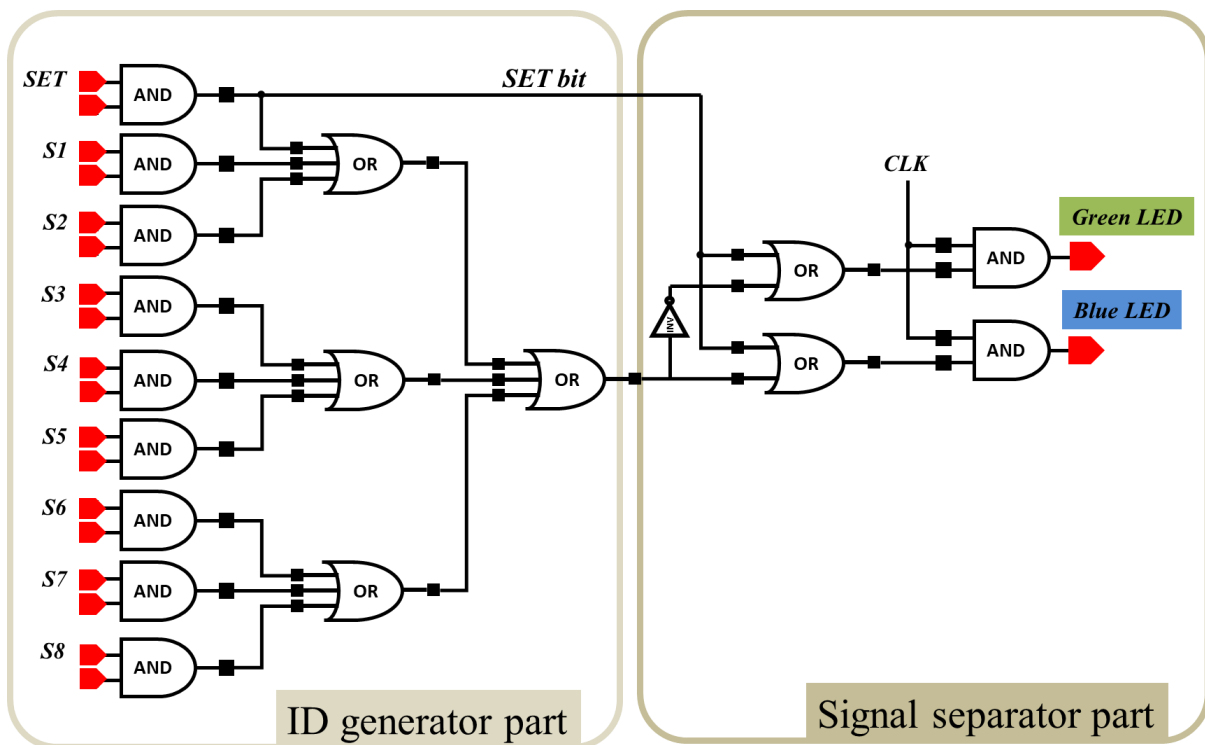
Figure 21 Schematic of LED drivers.
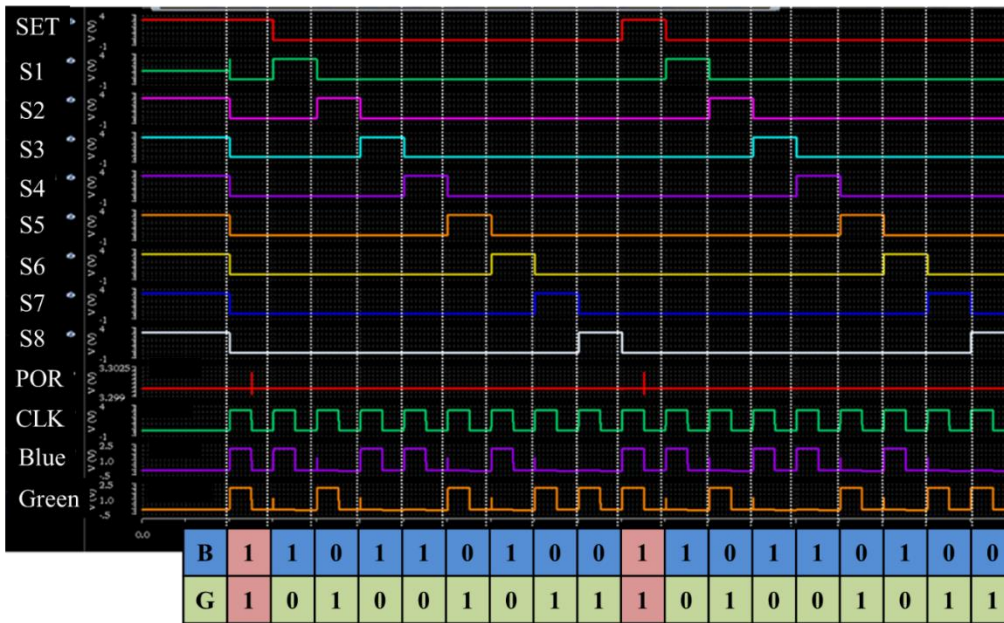
Figure 22 Simulation result and output table of LED drivers.

The ID is selectable by selecting the input of 2x1 AND logic gates on the left-hand side in Fig. 21. One the leg of the AND gates are already connected to the output signal from the scanner to control its operation time. Another leg can be connected to reference voltage (VDD) or ground (GND). Table 3 shows the logic table of the ID input. For example, if the AND gate connects to VDD and S2, the blue LED blinks in the second bit of the ID. On the other hand, if the AND gate connects to GND and S2, the green LED blinks in the second bit of the ID. In actual application, the ID input provides the different ID for each device, which is available more than 200 different ID to identify itself with the IoT system.
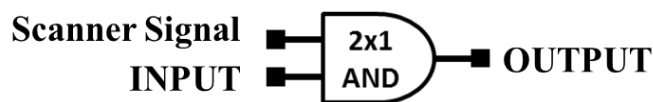
Table 3 Logic table of ID input.

Input	Output signal	Operating LED
VDD	1	Blue
GND	0	Green

4.3.4 Layout Design

After completed schematic designing and simulating the dual-stage optical power-transfer with an optical ID circuit, the next step is layout design. The main idea design of this layout is to optimize the space for minimizing device size. Figure 23 shows the layout of the dual-stage optical power-transfer with an optical ID circuit. This layout also includes a metal-4 protection layer, I/O pads, and electrostatic discharges (ESD). The size of the dual-stage optical power-transfer with an optical ID chip is $702.5 \times 702.5 \ \mu m^2$. The details of input and output pins (I/O pads) are shown in Table 4.

Layout of the optical power-transfer with optical ID circuit
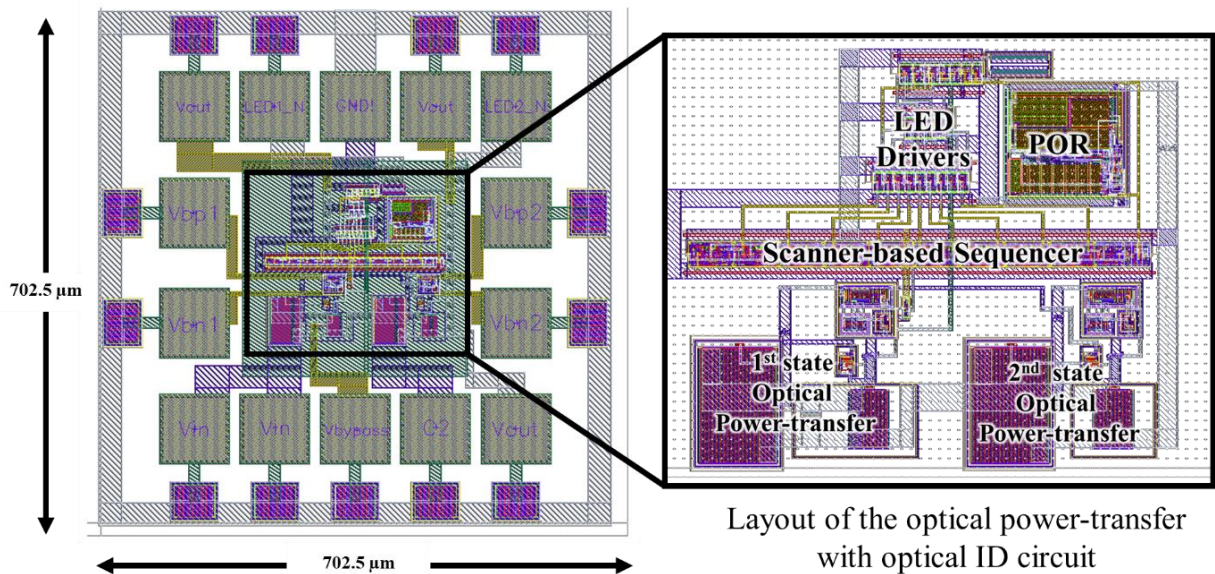
Figure 23 Layout of the dual-stage optical power-transfer with an optical ID chip.
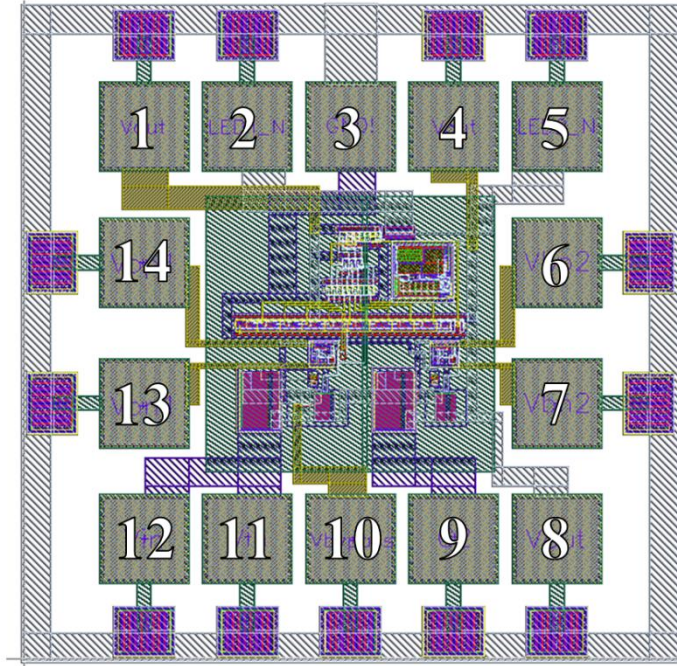
Table 4 Detail of each pad in the dual-stage optical power-transfer with an optical ID chip.

PAD number	PAD name	I/O	Connection node
1	Vout	O	P side of blue and green LEDs
2	LED1_N	I	N side of blue LED
3	GND!	I	ground
4	Vout	O	*spare pad for V_{out}
5	LED2_N	I	N side of green LED
6	Vbp2	I	photodiodes
7	Vbn2	I	photodiodes
8	Vout	O	load: target implantable device
9	Cap2	I/O	capacitor 2
10	Vbypass	I	photodiodes
11	Vin	I/O	photodiodes and capacitor 1
12	Vin	I/O	*spare pad for V_{in}
13	Vbn1	I	photodiodes
14	Vbp1	I	photodiodes

To characterize the circuits and demonstrate the concept of the designed optical power transfer technology, the CMOS chip was fabricated using a 0.35 μm two-poly, four-metal standard CMOS process. Figure 24 and Table 5 display the layout and specifications of the CMOS chip, respectively.
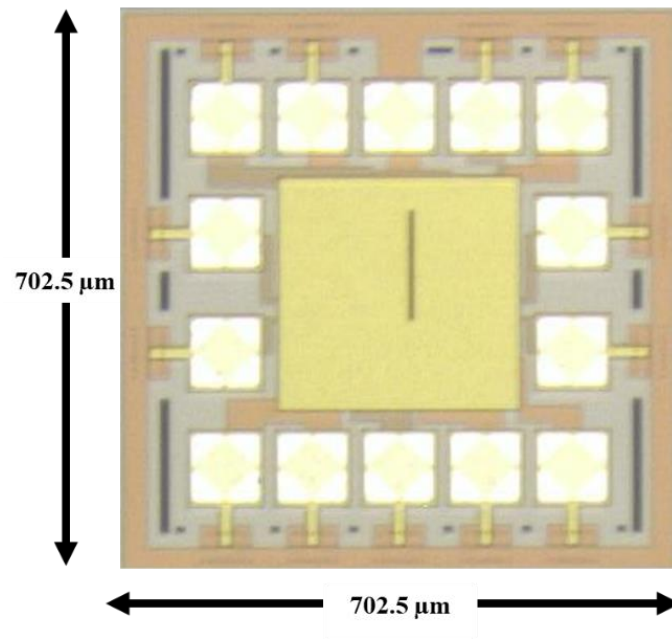
Figure 24 Photograph of actual dual-stage optical power-transfer with an optical ID chip.

Table 5 Specifications of CMOS optical power-transfer chip.

Specification	Details
Process	0.35 μm two-poly four-metal standard CMOS
Operating voltage range	2.2 ~ 2.6 V
Chip size	702.5 × 702.5 μm^2
List of included circuits	Optical power-transfer circuits, Optical ID circuit
Required external components	Two serially connected photodiodes for powering and biasing, two capacitors, two LEDs

4.3.5 Printed Circuit Boards (PCB) for evaluation

A printed circuit board was designed for connecting the optical power-transfer with optical ID chip and other required external components, which are a blue LED, a green LED, two 4.7μF capacitors, and two sets of photodiode arrays for input power and a bias circuit. Table 6 and Figure 25 show the comparison of three versions of the designed PCB that had been developed. The design of the first version consists of two boards that can be separated. The left one is for the chip, capacitors, and LEDs. The right one is for series connecting photodiodes. The first version PCB also has vias for connecting header pins. These header pins were connected with measuring equipment, such as an oscilloscope. Moreover, they also connect between two boards for evaluation of the designed chip. Then, the second and third version was developed after the chip evaluation for matching the implantable application with a more compact size.

Table 6 Specifications of all three versions of optical power-transfer PCB.

	Version 1	Version 2	Version 3
Size	5×5 cm^2 (each board)	2×2 cm^2	Less than 1 mm^2
PCB shape	square	square	round
Front components	Left: PD arrays Right: Chip, LEDs, C	PD arrays	PD arrays, LEDs
Back components	-	Chip, LEDs, C	Chip, C
Number of PDs	20	20	15
Photodiode type	Surface mount	Surface mount	Bare chip
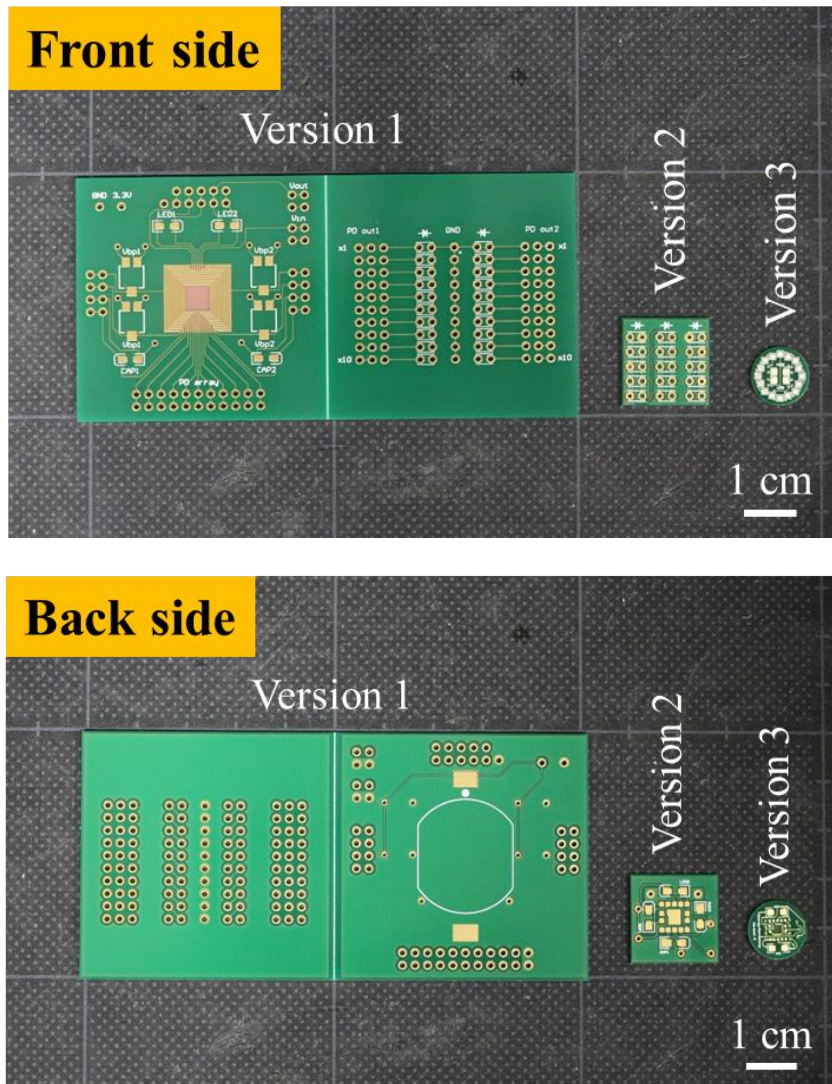
Figure 25 Photographs of the top and bottom side of PCB three versions.

4.4 Device Evaluation

4.4.1 Operation of Controllable Voltage detector in Dual State Circuit

To confirm the operation of the voltage detector in a dual-state optical power-transfer circuit, a 4 Vp-p ramp voltage was applied to the circuit as an input voltage, Vin. A resister was connected to the output line as a load to discharge the accumulated power. The relationship between the threshold voltages (V_{TH1}, V_{TL1}, V_{TH2}, and V_{TL2}) and bias voltages (V_{bn1}, V_{bp1}, V_{bn2},

and V_{bp2}) of each state in Fig. 26 is assessed by applying a matrix of bias voltages from 0.4 to 2.8 V and measuring the corresponding threshold voltages. The results from both states are similar to the result of the single-state optical power-transfer circuit in Chapter 3.3. The two-state operation of the dual-state circuit does not affect the operation of the controllable voltage detector in the basic design. Therefore, these results indicate that the threshold voltages can be adjusted by changing the bias voltages, as designed.
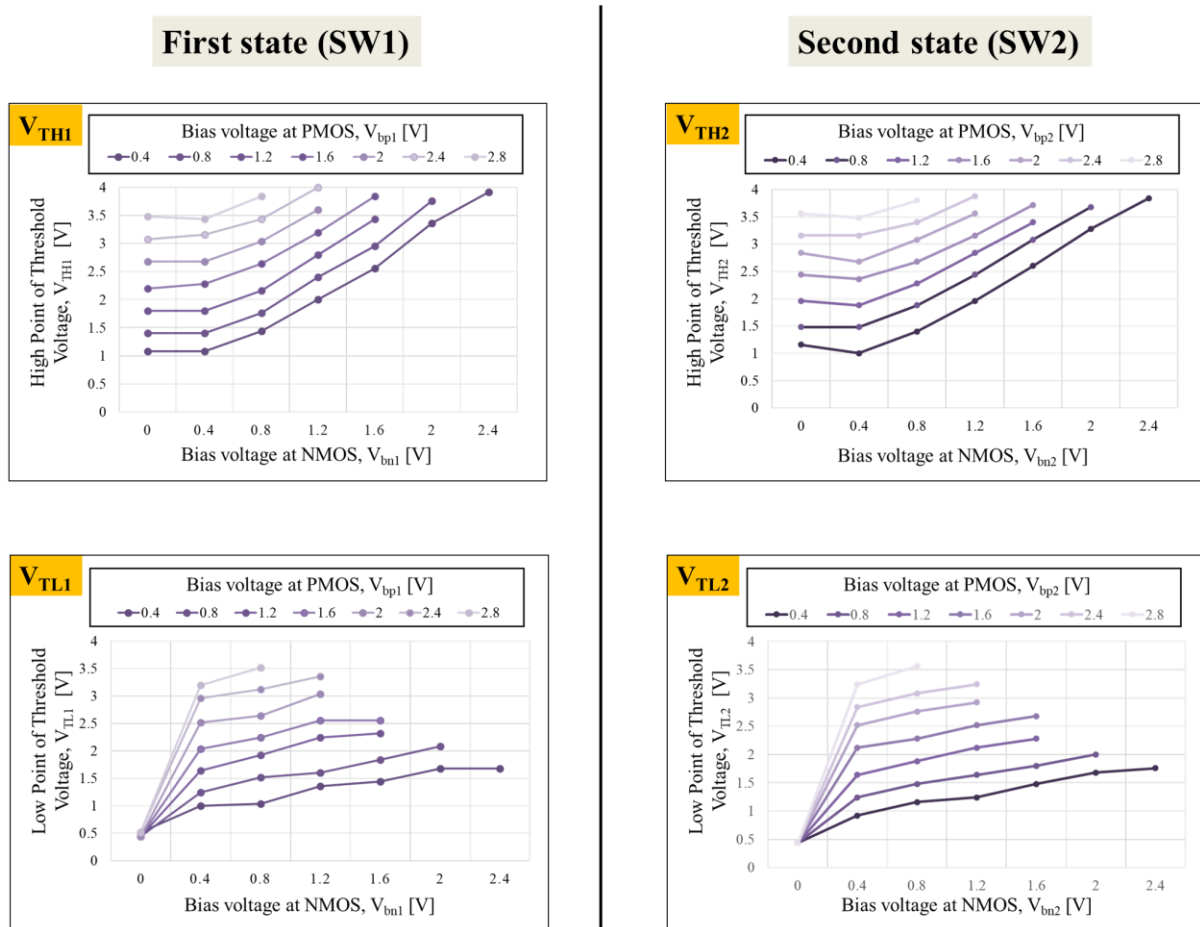
Figure 26 Relationship between threshold voltages and bias voltages in both first and second state optical power-transfer circuits.

From the relationship between threshold voltages (V_{TH1}, V_{TL1}, V_{TH2}, and V_{TL2}) and bias voltages (V_{bn1}, V_{bp1}, V_{bn2}, and V_{bp2}) of each state in the previous experiment, the bias voltages were chosen using "$V_{TH1} > V_{TL1} > V_{TH2} > V_{TL2}$" condition (1: the first power-transfer circuit,

2: the second power-transfer circuit). Under this condition, the dual-state optical power-transfer circuit accumulates and supplies continuous power and a clock signal.

To confirm the signal transmission from the voltage detector to the CMOS switch in both state, the same 4 Vp-p ramp voltage was used as the input voltage. For load, an LED was connected and also used to indicate the amount of the output voltage that enough to operate the LED. Figure 27 is an example of the oscilloscope signals from the dual-state optical power-transfer circuit at $V_{bn1} = 0.3$ V, $V_{bp1} = 2.5$ V, $V_{bn2} = 0.18$ V, and $V_{bp2} = 1$ V. The switch in the first state (SW1) turns on when V_{in} is higher than 1.04 V which is V_{TH1}. The switch in the second state (SW2) turns on when V_2 is higher than 2.04 V and turns off when V_{in} is lower than 1.08, which are the high and low threshold voltage of the second state (V_{TH2}, V_{TL2}). The connected LED illuminates when the SW2 turns on. Therefore, the signals confirm that the signal from the voltage detector turns on-off the CMOS switch, and the operation works properly.
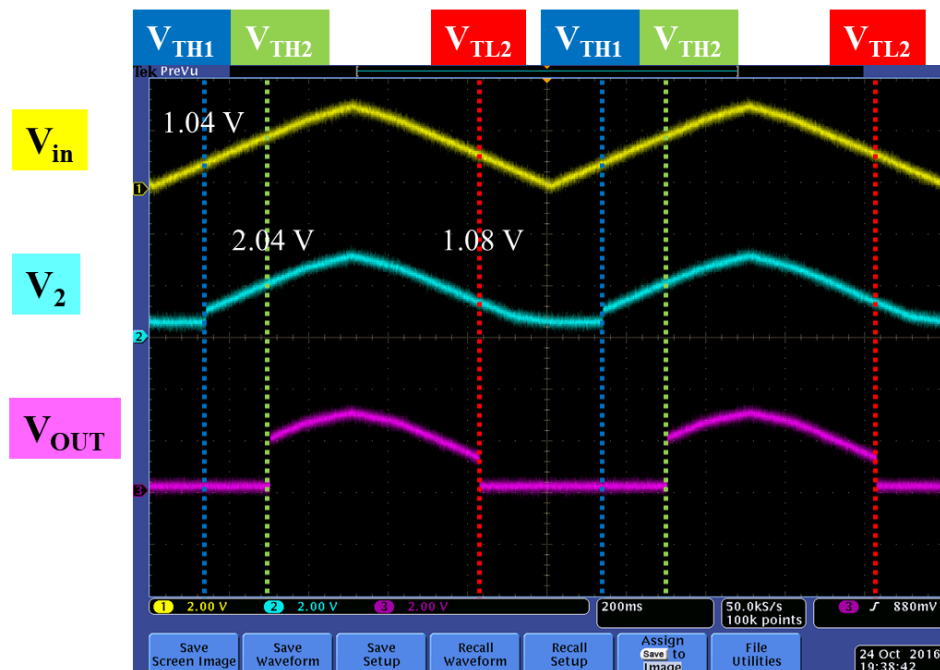
Figure 27 Voltage signals of the dual optical power-transfer circuit

with 4 Vp-p ramp input voltage.

4.4.2 Fully Wireless Operation of Optically Powered Optical ID Device

The fabricated dual-stage optical power-transfer chip was integrated at the board level, with 10 serially connected discrete photodiodes operating as small-current optical power converter to obtain sufficient voltage (approximately 4 V), and another set of 10 serially connected photodiodes as the bias circuit. Furthermore, I integrated external blue and green LEDs [54-55] as an ID display, as well as two discrete 4.7 µF capacitors[56], C1, and C2. For device evaluation, the first version of the designed PCB was used as the board of the device. Since the first version consists of two boards, the setting of the bias voltages must be designed for photodiode connection. In the previous experiment, the bias voltages were varied to find the appropriate setting for the optical ID circuit and the target load. From the variation experiment under the "$V_{TH1} > V_{TL1} > V_{TH2} > V_{TL2}$" condition, the appropriate setting of the bias voltages for this device is $V_{bn1} = 0.8$ V, $V_{bp1} = 1.6$ V, $V_{bn2} = 1.2$ V, and $V_{bp2} = 1.2$ V. The voltage for control the bypass switch is 2.5 V. The designed wiring inside the bottom board of the first version directly connects the photodiodes as two sets of series connection. Therefore, the V_{in}, V_{bn1}, V_{bp1}, V_{bn2}, V_{bp2}, V_{bypass}, and ground of the top board must connect to the tenth, second, fourth, third, third, fifth photodiode and ground point of the photodiode, respectively in the series-connected photodiode of the bottom board. Figure 28 shows the illustration of the components and connection between two boards of the first version PCB. Figure 29 shows images of the integrated prototype CMOS-based optical power-transfer circuit for bio-implantable and Internet of Things (IoT) devices.
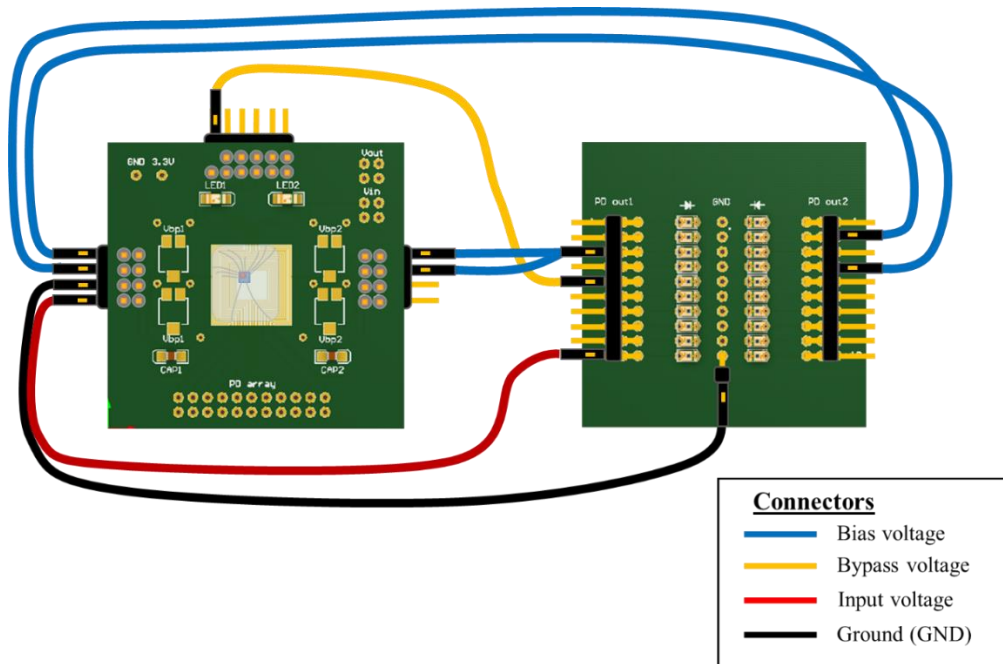
Figure 28 Illustration of components and connection between two boards of PCB version 1.
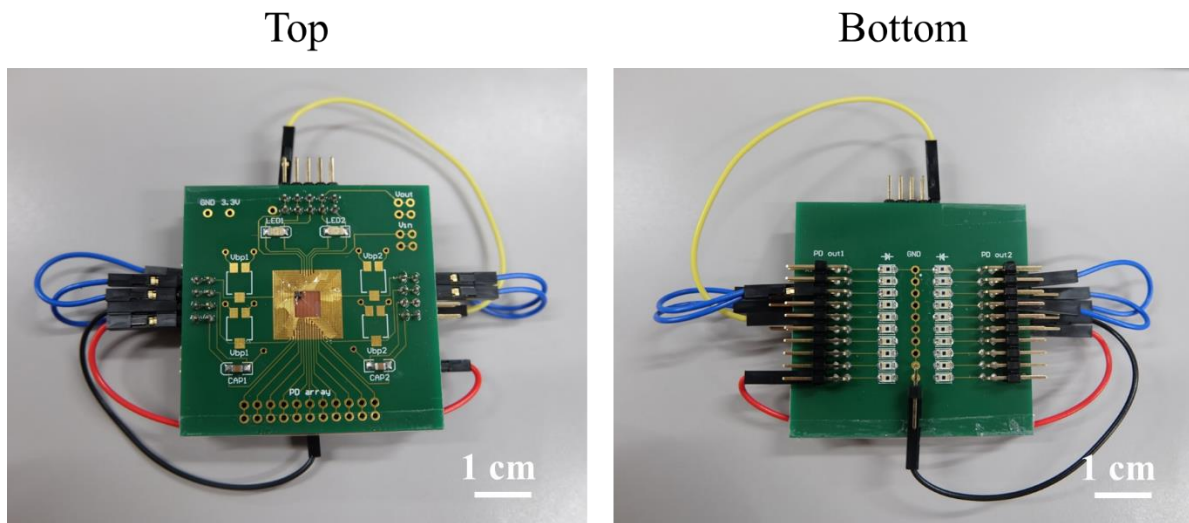
Figure 29 Photographs of top and bottom side of the finished PCB version 1.

After fabricating the device, the device was evaluated. To confirm the optical ID transmission of the prototype device, an IR light was emitted to the photodiodes side of the device (bottom). The result shows that the prototype device can wirelessly operate without any battery support or additional power source; the only power source for this device is light. Figure 30 shows traces of the input voltage, the voltage at C2, and $V_{Cathode}$ of the two LEDs, acquired

during the fully optically powered operation. The waveforms are completely consistent with the simulations, indicating that the circuits operate as expected. The optical power-transfer circuit controls the charging of the two capacitors and supplies both continuous and pulse voltages to the optical ID circuit. The LEDs operated successfully in the designed sequence, synchronously with the pulses generated by the first state circuit (a drop of V_{in}). Note that the anodes of both LEDs are pulled up to V_{out}, and the LED operations are controlled at the cathode sides.

Therefore, the short negative pulses to the 0 V observed in the lower two traces in Fig. 30 indicate that each LED is powered. From the result in Fig.16, the operation of the bypass switch also confirmed as the capacitor in the second-state was also charged when the first-state still turns on. The device also can operate under other light wavelengths such as a flashlight. A Movie 1 in the appendix showing the device in the fully wireless under flashlight, photoelectric operation is also provided as a supplementary data.
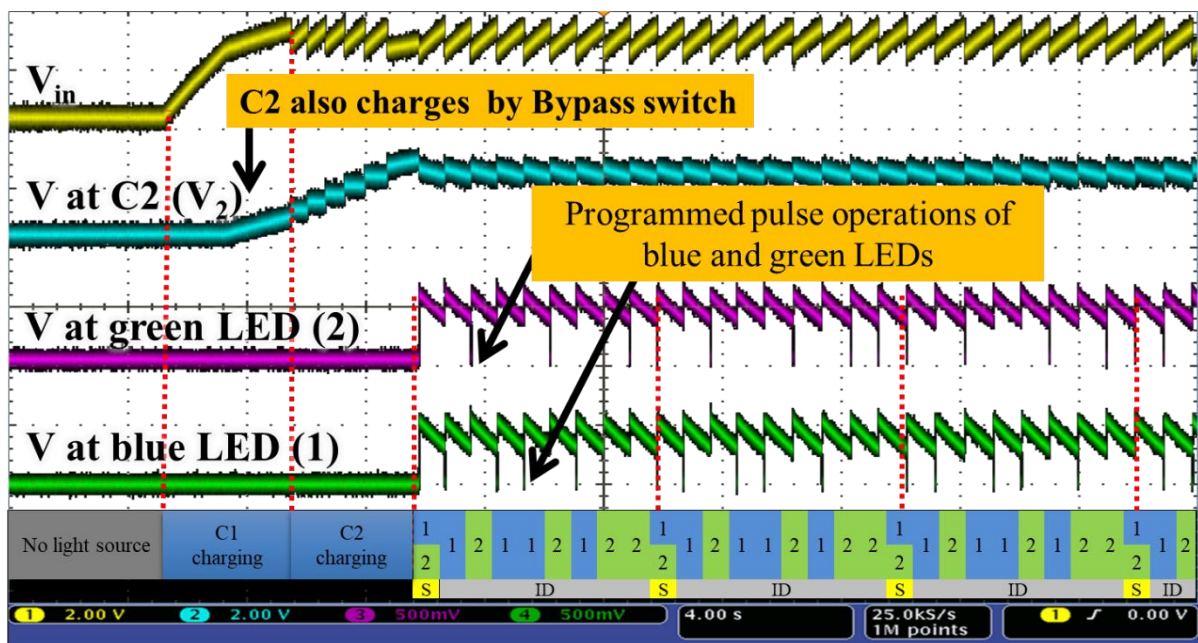
Figure 30 Traces of the signals acquired of the optical power-transfer with optical ID for the implantable device during the fully optically powered operation.

The energy conversion efficiency of an optical power-transfer device mainly depends on the powering photodiode. According to the measurement, the conversion efficiency of a single photodiode is approximately 7%. Considering that the powering photodiode is 10 series-connected photodiodes, means 10 photoelectrons are used to generate one high voltage electron. Thus, the conversion efficiency of the optical power-transfer device is approximately 0.7%.

Then, a water bath experiment was also performed to test a temperature tolerance of the optical power-transfer for bio-implantable and IoT devices. The water temperate in this experiment is from 2 to 60 degrees Celsius. The result confirms that the device works fine between 2 and 60 Celsius. The experiment of higher and lower temperatures was not provided because this temperature range is enough for the primary target application, which is bio-implantable. Note that, the third version of the optical power transfer device was used in the water bath experiment due to it is the only version that has no external wiring semi-waterproof.

4.4.3 Device Development

After evaluating the device performance, I develop another two versions of the PCB, as mention in Chapter 4.3.5. Figure 31 shows the photos of the top and bottom sides of the second version optical power-transfer device. According to the appropriate setting of the bias voltages in the device evaluation, the maximum bias voltage uses only four series connecting photodiode. Therefore, the second version can reduce the number of photodiodes for bias voltages from 10 to four diodes. However, five photodiodes were used as the bias photodiode for symmetrical and beautiful design.
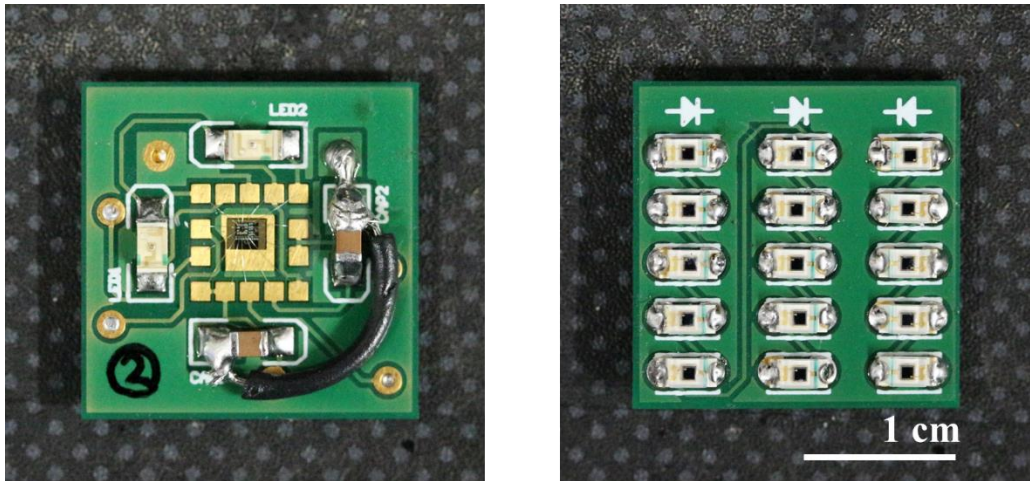
Figure 31 Photographs of top and bottom side of the finished PCB version 2.

Lastly, the third version device was designed. The last version aims to minimize size, reduce sharp edge, and introduce the waterproof ability to the device. Instead of photodiodes with the package, bare chip photodiodes mentioned in the early of this chapter was used. Also, the size of the LEDs and gold pads on the PCB are smaller. After assembling all the components on the board, the device was covered by clear epoxy for the protection and increase waterproof ability as shown in Fig. 32. Figure 33 shows the photos of the operating final version device under the low and high intensity of the IR light. According to bias voltages using photodiodes, the slight change of the bias voltages depends on the intensity of the light source. Therefore, the LED intensity is stronger when the intensity of the light source is higher. By applying the same way as the lower intensity light source, the LED intensity becomes weaker. The operation video of the final version CMOS-based optical power-transfer for bio-implantable and IoT devices is in Movie 2 in the appendix.
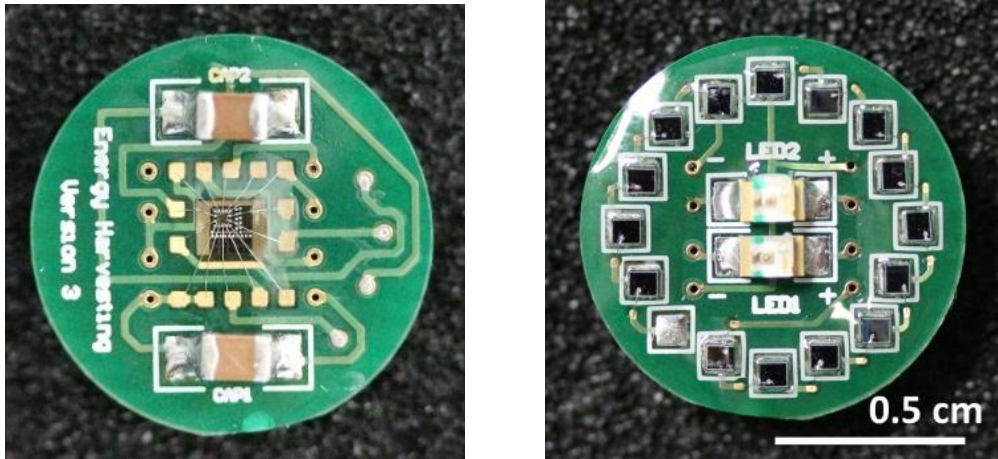
Figure 32 Photographs of top and bottom side of the finished PCB version 3.
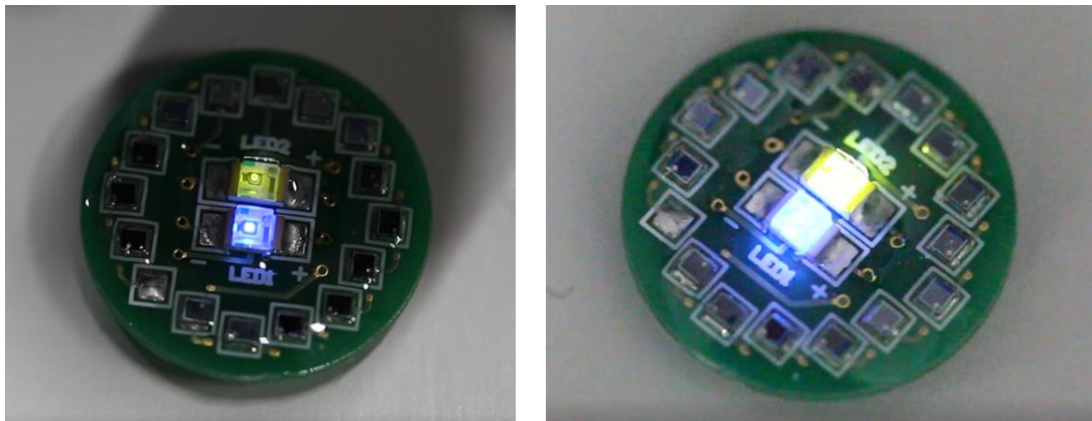
Figure 33 Photograph of operating 3rd version optical power-transfer with optical ID device.

4.5 Summary & Discussion

To comply with various application requirements, including those of the biomedical and IoT fields, a CMOS-based optical power-transfer technology was proposed and demonstrated. The schematic and layout of the proposed circuit were designed using a CAD program. Then, the chip was fabricated using a 0.35 μm 2-poly, 4-metals standard CMOS process. To evaluate and attach the designed chip with external components, which are an external photodiode array

and capacitors, I designed and developed three versions of PCBs. The finished integrated prototype CMOS-base optical energy harvesting device's size is round shape with a 1 mm diameter. The evaluation results indicate that the circuits operate as expected. The threshold voltages can be adjusted by changing the bias voltages. A battery-less, photoelectrically powered, optical ID device was developed based on the proposed optical power-transfer system. The device can operate under both IR light and flashlight. The device was developed to match with the implantable application. The final integrated prototype CMOS-based optical power-transfer device is round in shape with a 1 cm diameter. Even the 0.7% efficiency is a drawback of the optical power-transfer device but not the main concern as it is enough to drive the ID circuit. The principal aim of the device that we successfully came across is a simple circuit design.

In terms of further improvements, the size and performance of the overall device must be considered, because the size is significantly important in the implantable device, and also current and a voltage obtained by photodiodes are limited. Figure 34 shows the future concept of the CMOS-based optical power-transfer for biomedical and IoT devices. The future design cuts out the PCB, so the size is as small as the CMOS chip size, in which the size is less than 1 mm. The device includes two external capacitors, two LEDs and an optical power-transfer chip. This chip contains not only the optical power-transfer with an optical ID circuit as the original design, but it also includes two sets of build-in photodiode arrays. The optical ID circuit will be developed for modifiable ID.
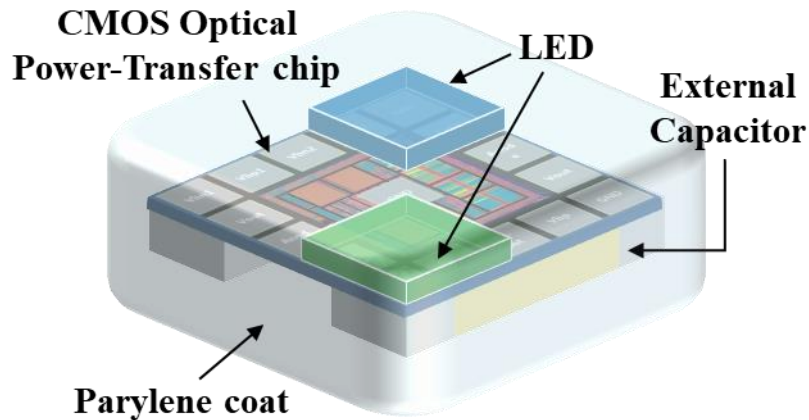
Figure 34 Future concept of CMOS-based optical power-transfer

for biomedical and IoT devices.

The original design of the optical ID circuit is designed to have already fixed a device's ID at the circuit design stage. Therefore, the user cannot change the device's ID after the device was fabricated. To develop the optical ID circuit, the input from the scanner signal remained, but another input is connected with both VDD and GND by using MET4; the most top metal layer in the chip, this MET4 can be cut by laser cutter machine to choose the VDD or GND input after fabricated the chip. From this new design, the user can design eight ID data bits by themselves, so the device is more flexible in terms of function.

To reduce the size of the device, the series-connected external bare chip photodiodes are replaced. Due to the CMOS technology, arrays of n-well p-sub photodiodes directly, including in the optical power-transfer chip [36, 41, 57-58] is possible. Figure 35(a) shows a layout of a single build-in photodiode, which the Vout pad is P side, and the GND pad is the N side of the photodiode. To obtain enough power, the build-in photodiode is connected in series as shown in Fig. 35(b).
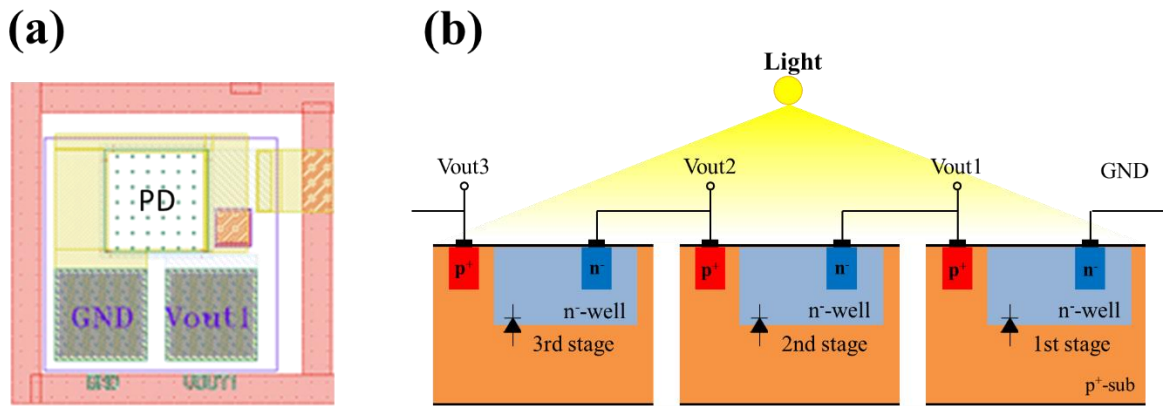
Figure 35 Design of integrated CMOS-based photodiode.

(a) is the layout of the single build-in photodiode (b) is the wiring of build-in photodiodes

Moreover, this designed optical power-transfer with IoT devices is not limited to only the implantable application. It can be used as an IoT node for smart house applications as shown in Figure 36. Using this design, the device supplies power to the sensor or device in the smart house and provides ID of each sensor for the IoT system.
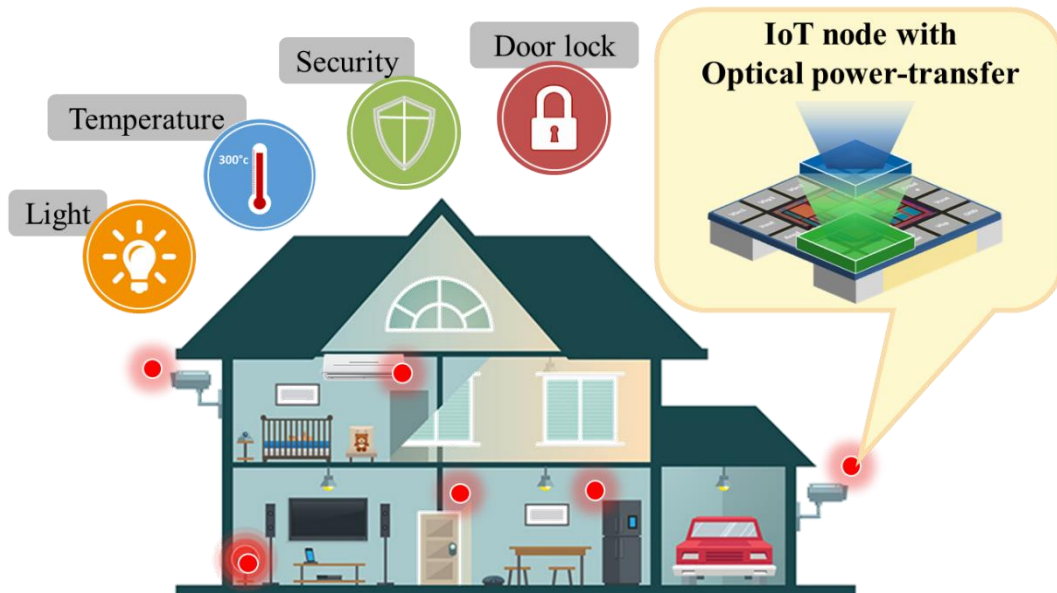
Figure 36 Concept of optical power-transfer with optical ID for smart home application.

Chapter 5

Second Application:

CMOS-based Wearable Device

for Non-invasive Glucose Monitoring

5.1 Overview

The second application for examining the operation of the optical power-transfer circuit is a wearable health monitoring device. In this chapter, a CMOS-based wearable device for noninvasive health monitoring operated by optical power transfer was presented. The device was designed based on the idea of a pain-free and more convenient health monitoring device. The power system of this device was adapted from the basic single-state optical power-transfer circuit in Chapter 3 to accumulates a small amount of photoelectrically converted energy in an external capacitor and intermittently supplies this power to a measurement circuit. In the measurement circuit, a CMOS-based amperometric measurement was also developed for operating and transmitting data from a three-electrodes electrochemical sensor. Among various target metabolites of the sensor, glucose was chosen as the target to set an example health monitoring application. The purpose, design, and evaluation of the CMOS-based wearable device for noninvasive glucose monitoring operated by optical power transfer is explained in detail in this chapter.

5.1.1 Power System for Wearable Device

The wearable device is a smart electronic device that can be comfortably attached or worn closed to the surface of the skin without interrupting or limiting the user's movement. This wearable device is used for detecting and tracking information on a real-time basis. It also can analyze and transmit the detected information to other smart devices such as a smartphone. To make the most advantage out of the structure of epidermal attachable/wearable device advantages, a battery-free approach was introduced.

One of the bottlenecks of a wireless wearable device technology is a battery due to its system lifetime limitation, system volume requirement, and unhandy maintenance. However, most of the power supply systems of the wireless devices are still dependent on it. To get rid of the battery, the proposed single-state optical power-transfer circuit in Chapter 3 was introduced in the wearable device. Comparing to battery, the circuit provides a smaller volume and extend the lifetime of the device. Moreover, the uniqueness of the circuit, which is a periodic power supply signal can be used for data transmission of the health monitoring wearable device.

5.1.2 Wearable Device in Personal Healthcare Perspective

More than ten years ago, wearable technology had been introduced into our society and became the norm in recent years. The applications of the wearable device are various and gradually grow as the field itself expands. The most commonly seen and widely used wireless wearable device in our daily life is a smartwatch that can be used as an activity tracker. Besides the commercial smartwatch, wearable technology is also being incorporated into other fields such as a navigation system, an advanced textile, and a healthcare system. Especially in terms

of healthcare, wearable technology is also considered as an innovative solution for the medical healthcare industry.

The medical healthcare industry has been dramatically changed in the past decade. The main focus of medical devices moves from a one-size-fit-all concept to a more personalized concept. The concept of personalized medical devices improves medical health care to better match individual and specific needs. It not only helps patients but also helps healthcare professionals to prevent, detection, diagnosis, follow-up, and decision making by improving the capability to predict health risks, to determine and quantify the dynamics of disease development, and to target therapeutic approaches to the needs of the individual patient. From the aspects of health, the most caring point is that the users feel comfortable with the health services provided to them, which is a lacking point of current healthcare technology. Therefore, a key in personalized medical devices is the development of portable tools that patients can easily carry in a daily basis. That is where the demand for wearable devices has increased for many healthcare applications. The wireless epidermal attachable devices are not only helping to break the uncomfortable health monitoring device barrier but also providing a minimally invasive or completely non-invasive, which less pain, freely to move and more suitable for daily life. Especially personalized medical application, the concept of the attachable devices has been more widely considered as a personalized health monitoring by combining them with biosensors. However, it is by far one the most complicated areas, and that is why wearable technology has the potential to make such a major impact.

5.1.3 Electrochemical Sensor

For the health monitoring application, biosensors play an important role in this space providing direct detection of disease markers. There are a variety of sensor types for personalized health monitoring sensors that measuring vital signs such as heart rate, bodily motion, and brain activity but still lacking chemical activity monitoring. The most considerable chemical sensor in the area of on-body sensing is an electrochemical sensor. Electrochemical sensors offer considerable promise as wearable chemical sensors that are suitable for diverse applications owing to their high performance, portability, simplicity, and low cost [59].

The electrochemical sensor is a device that transforms electrochemical information into an analytically useful signal, such as an electrical signal. Electrochemical sensors are usually composed of two basic components, a chemical (molecular) recognition system, which is the most important part of a sensor and a physicochemical transducer, which is a device that converts the chemical response into a signal that can be detected by modern electrical instrumentations [60]. The electrochemical sensor measures the concentration of a target metabolite by oxidizing or reducing the target metabolite at electrodes on the electrochemical sensor. From the oxidation/reduction reaction, electrons are produced/reduced. The electron exchange creates a current at Bio/CMOS interface, which has the opposite direction in oxidation and reduction. The current from these reactions is called "Faraday current" as an example of glucose oxidation in Fig. 37. The value of the faraday current depends on the target metabolite concentration. There are such as two-, three- or four-electrode sensors. Among these types, a three-electrode sensor was applied in this work. The three-electrode sensor consists of a working electrode (WE) which contains all the bio- and nano-materials required by the bio-detector such as an oxidase/reductase of a target metabolite, a reference electrode (RE) which

supplies a right potential to get the right reaction, and a counter electrode (CE) which make it possible to measure the faraday current [61-63].

$$Glucose + O_2 \xrightarrow{\text{GOx}} Gluconic\ acid + H_2O_2$$
$$H_2O_2 \xrightarrow{\text{Oxidation voltage}} O_2^+ + 2H_2O + 4e^-$$
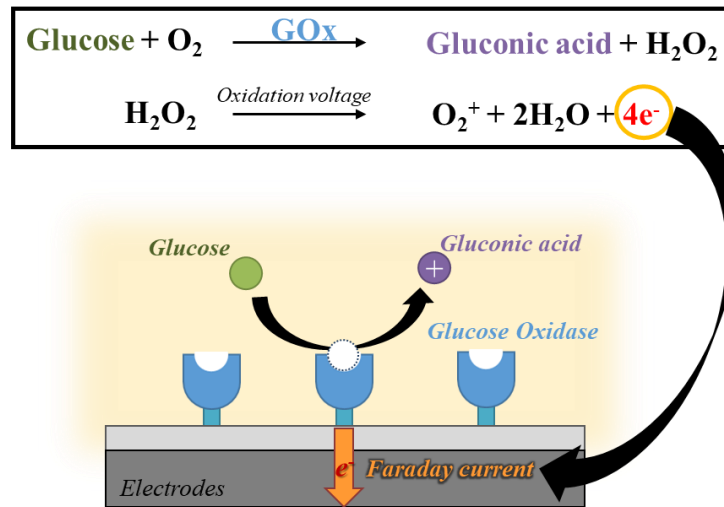
Figure 37 Chemical reaction and illustrator of the glucose oxidation reaction.

Moreover, a wide range of electrochemical sensors has been developed for noninvasive measuring electrolytes in biofluids, such as sweat, tear, or saliva as an indicator of health status. With continued innovation and attention to key challenges, such non-invasive electrochemical sensors are expected to open up new exciting avenues in the field of wearable wireless sensing, and thus find considerable use in a wide range of personal health-care monitoring applications [59, 64-66].

5.1.4 Diabetes

Diabetes is a disease that causes high blood sugar or blood glucose levels. Glucose was brought into the body by consuming food. This disease involves problems with the hormone insulin. The hormone insulin is released from the pancreas. This is a key hormone that helps glucose get into cells to be stored or give them energy. With diabetes, the pancreas does not

produce insulin or a minimal amount of insulin, or the body does not respond effectively to insulin. This causes a high blood glucose level. Over time, untreated high blood causes serious problems. It can damage nerves, blood vessels, eyes, kidneys, and lead to heart disease or other health problems. Therefore, people with diabetes must monitor and treat their blood glucose levels. There are three types of diabetes, which are Type 1, Type 2, and Gestational diabetes [67-68].

Type 1 diabetes occurs when the body cannot produce enough insulin. The immune system attacks and destroys cells in the pancreas. That causes the loss of insulin production. Since the pancreas of diabetes patients cannot release enough insulin to control the blood glucose level, their blood glucose level can be too high. When blood glucose is high, the patient must receive insulin injections to fulfill the amount that his/her pancreas cannot provide. This diabetes type most often appears in children and young adults but can appear at any age [69-70].

Type 2 diabetes occurs when the body does not use insulin properly or becomes resistant to insulin. The body is unable to metabolize glucose and still remain in blood. This leads to high blood glucose levels. This diabetes type is the most common and can be delay or prevent by changing lifestyle. People with type 2 diabetes may be prescribed tablets and/or injectable medication to helps the body to respond better to insulin. Blood glucose monitoring is significantly beneficial for patients. It provides immediate feedback and improvement of the blood glucose level to their food, lifestyle, and medical treatment [71-73].

Gestational diabetes occurs especially in women during pregnancy. One of the most significant causes of gestational diabetes is placental hormones. The placental hormones reduce the effectiveness of insulin, and their level is required higher as the baby grows. Therefore, further into pregnancy, women are a higher likelihood of developing insulin resistance.

Gestational diabetes does not happen in all women and usually subsides after pregnancy. However, it can sometimes remain as type 2 diabetes.

Nowadays, there is no cure for permanently fixing the blood glucose level. People with diabetes need to maintain their disease to stay healthy. To maintain and checkup health conditions, patients must measure their glucose concentration levels by a suitable device. A commonly used method for glucose detection is electrochemical glucose sensing and mostly blood-based type [74].

5.1.5 Glucose Monitoring Technology

Glucose monitoring is essential for diabetes patients because they require 24-hour management to control their blood glucose/sugar level. The most popular and conventional blood glucose monitoring device is self-monitoring blood glucose (SMBG) meter (Fig. 38). The SMBG uses a drop of blood from finger pricking, which is a well-known method for measuring blood glucose levels. One set of the SMBG consists of a glucose meter, a test strip, a lancing device, and a lancet, which is a needle used to prick the end of the finger to produce a drop of blood to measure the blood glucose. Without one of these equipment, the glucose measurement cannot perform. The figure pricking is the easiest method but has limitations for patients because of the pain, inconvenient to carry much equipment, and accompanying intense stress of repetitive blood collection, usually 3-4 times per day [75].

Figure 38 Commercial self-monitoring blood glucose (SMBG) meter.

Ref.: https://www.cnbc.com/2018/11/16/alphabet-verily-stops-smart-lens-glucose-measuring-contact-lens.html

Ref.: https://time.com/4703099/continuous-glucose-monitor-blood-sugar-diabetes/
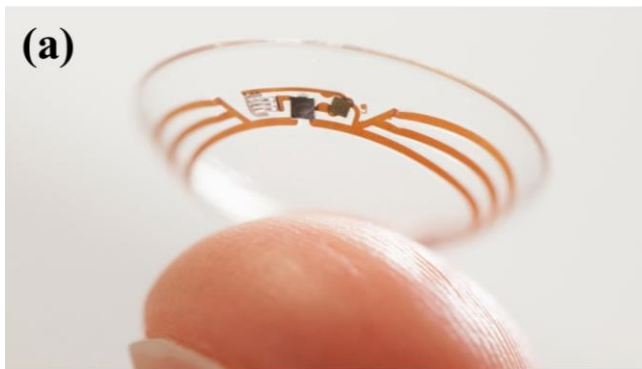
Figure 39 Minimally/Noninvasive glucose monitoring devices.

(a) Glucose monitoring contact lens by Google

(b) Minimally invasive glucose monitoring device by FreeStyle Libre

Since diabetes can happen not only adults but also children and older people, a method for painless and stress-free glucose monitoring is highly desirable. This need can be fulfilled by combining a minimally/noninvasive electrochemical sensor for glucose with a wearable device [76-77]. There are many studies and some products based on this concept, such as a contact lens by Google and Novartis that noninvasively detect glucose from tears (Fig. 39 (a)).

A minimally invasive continuous glucose monitor with a thin, flexible filament inserted under the skin to measure glucose (Fig. 39 (b)). In this work, a sweat analysis was chosen for a glucose detecting method.

According to the pilot studies of transdermal continuous glucose measurement in 2008 [78], a noninvasive electrochemical sensor is possible to monitor glucose concentration in blood with the help of ultrasound skin permeation methodology. The performance of noninvasive glucose monitoring was also equivalent to abrasion glucose monitoring. The noninvasive method could facilitate strict blood glucose control, potentially rendering safer self-management and improved long-term health benefits [79].

5.2 Purpose

The purpose of this work is to design and evaluate a CMOS-based wearable device for noninvasive health monitoring operated by optical power transfer. Among various sensing possibilities, glucose was chosen as an example of the target metabolite. This device also presents as one of the example applications of the single-state optical power-transfer circuit in Chapter 3. The device includes three technologies, which are the optical power transfer, a wearable device, and a sweat-based noninvasive electrochemical sensor to improve the health monitoring system. The CMOS-based optical power-transfer circuit was introduced into the device as a power supply system instead of a battery. This device was designed to easily attach/wear on human skin like a band-aid and detect glucose concentration from sweat. It also requires only a smartphone for light source and data display. This method provides less pain, freely movement, and more convenient.

Figure 40 is a conceptual illustration of the battery-free attachable glucose monitoring device's application. The device operation is simply started by using a smartphone flashlight as a light source of an optical power-transfer system. Then, the power from the power-transfer system operates a measurement system and detects a glucose concentration from sweat. The data display system receives the measured glucose concentration and generates a data signal. This data signal can be collected and displayed by a camera on the smartphone.
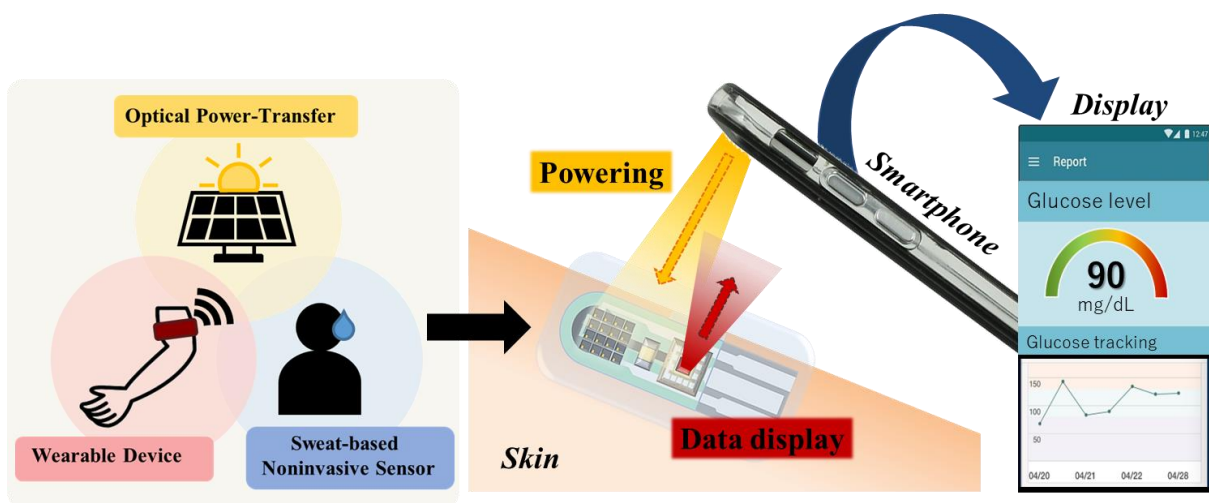
Figure 40 Conceptual application of the battery-free attachable glucose monitoring device.

5.3 Circuit Design

5.3.1 Device Overview

The design of the wearable device for noninvasive glucose monitoring operated by optical power transfer focused on the idea of painless, convenient, and freely-movement device. For convenient and flexible movement, the device must be able to complete the measurement without too much equipment and within only a compact size. The designed device requires only the device itself and the smartphone that everyone has already carried

around every day. In order to minimize the device size, the single-state optical power-transfer circuit presented in Chapter 3 was used as the power supply system of this device. The measurement circuit was also designed to complete its function within a single powering pulse. For optical data display, the advantage of the pulse power supply from the single-state circuit was applied to a pulse width modulation (PWM) method for transferring and displaying the data.

Figure 41 shows the block diagram of the proposed battery-free glucose monitoring device with an optical power-transfer platform. The device has external serial-connected photodiodes, a capacitor, a three-electrode electrochemical glucose sensor, a LED, and a CMOS optical health-monitoring chip. The CMOS chip is the main component to control the device power system and measuring system [46]. It consists of an optical power-transfer part and a functional part, including a single-potential amperometric measurement circuit and a pulse-width-modulated (PWM) light pulse data display. Due to the photodiodes, the device is simply powered by an external light source, such as the LED illuminator of a flashlight in smartphones. A photocurrent generated by photodiodes is charged into a capacitor, which is used as primary power storage. An optical power-transfer part monitors the voltage of the capacitor (V_C), and controls the operation. When the capacitor accumulates enough power, the power-transfer system supplies the power to the functional part. In the functional part, an amperometric measurement was used as the measurement method to work with the electrochemical sensor. Then, a PWM light pulse transfers the measured value and displays the value using a LED. The light pulse from LED will be collected by the camera and converted into a numeric concentration on the smartphone.
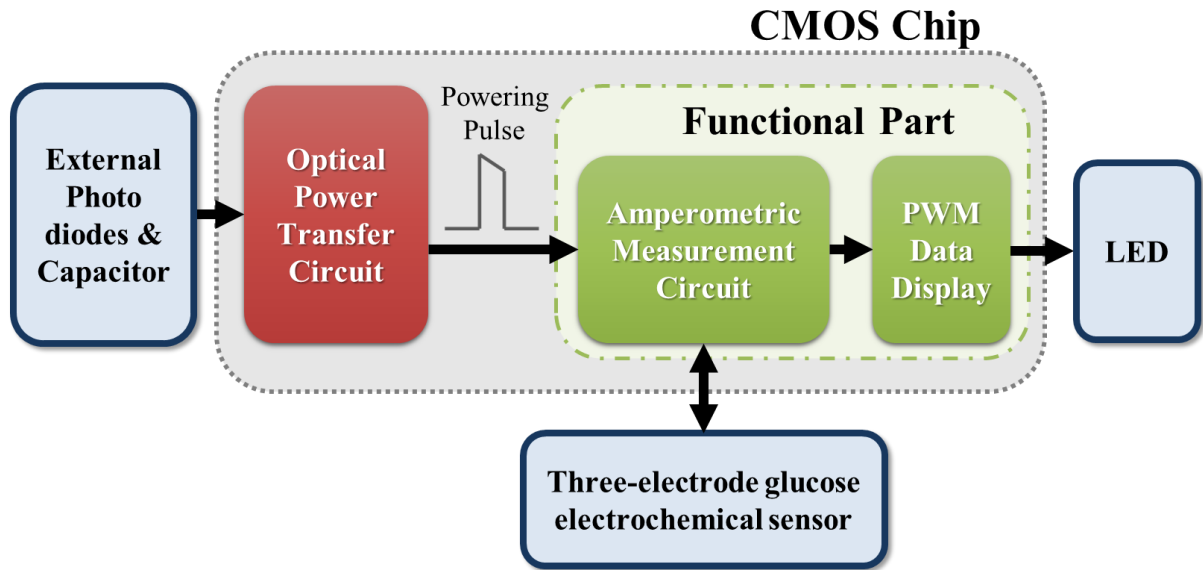
Figure 41 Block diagram of the battery-free attachable glucose monitoring device.

5.3.2 Optical Power Transfer part

An optical power-transfer part is an important power supply system in this device for providing a suitable power supply to the functional part. Due to the single pulse operation of the functional part, the design of the single-state optical power-transfer circuit in Chapter 3 with some modification in the voltage detector was employed as the optical power-transfer part of this device. The modification aims to reduce the power consumption of the optical power-transfer part. For low power consumption, current limiting transistors were introduced in the voltage detector by adding them at the instantaneous transition current flowing through two inverters consisting of Mp2, Mn2, Mp3, and Mn3 in the voltage detectors.

Figure 42 is a schematic of the voltage detector in the CMOS optical health-monitoring chip. According to the modification, this voltage detector requires four bias voltage to control power supply and reduce power consumption. To control the supply voltage level (V_{TH} and

V_{TL} levels), V_{bn} and V_{bp} voltages from the bias circuit are crucial. In addition, V_{limit} at a current-limiting transistor set (Mn4 and Mn5) utilizes for reducing the current consumption of the optical power-transfer circuit.
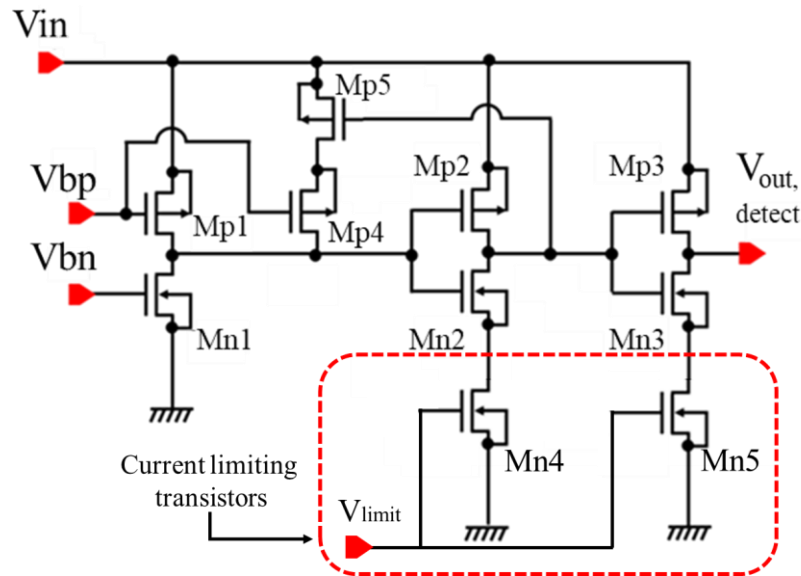
Figure 42 MOS-level schematic of the low power consumption voltage detector.

The overall function and block diagram (Fig. 43(a)) of the new optical power-transfer circuit basically remain the same as the original single-state optical power-transfer circuit. The circuit consists of two sets of external photodiodes, an external capacitor, a voltage detector, and a CMOS switch. The two sets of photodiodes included one set of 10 series-connected photodiodes, called "main photodiodes," to obtain sufficient voltage for the circuit operation, and another set of six series-connected photodiodes as a bias voltage source, called "bias photodiodes," to control on-off voltages and current limitation that are required for operation.

The operation begins when emitting light to the photodiodes. The photodiodes convert light to electrical power then, charge the external capacitor with the current generated by the photovoltaic effect. When the capacitor voltage (V_C) reaches V_{TH}, the voltage detector turns on a CMOS switch and supplies power to the functional part means the external capacitor is discharged. After a discharge phase, when the capacitor voltage decreases to V_{TL}, the voltage

detector turns off the CMOS switch and stops supplying power. During the phase, when no load is present, the capacitor is recharged to repeat the operation, as shown in Fig. 43(b). Therefore, the supply power signal is intermittent pulses with voltage decay. The pulse period starts with the turn-on threshold voltage V_{TH} and terminates at the turn-off threshold voltage V_{TL}.

Importantly, the pulse width of the capacitor discharge period (yellow arrow in Fig. 43(b)) depends on the power consumption of the functional part. As the supply voltage is almost constant, it means that the pulse width depends on the current consumption of the functional part. This relationship between the pulse period and the current consumption was employed for data-display in the functional part.
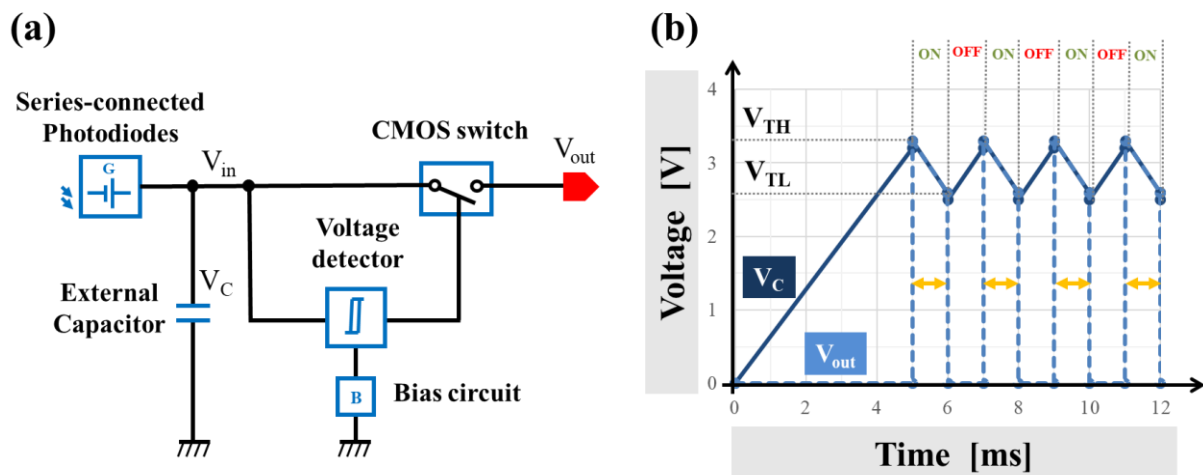
Figure 43 Optical power-transfer part in the glucose monitoring device.

(a) Block diagram and (b) Simulated operation of the optical power-transfer part.

5.3.3 Functional Part

In the functional part, there is a measurement part connected with a noninvasive electrochemical sensor and a data display part connected with a LED. For the measurement part, a three-electrode amperometric measurement circuit, which is a common measurement method for the electrochemical sensor, was chosen to control and collect measurement data from the sensor. For the data display part, we employed a pulse-width-modulated (PWM) light pulse circuit using the relationship between the pulse period and the current consumption of the functional part to transfer the measured value as shown in Fig. 44.
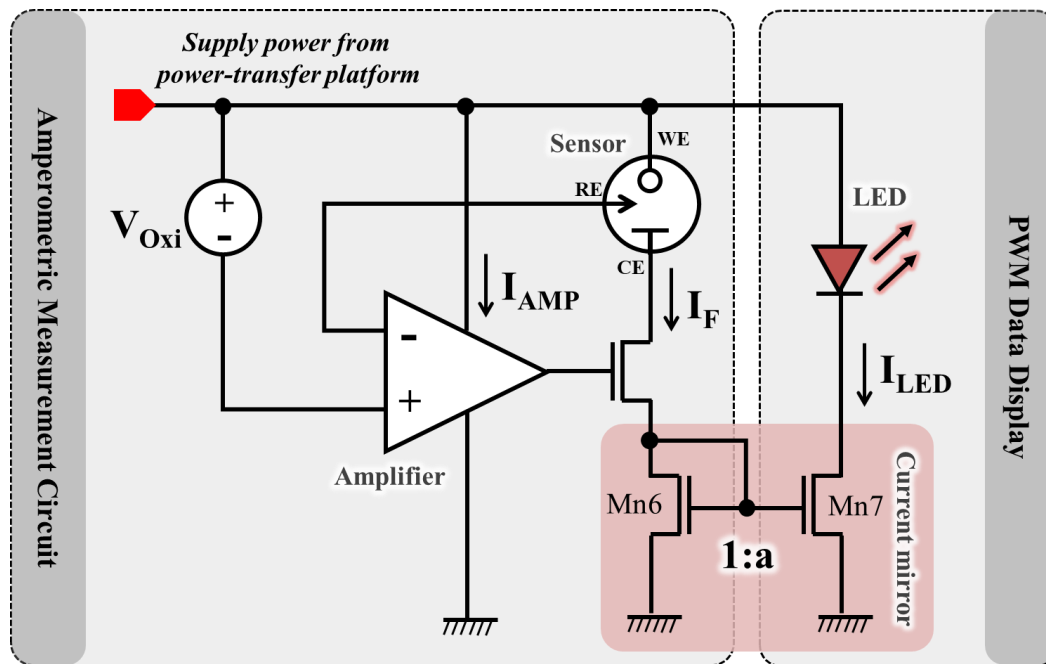
Figure 44 Block diagram of the functional part.

Amperometry or amperometric method is one of a family of electrochemical methods. This method applies a fixed voltage to the sensor to control the chemical reaction and instrument. The voltage is applied between two electrodes during measurement. Then, measures the current occurring, which is a consequence of oxidation/reduction at the electrode surface as the analytical signal. As the concentration of the target metabolite higher, the more

chemical reaction (oxidation/reduction), the higher number of exchanging electron on the electrode surface, means the higher current value. Therefore, the current depends on the concentration of the target metabolite. This current is measured only while the potential is applied. It is called "Faraday current," as mentioned in the introduction. A typical application of amperometry is the determination of glucose concentration [80].

Typically, an amperometric measurement demands a continuous power supply means it is reasonable to implement a voltage regulator circuit in the power-transfer platform to operate the amperometric measurement circuit, but it requires additional current. In order to minimize the current overhead, I configured the amperometric measurement circuit to work with a temporary-varying operation voltage and utilize the relationship of the supply power pulse width and the current consumption of the functional part for the data-display scheme.

For the specification of the amperometric measurement circuit, the three-electrode electrochemical sensor requires a constant and correct potential between the working electrode (WE) and the reference electrode (RE) to get the right reaction and maximum sensitivity of the sensor. A feedback loop using a simple differential amplifier without cascade transistors was introduced to fulfill the sensor requirement. The schematic and symbol of the amplifier in the feedback loop is shown in Fig. 45. In this work, the voltage between WE and RE (V_{WE-RE}) was kept at approximately 0.4 V, which is a glucose oxidation voltage (V_{oxi}) of this specific sensor. V_{oxi} is generated by micro-photodiodes, similar to other bias voltages. At the right V_{oxi} value, a glucose oxidation reaction generates the faraday current (I_F) based on a glucose concentration. The current flows from WE into the collection electrode (CE) and transmits to the data display part via current mirror transistors.
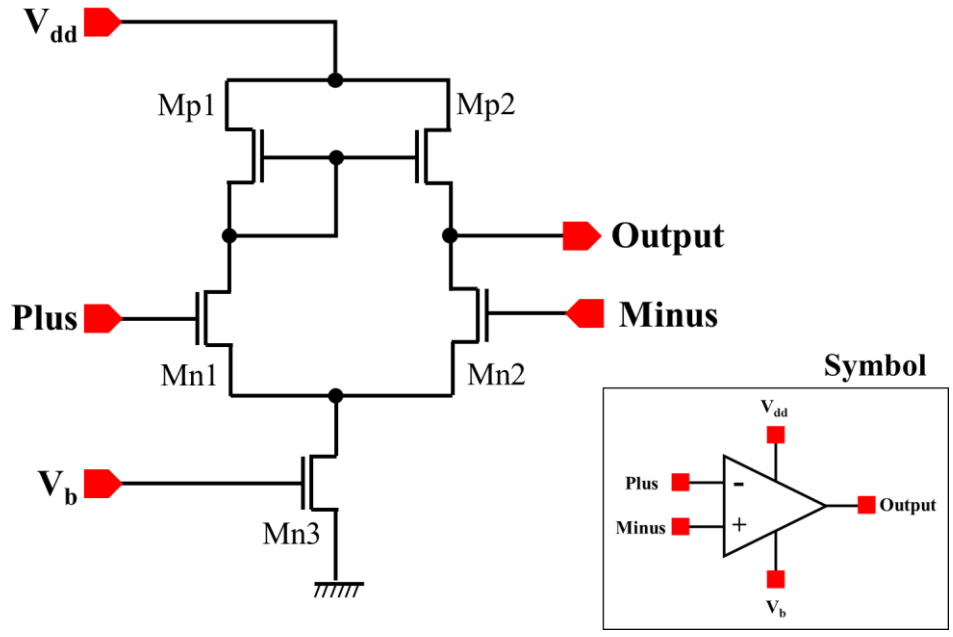
Figure 45 MOS-level schematic and Symbol of the amplifier.

In the data display part, the current mirror transistors were integrated to copy the faraday current from CE and build up a new LED current to transmit the measured value. The power from the optical power-transfer circuit supplies the amplifier and the electrochemical sensor in the amperometric measurement circuit. Moreover, the LED also shares power with the amperometric measurement circuit. This means that the total current consumption of the functional part (I_{Total}) that flows from the external capacitor (see Fig. 46) is

$$I_{Total} = I_{AMP} + I_F + I_{LED} \qquad (1)$$

Thus, the LED current is regulated to be proportional to the faraday current. The ratio between LED current and faraday current depends on the ratio between the width of two current mirror transistors (Mn6:Mn7 is 1:a). Therefore, the total current consumption of the functional part is

$$I_{Total} = I_{AMP} + (1+a) I_F \qquad (2)$$

As the amplifier is expected to operate only in feedback to keep the operating point within the designed condition and the amplifier current (I_{AMP}) is expected to be nearly constant during operation. Thus, the total current consumption depends purely on the faraday current (I_F). On the other hand, the optical power transfer circuit (voltage detector and switch) is configured to provide the power pulse while V_C is between V_{TH} and V_{TL}. Therefore, a single powering pulse delivers a total charge of

$$Q_{Pulse} = C \times (V_{TH}\text{-}V_{TL}) \tag{3}$$

Therefore, the pulse duration of a single pulse is

$$T_{Pulse} = Q_{Pulse} / I_{Total} \tag{4}$$

Now that the total current consumption depends on the faraday current and C, V_{TH}, V_{TL}, (1+a), and I_{AMP} value can be determined from design and/or calibrated parameters. Therefore, the faraday current (I_F) can be estimated from T_{Pulse} based on Eq. (1) to (4). Moreover, since the LED was designed to operate by the power pulse from the optical power transfer circuit, the LED emitting pulse period equals the pulse duration of a single pulse (T_{pulse}). For that reason, the faraday current also can be estimated from the duration of the LED emitting pulse. Then, it converts the faraday current back to the glucose concentration from the sensor calibration. Figure 46 shows the overall schematic level of the wearable device for noninvasive health monitoring operated by optical power transfer.
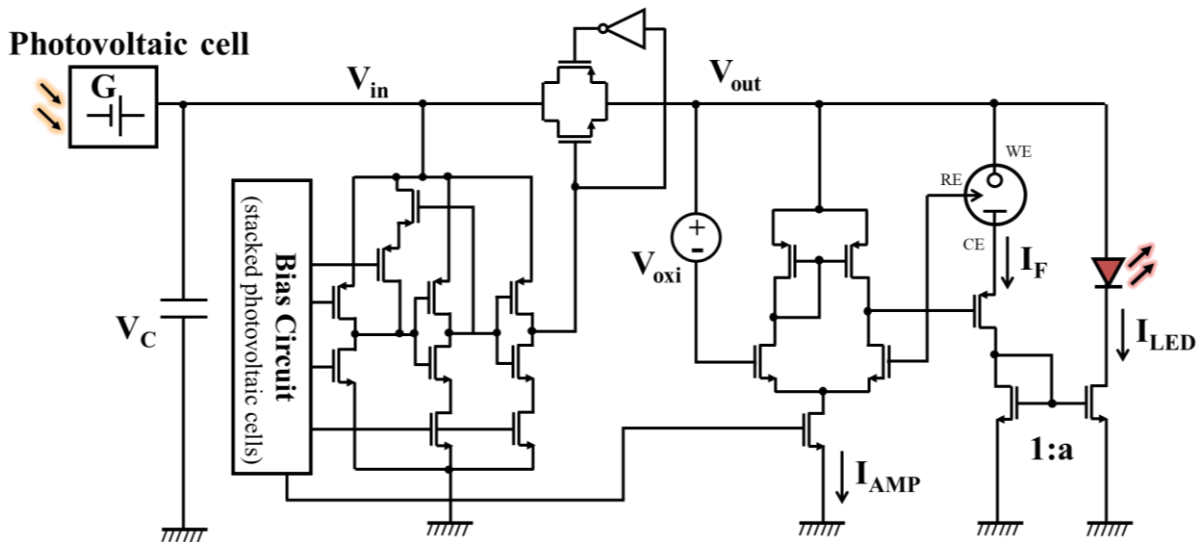
Figure 46 MOS-level schematic of the battery-free attachable glucose monitoring device.

5.3.4 Electrochemical Sensor Model for Simulation

The CMOS chip was designed using a 0.35 μm standard CMOS process. In this simulation, a glucose sensor is used as an example of a health monitoring target, but the actual physical electrochemical glucose sensor (Fig. 47) cannot be included in the simulation. Therefore, the glucose sensor model must be used in the simulation. Figure 48 is an equivalent circuit of the electrochemical glucose sensor that widely uses in many journals. The commonly used model is designed based on the Randles equivalent circuit [81-83]. The circuit can vary glucose concentration by using the variable resistor. However, this equivalent circuit has a deviation when the sensor does not operate at oxidation or reaction voltage. To solve this problem, the new equivalent circuit of a three-electrode electrochemical sensor in Fig. 49 was designed and used as the glucose model in this work.
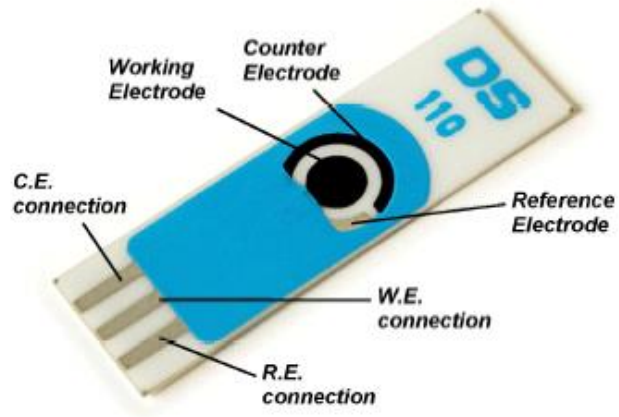
Figure 47 Image of the physical electrochemical glucose sensor.
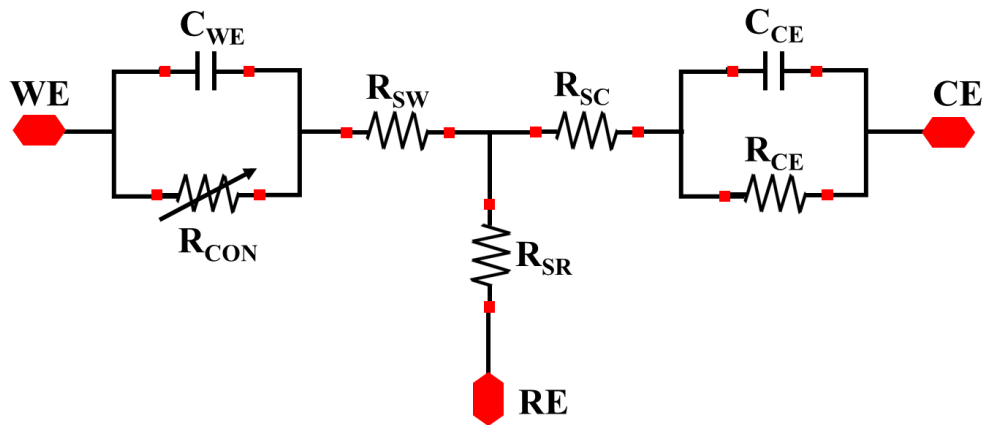
Figure 48 Equivalent circuit of a commonly used three-electrodes electrochemical sensor.
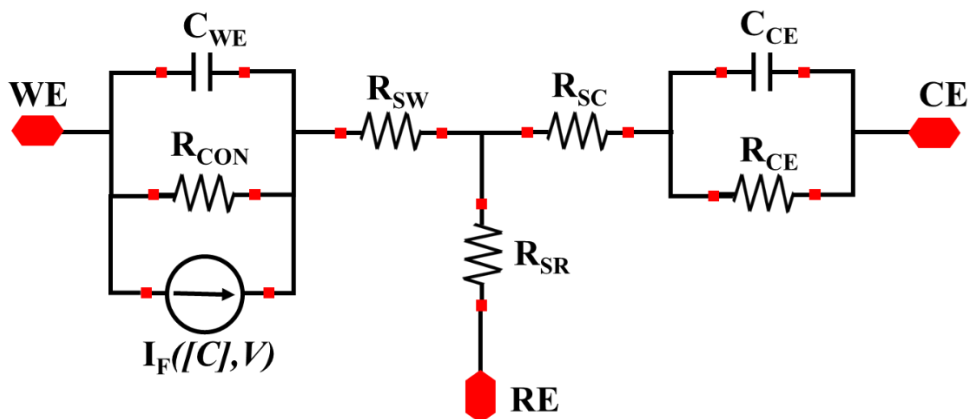
Figure 49 Equivalent circuit of new design three-electrodes electrochemical sensor.

According to the characteristic of the electrochemical sensor [61], a current generator between the working electrode and the reference electrode generates faraday current (I_F), which relates to the concentration of the measured biological substance/target metabolite. The relation between the concentration and applied voltage between RE and WE to faraday current value defines by

$$I_F([C], V) = I_{max}\, e^{-\frac{(V-VF)^2}{Peak\,width^2}} \tag{4}$$

V_F is the oxidation voltage, which is the voltage at the peak position of the cyclic voltammetry curve. I_{max} is the maximum faraday current of the peak position, as shown in Fig. 50. The other parameters in the equivalent circuit have a constant value, and they are dependent on the characteristic of the electrochemical sensor except for the concentration resistor at the working electrode:

$$R_{CON} = V_F / I_{max} \tag{5}$$
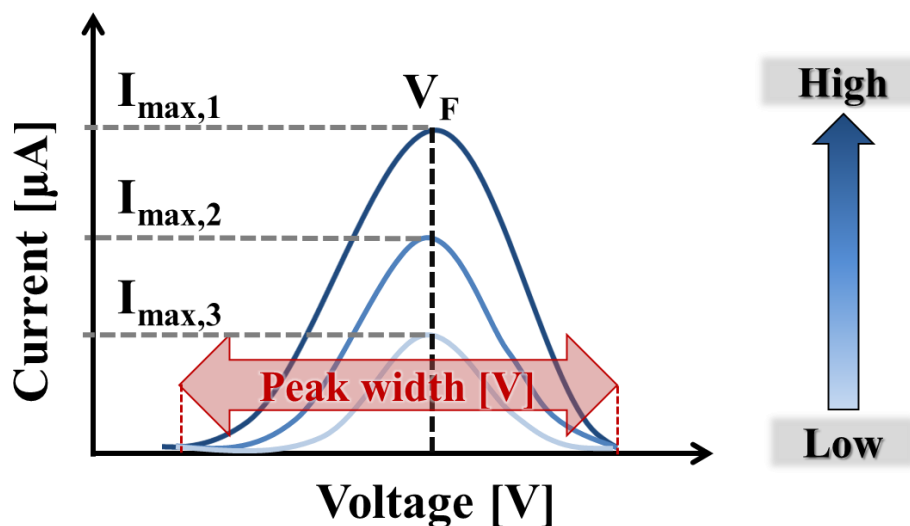
Figure 50 Example of cyclic voltammetry curve in the oxidation reaction.

(Note that, plots "Imax, 1", "Imax, 2", and "Imax, 3" are

the maximum current from high to low concentration.)

According to [84], the characteristic of their glucose sensor is used as reference data of testing the designed glucose sensor model in the simulation. Fig. 51 is an oxidation curve of cyclic voltammetry (CV) and the relationship between faraday current and glucose concentration results of the actual glucose sensor. From the oxidation curve, the oxidation voltage (V_F) is approximately 0.47, I_{max} varies from 30 to 80 µA, and the peak width is approximately 0.25 V.
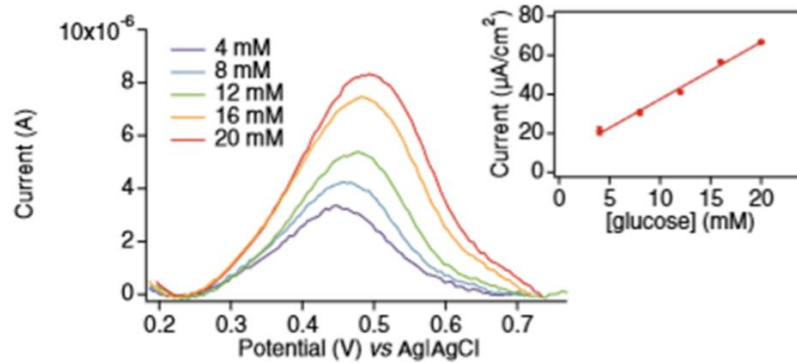
Ref.: **Fast synthesis of platinum nanopetals and nanospheres for highly-sensitive non-enzymatic detection of glucose and selective sensing of ions** --Irene Taurino, Gabriella Sanzó, Franco Mazzei, Gabriele Favero, Giovanni De Micheli1, and Sandro Carrara

Figure 51 Oxidation curve from CV and Calibration curve of the reference glucose sensor.

To evaluate the characteristic of the new sensor model, a DC voltage and a 1 kOhm resistor were applied between WE and RE as an oxidation voltage (V_F) and at CE as a load. Then, a DC analysis with a vary oxidation voltage from 0 to 1 V was used for simulation. A parametric analysis with a varying current from 30 to 80 µA was also used for representing the different glucose concentrations. For other constant parameters, the value of R_{CE}, R_{SC}, R_{SW}, R_{SR}, C_{CE}, and C_{WE} chose according to [82-83], are set to 1 kOhm, 10 Ohm, 10 Ohm, 6.3 kOhm, 1µF, and 1 nF. Note that these parameter values can be adjusted to fit with the characteristic of the actual sensor. However, the main focus of this simulation is the operation of the designed health monitoring circuit, not the sensor characteristic. Therefore, these estimated parameter values are enough to simulate the characteristic of the glucose electrochemical sensor in the circuit simulation.

The simulation result in Fig. 52 shows that the designed equivalent circuit of the electrochemical sensor has the same characteristic exponential curve as the actual electrochemical sensor. On the other hand, the commonly equivalent used circuit was simulated using the same DC analysis by varying oxidation voltage from 0 to 1 V. The simulation result in Fig. 53 shows that the relationship between the faraday current and oxidation voltage of the common one is a linear. Comparing these two equivalent circuits, the new design circuit has more similar characteristics to the actual sensor than the commonly used one. The simulation result from both equivalent circuits might not be much different when the sensor operates at oxidation voltage or lower. However, when the voltage between WE and RE is higher than the oxidation voltage, the faraday current from the commonly used equivalent circuit is higher than the faraday current at oxidation voltage. In contrast, the actual sensor and the new design generates lower faraday current than the faraday current at oxidation voltage. Therefore, the new design equivalent circuit in this work is more accurate than the commonly used circuit.
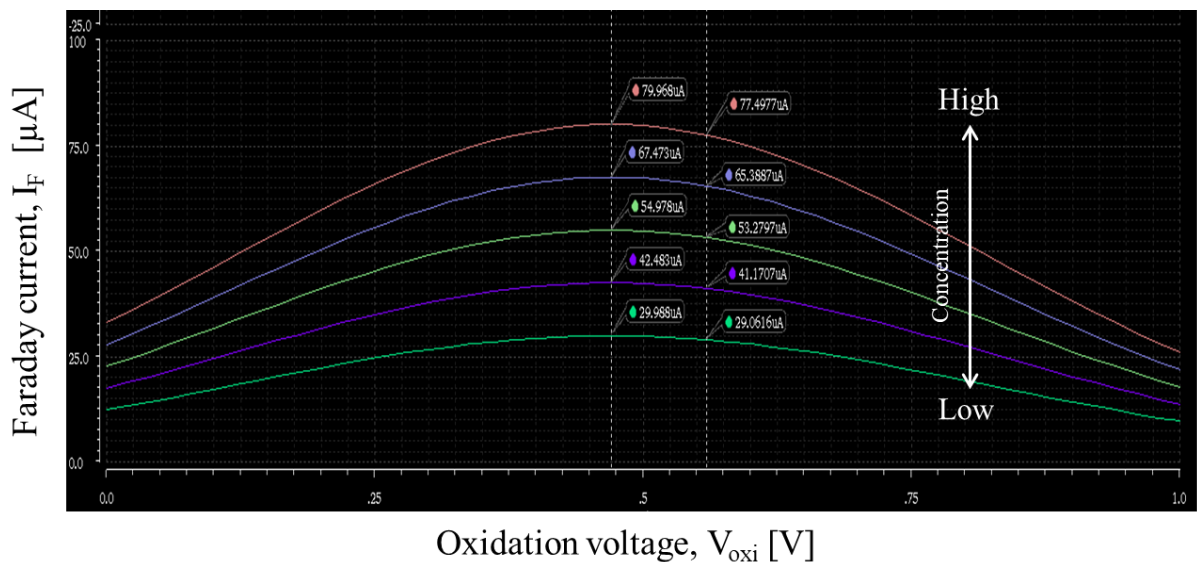
Figure 52 Simulation result of the oxidation curve from the new design three-electrodes electrochemical sensor.
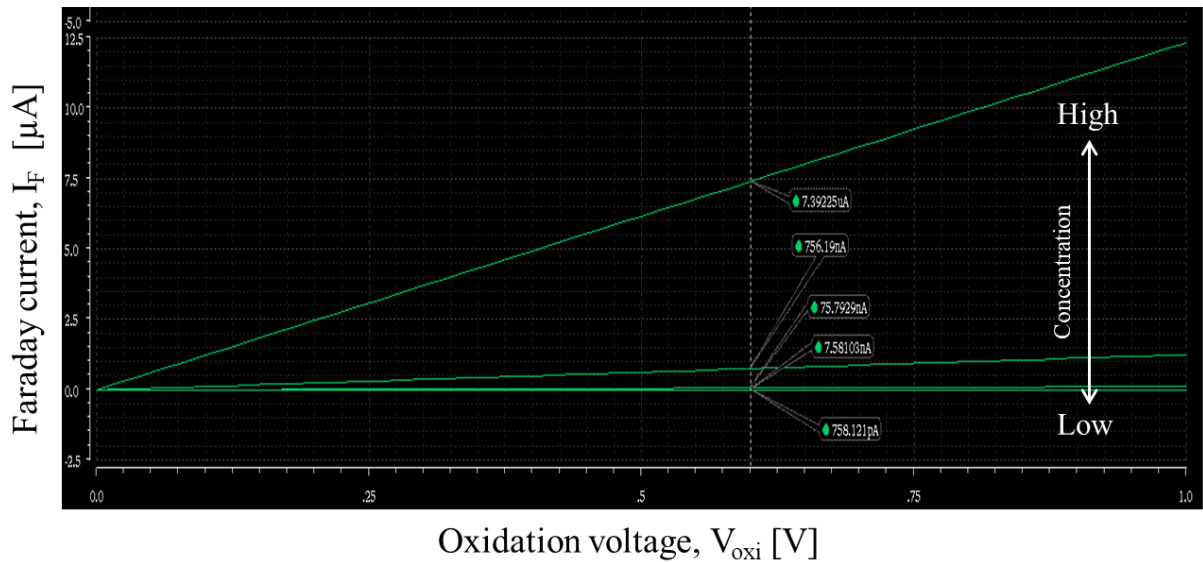
Figure 53 Simulation result of oxidation curve from the commonly used three-electrodes electrochemical sensor.

5.3.5 Device Simulation

By including the designed sensor model, the designed schematic of the wearable device for noninvasive health monitoring operated by optical power transfer was simulated. To evaluate the relationship between glucose concentration and the duration of LED emitting pulse, a parameter analysis was used. The parameter analysis varies I_{max} value for representing different glucose concentrations. The high I_{max} value means high concentration, and the low I_{max} value means low concentration. The schematic and parameter values for simulation are in Fig. 54 and Table 7. Using transient analysis, the result of the simulation in Fig. 55 shows that at high I_{max}, the V_{LED} period is shorter, and at low I_{max}, the V_{LED} period is longer. Therefore, the LED emitting period depends on the I_{max} value, which is a glucose concentration.
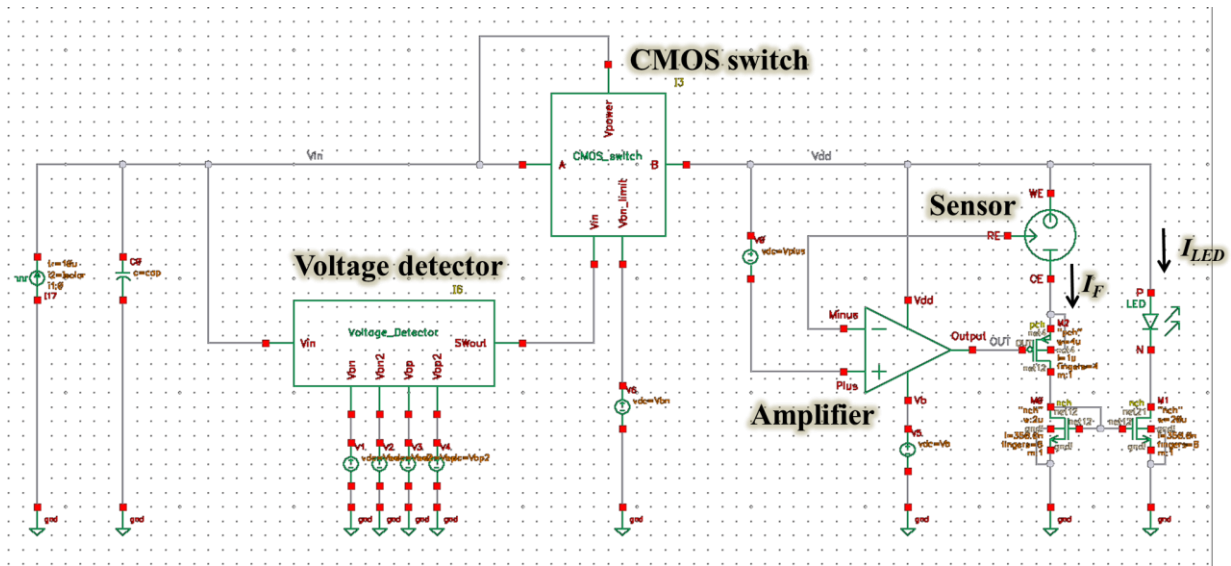
Figure 54 Schematic of the battery-free attachable glucose monitoring device for simulation.

Table 7 Set up parameter value for simulation.

Parameter	Value
I solar	10 μA
C	20 μF
V_{bn}	0.4 V
V_{bn2}	0.4 V
V_{bp}	2.4 V
V_{bp2}	2 V
V_b	0.8 V
V_{oxi}	0.47 V
I_{max}	0.01-100μA
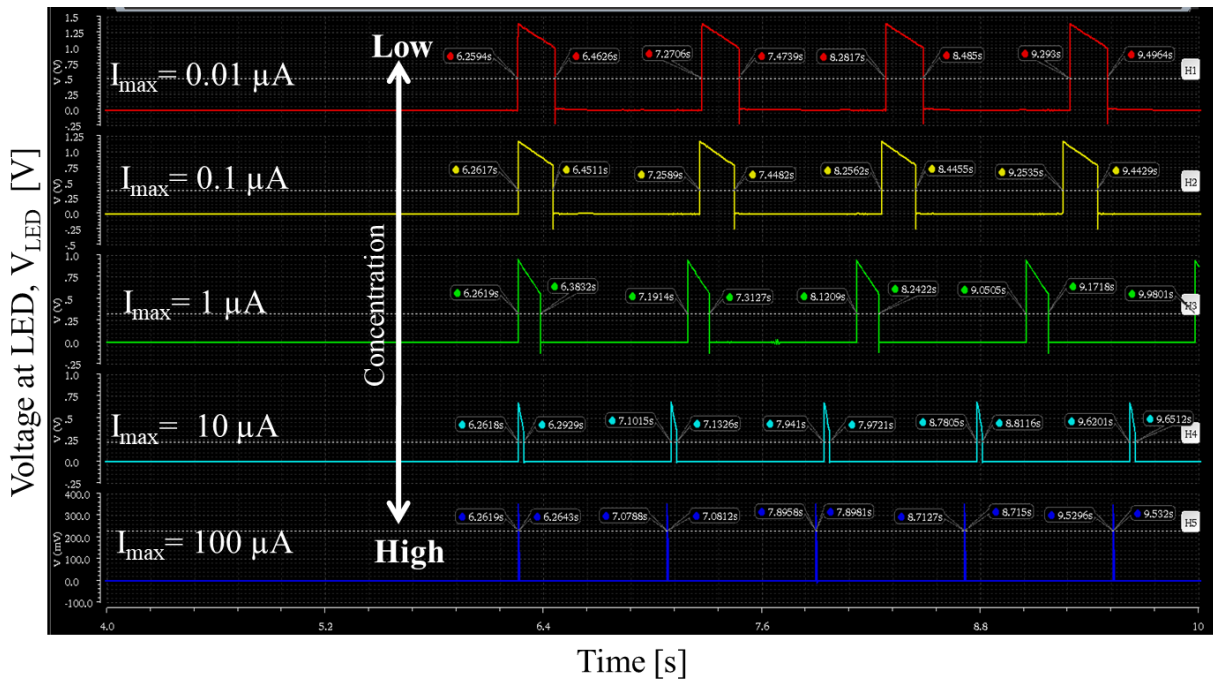
Figure 55 Simulated operation (LED pulse duration) for various I_{max}

representing different glucose concentrations.

At a constant voltage between the working electrode and the reference electrode, the faraday current (I_F) equals to I_{max}. The higher the faraday current (I_F) means, the higher concentration and also indicates a higher LED current and a higher total current consumption (I_{Total}). Now that a higher current is being drawn, the period of the capacitor discharge and the LED pulse duration become shorter. Moreover, the LED brightness also becomes brighter. Therefore, the results of the simulations indicate that the amperometric measurement and data-display with the optical power-transfer circuit works as expected. According to the simulation results, the best ration between two transistors in the current mirror circuit is 1:10 (Mn6:Mn7). Figure 56 shows the complete block diagram of the noninvasive health monitoring with optical power transfer circuit and the relationship between each part.
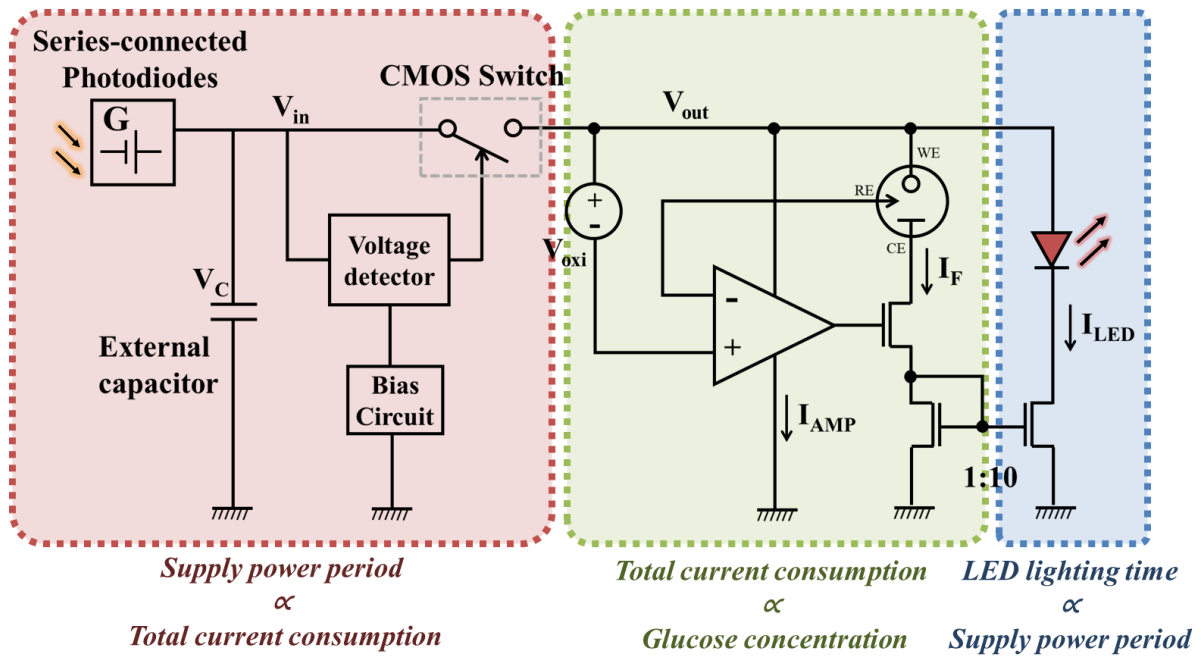
Figure 56 Complete block diagram and relationship of the noninvasive health monitoring with optical power transfer circuit.

5.3.6 Layout Design

After completed schematic designing and simulating the noninvasive health monitoring with an optical power transfer circuit, the next step is layout design. The main idea design of this layout is to optimize the space for minimizing device size. Figure 57 shows the layout of the noninvasive health monitoring with optical power transfer circuit. This layout also includes a metal-4 protection layer, I/O pads, and electrostatic discharges (ESD). The size of the finishing circuit layout is 67.15×50.35 μm^2, and the size of the whole chip in Fig. 58 is 617×641 μm^2. The details of input and output pins (I/O pads) are shown in Table 8.
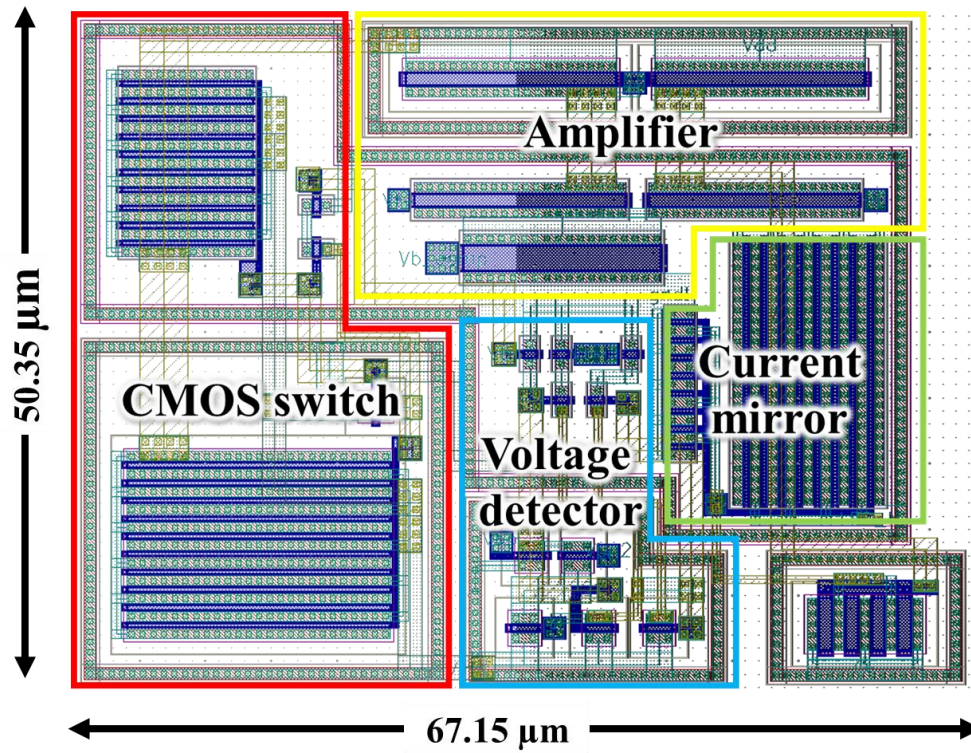
Figure 57 Layout of the noninvasive health monitoring with optical power transfer circuit.
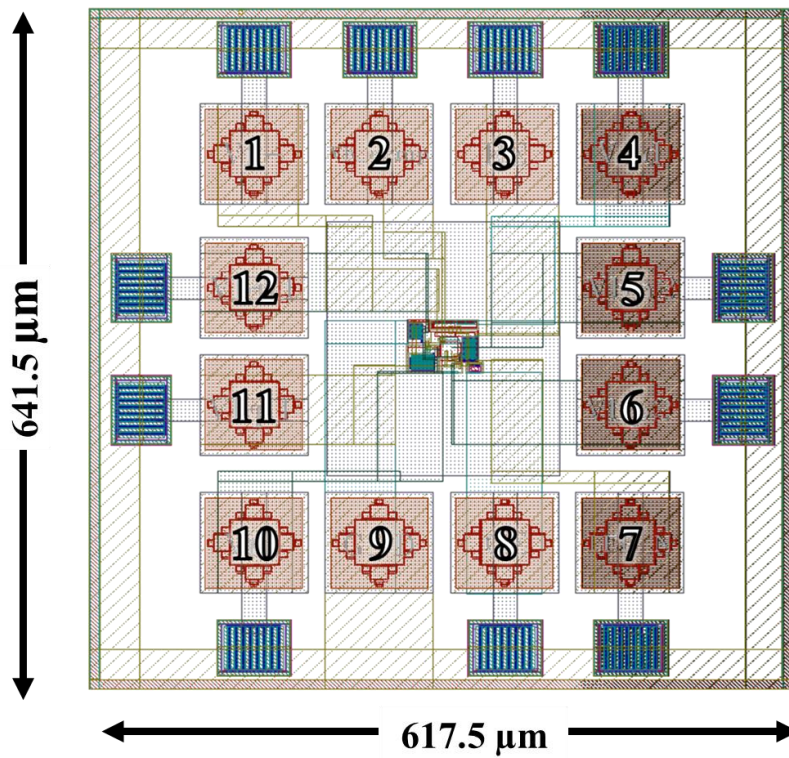
Figure 58 Layout of CMOS noninvasive health monitoring with optical power transfer chip.

Table 8 Detail of each pad in the health monitoring with optical power transfer chip.

PAD number	PAD name	I/O	Connection node
1	Vdd	I/O	1. plus of oxidation voltage 2. working electrode of sensor 3. P side of LED
2	RE	I/O	reference electrode of sensor
3	Vb_amp	I	photodiodes
4	Voxi-	I	minus of oxidation voltage
5	Vbn1	I	photodiodes
6	Vbp1	I	photodiodes
7	Vin	I/O	PDs and Capacitor (C= 20 µF)
8	GND	I	ground
9	CE	I/O	counter electrode of sensor
10	LED_N	I	N side of LED
11	Vbp2	I	photodiodes
12	Vbn2	I	photodiodes

To characterize the circuits and demonstrate the concept of the proposed battery-free health-monitoring device with optical power-transfer platform, the designed CMOS chip was fabricated by a 0.35 µm two-poly, four-metal standard CMOS process. Figure 59 and Table 9 display the layout and specifications of the CMOS chip, respectively.
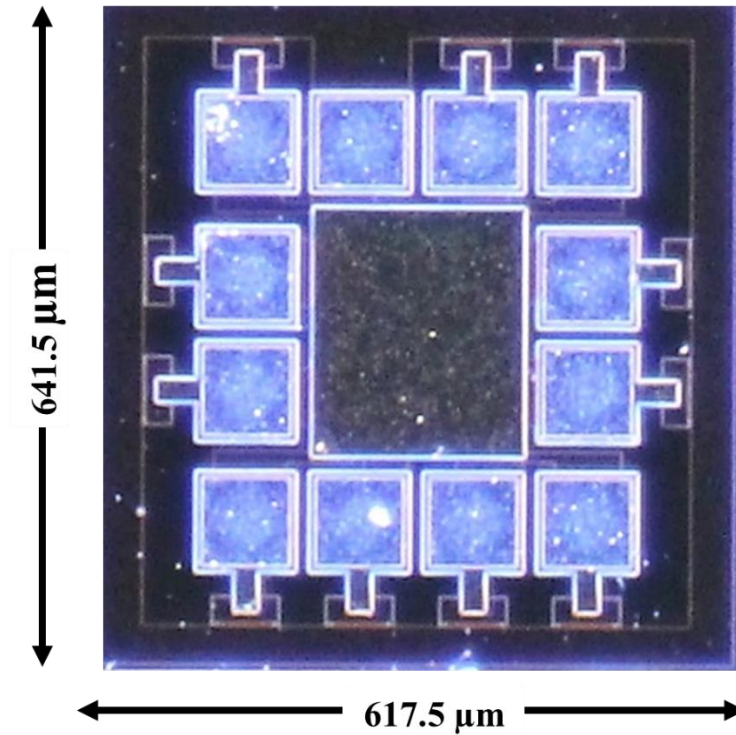
Figure 59 Photograph of actual health monitoring with optical power transfer chip.

Table 9 Specifications of CMOS actual health monitoring with optical power transfer chip.

Specification	Details
Process	0.35 µm two-poly four-metal standard CMOS
Operating voltage range	2.6 - 4 V
Chip size	641.5 x 617.5 µm^2
List of included circuits	- Optical power transfer circuit - Amperometric measurement circuit - Pulse-width-modulated (PWM) data display circuit
Required external components	- Two serially connected photodiodes for powering and biasing - Three-electrode electrochemical sensor - Capacitor - LED

After preparing all the components, the evaluation boards were fabricated. Fig. 60 shows the fabricated evaluation boards. The (a) board on the top side consists of a CMOS chip, a capacitor, and a LED. On the bottom side, the (b) board is for glucose sensor. A commercial disposable blood glucose test strip was used as a glucose sensor and connect with other components using a connector.
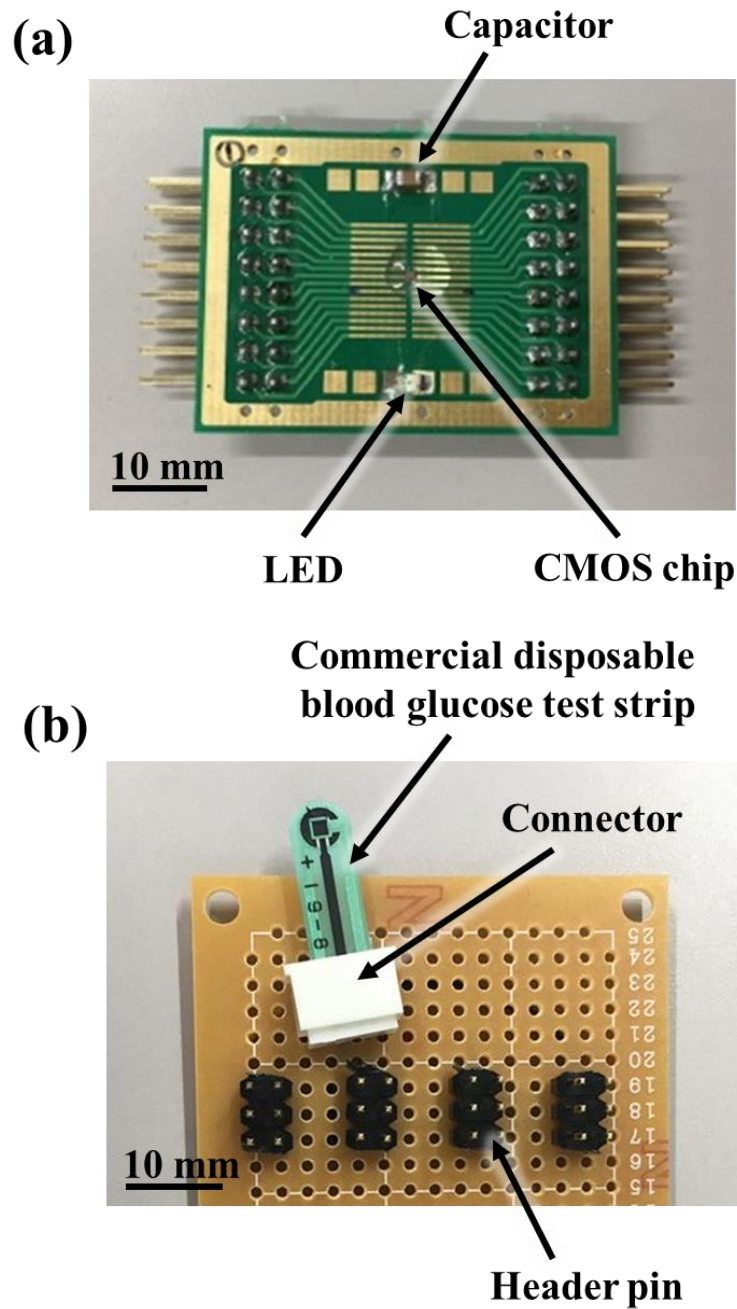
Figure 60 Photographs of the evaluation boards for battery-free glucose monitoring device.

5.4 Device Evaluation

5.4.1 Intermittent Operation of Optical Power-Transfer

To confirm the operation of the optical power-transfer part, a function generator was used as an input voltage (V_{in}) instead of serially connected photodiodes and capacitor for stability control/most accurate results in this experiment. In actual applications, the initial stage of the capacitor voltage is zero, and increase its value by the current from the photodiodes. Then, decrease the value by discharging to the functional part. To mimic these characteristics of the capacitor voltage, a 0-4 V ramp voltage from the function generator was chosen. The 0-4 V ramp voltage, DC voltage generators, two resisters, and a LED were used as the input voltage, bias voltages, a glucose sensor, and a data display LED for analyzing the on-off period of the optical power-transfer. If the optical power-transfer part works properly, the CMOS switch is turned on when the input voltage reached a high threshold voltage level (V_{TH}) and turned off when the input voltage dropped lower than the low threshold voltage level (V_{TL}). Therefore, the output supply voltage (V_{OUT}) to the functional part occurs only when the switch turns on. Otherwise, the output supply voltage has the same value as the input voltage if the optical power-transfer part is not a function. The result in Fig. 61 shows that the optical power-transfer part correctly intermittent supplies power to the functional part as expected. At the appropriate bias voltages, the circuit starts to supply power (V_{OUT}) when the input voltage reached 3 V (V_{TH}) and stops supply power when the voltage dropped to 2.6 V (V_{TL}). Therefore, the output voltage has the same level as the input voltage only when the CMOS switch turns on and reminds almost zero volts when the switch turns off. The LED also only emits light when the CMOS switch turns on, which means the output voltage is properly supplied to the functional part.
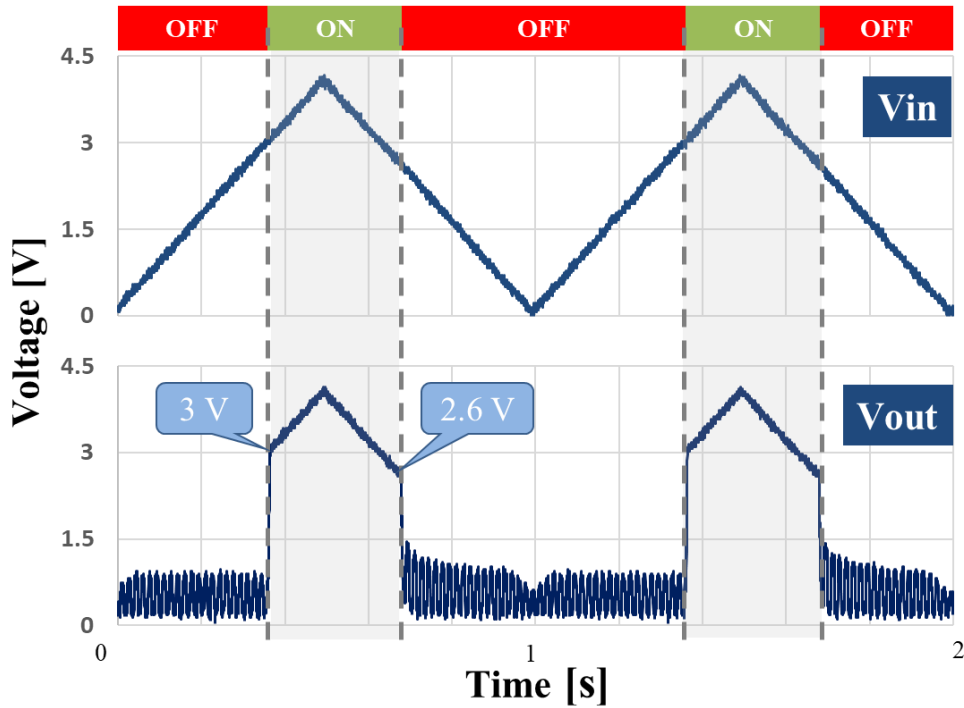
Figure 61 Voltage signals of the optical power-transfer part with 4 Vp-p ramp input voltage.

As mentioned in section 5.3.2, the bias voltages in the optical power-transfer part were designed to supply by photodiodes. Therefore, the variations of V_{bn} and V_{bp} from light intensity may cause some shifts in on and off voltage values. By changing the light intensity, it might slightly change the on-off voltage level but not completely stop the operation. The limitation of the operation is the illumination at the powering PDs, not the biasing PDs.

5.4.2 Glucose Detection Using Amperometric Measurement

To evaluate the function of the measurement part, the same 0-4 V ramp voltage was applied to the circuit input instead of photovoltaic power generation. The LED was also replaced with a resistor to monitor the current flowing at LED. The commercial glucose-sensing strip was used as the glucose electrochemical biosensor. In this experiment, glucose powder was used to prepare a glucose solution and drop the solution on the strip for testing

glucose detecting as a substitute for sweat. The result of two powering pulse cycles of the LED voltage from non-glucose to higher than 600 mg/dL glucose concentration is shown in Fig. 62. Due to the experimental setup, the function generator fixes the pulse duration of the LED. Therefore, the measurement result is not shown as pulse duration, but only as pulse height. At the higher concentration, the circuit successfully obtained a larger faraday current. On the other hand, the circuit obtained a smaller faraday current at a lower concentration. This result shows the amperometric measurement circuit works as expected.
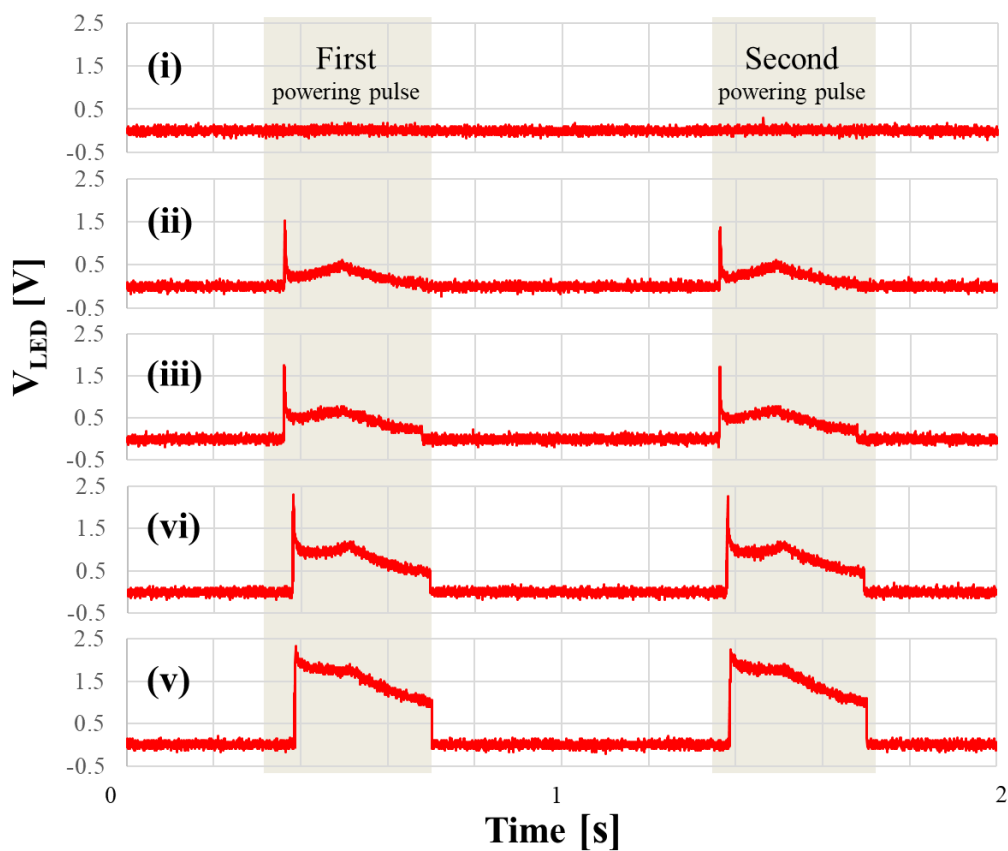
Figure 62 Voltage at LED at various glucose concentration using 4 Vp-p ramp input voltage: "(i)" is 0 mg/dL (non-glucose), "(ii)" is lower than 20 mg/dL, "(iii)" is 109 mg/dL, "(vi)" is 495 mg/dL, and "(v)" is higher than 600 mg/dL glucose concentration.

5.4.3 Fully Optical Operation of Battery-free Glucose Monitoring Device

The prototype of the battery-free health-monitoring device operated by optical power was assembled for the device evaluation. The fabricated CMOS chip was connected with two sets of 10 series connected discrete photodiodes as the input photodiodes and the bias photodiodes to obtain sufficient voltage (approximately 4 V for each set). Furthermore, we connected a discrete 4.7 µF capacitor, an external LED as a power accumulator, and a data display LED, as well as a commercial glucose-sensing strip as the noninvasive electrochemical biosensor. This commercial glucose-sensing strip requires an oxidation voltage of approximately 0.4 V. For sweat detection, the same glucose solution was prepared at different concentrations. The details of the external components were summarized in Table 10. The device was activated by emitting light to both sets of the photodiodes and tracked its operation by an oscilloscope. The graphs in Fig. 63 show tracking signals from the oscilloscope of an input voltage at capacitor (V_C) and a voltage at LED (V_{LED}). As shown in the V_C graph, the device requires starting time about 2.5 seconds to accumulate initial power. This starting time can be shorter by using a stronger light source and conversely, it can be longer if the light intensity from the light source weaker. After the starting time, the glucose detection starts operation and shows the glucose concentration as the LED emitting pulse, as shown in the V_{LED} graph. In the V_{LED} graph, some noise occurs when the functional part is not measuring the glucose. However, it does not affect the display part because the display system focuses only when LED is emitting, and this noise has not enough voltage to operate the LED.

Table 10 Specifications of required external components.

Parameters		Details	Value
Input voltage		10 photodiodes from PD set1	4.0 V
Bias voltages in voltage detector	Vbn1	1 photodiodes from PD set2	0.4 V
	Vbp1	6 photodiodes from PD set2	2.4 V
	Vbn2	1 photodiodes from PD set2	0.4 V
	Vbp2	5 photodiodes from PD set2	2.0 V
Oxidation voltage (Voxi)		Individual single photodiode	0.4 V
Bias voltage in amplifier		1 photodiodes from PD set2	0.4 V
Electrochemical sensor		Commercial glucose strip	-
LED		470 nm Blue LED (Surface mount type)	-
Glucose solution		Glucose powder mixed with deionized water	125 mg/dL

*<u>Note</u>: PD set1 is input photodiodes, PD set2 is bias photodiodes
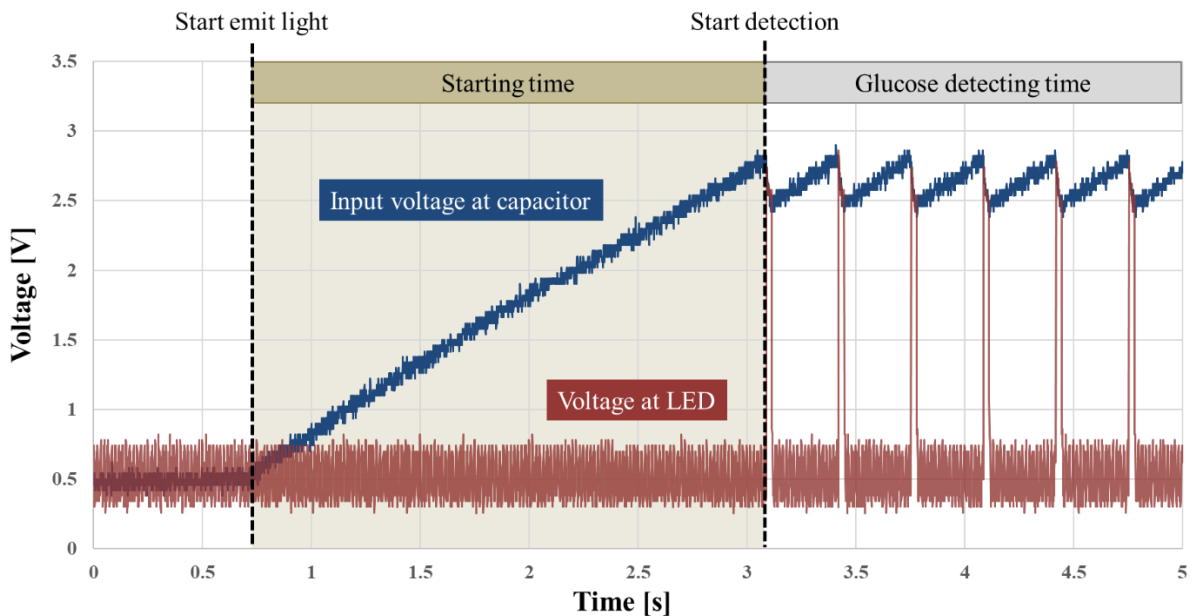
Figure 63 Traces of the signals acquired at 125 mg/dL glucose concentration

during the fully optically powered operation.

5.4.4 Relationship Between Concentration and PMW Light Pulse

As stated in 5.3.5, the faraday current (I_F) can be estimated from the pulse width of the lighting LED (T_{Pulse}). This faraday current value also represents the concentration of the glucose. This means the device can measure the concentration of the target biological substance from the lighting period of the LED by taking video and processing it on the smartphone. According to this process, the relationship between glucose concentration and LED lighting period is significant for measurement.

At the constant voltage between the working electrode and reference electrode, the higher glucose concentration means the higher faraday current (I_F) and also means the higher total current (I_{Total}) from Eqs. (1) in section 5.3.5. Due to the higher current consumption, the period of capacitor discharge and the LED emitting pulse is shorter. On the other hand, the lower glucose concentration means, the longer LED emitting pulse. Therefore, the glucose concentration shares an inverse relationship with the pulse width of the LED emitting pulse.

To confirm the relationship between the glucose concentration and the pulse width of the LED emitting pulse, we prepared various testing concentrations of the glucose solution. The testing glucose concentration range was designed base on the sensitivity of the example commercial SMGB for the commercial glucose-sensing strip, which is 20 to 600 mg/dL, and also the blood glucose level of healthy people and diabetes patients. According to the literature [67, 73], the blood glucose level for the majority of healthy individuals is between 70 to 110 mg/dL when fasting state and up to 140 mg/dL when two hours post-meal. For people with diabetes, their glucose level is higher than 140 mg/dL when fasting state without insulin injection, but the target blood glucose level for them is between 70 to 130 mg/dL before a meal and lower than 180 mg/dL after a meal. As their body does not produce enough insulin to absorb glucose until the glucose level gets back to normal, the blood glucose level can reach

over 200 mg/dL if they are not received the injected insulin. Therefore, we chose 30, 60, 125, 250, 500, and 1,000 mg/dL as examples of the glucose concentration to evaluate the device. With the same setup as the previous experiment, the result in Fig. 64 shows that the higher concentration is, the shorter the pulse width of the LED emitting pulse will be. Otherwise, the pulse width is longer when the concentration is lower. In the experiment, the LED emits light to display data in all the chosen concentration range but with small different brightness. By plotting the values of the glucose concentration and the average pulse period, the graph in Fig. 65 confirms that the glucose concentration shares an inverse relationship with the pulse width of the LED emitting pulse as expected.
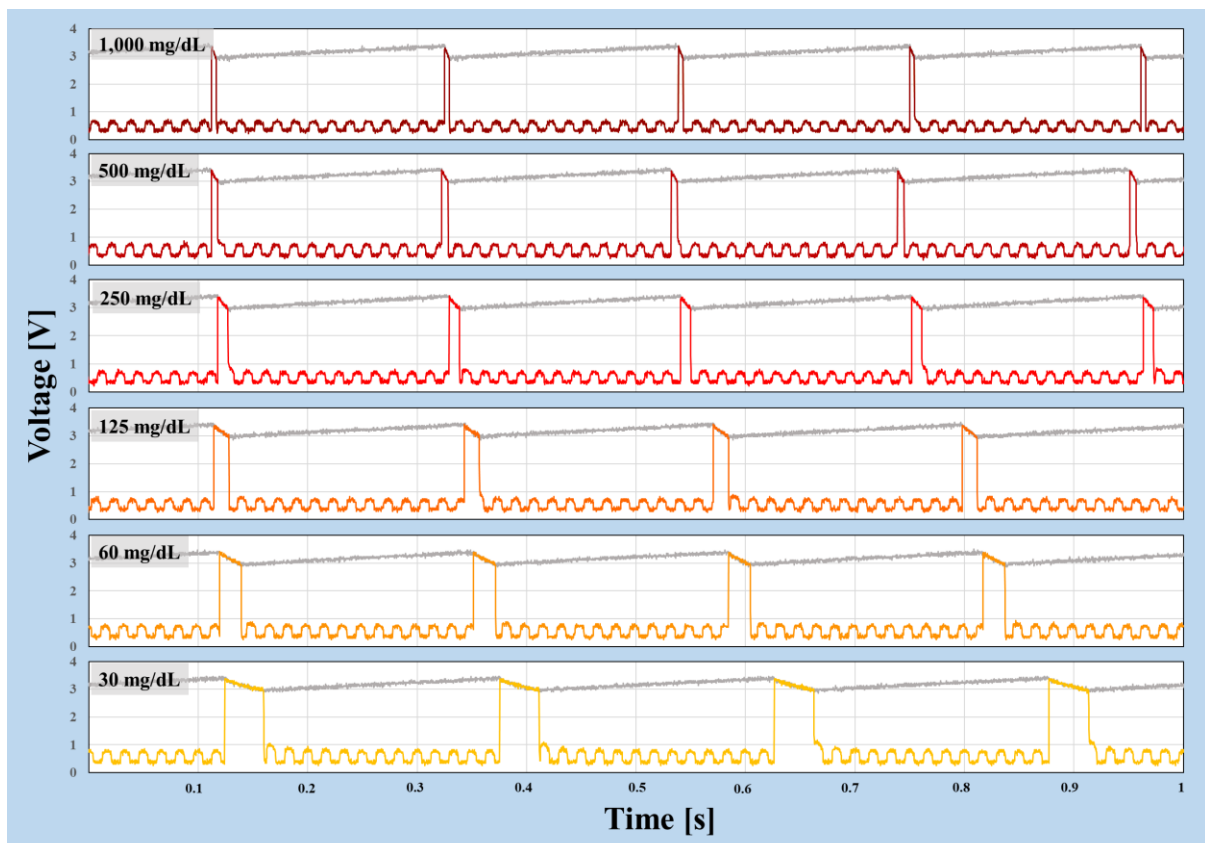
Figure 64 Oscilloscope signals in completely optically operation of voltage at LED in 30, 60, 125, 250, 500, and 1,000 mg/dL glucose concentration. (Grey line is input voltage)
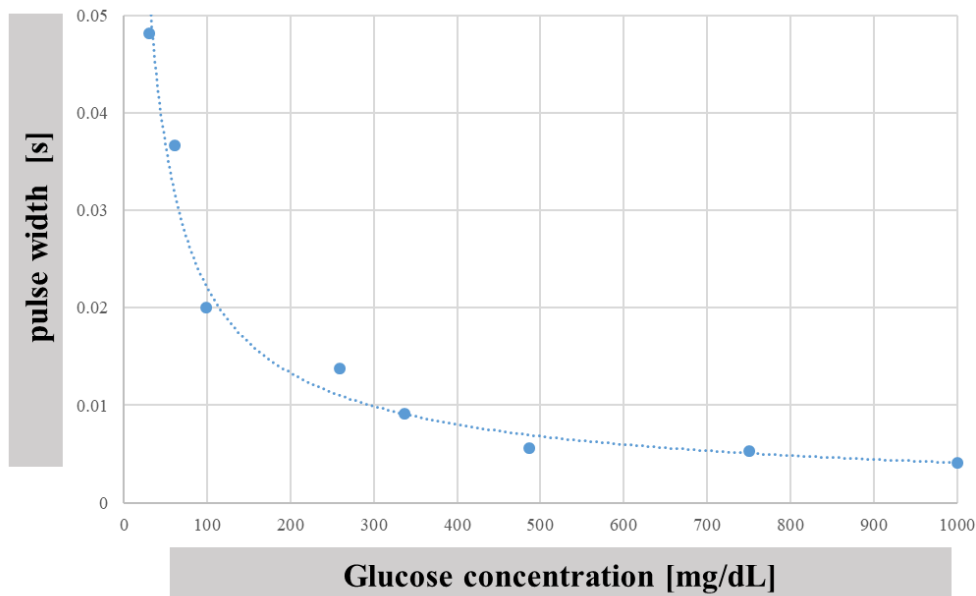
Expected concentration (mg/dL)	1,000	750	500	250	125	60	30	15
Pulse period (s)	0.004	0.005	0.006	0.009	0.014	0.020	0.037	0.048
LED blink	○	○	○	○	○	○	○	○

*Note that the average pulse period is the average value of 7 to 9 pulse from the same measurement.

Figure 65 Relationship between the pulse width of the LED emitting pulse

and glucose concentration.

However, the device works properly from 30 to 1,000 mg/dL but does not correctly work when the concentration is lower than 20 mg/dL due to the limitation of the commercial glucose strip sensitivity that is used as the electrochemical sensor.

5.4.5 Artificial Sweat Preparation and In-vitro Experiment

According to the design objective, this device is designed to attach to the body and noninvasively detect glucose from sweat. From the previous experiments, the device operation

under a completely optical power condition was confirmed. Next, the concept of sweat detection for glucose by this device was evaluated.

With the same experiment setting and the commercial glucose strip sensor as the previous experiment except for glucose solution (Table 10), the demonstration of the device was performed. Instead of the pure glucose solution, an artificial sweat or artificial perspiration solution (APS) with different glucose concentrations was used for demonstrating the actual application. According to the artificial sweat formula described in the literature, the sweat solution was prepared with the following composition listed in Table 11 [64, 85].

Table 11 Composition of artificial sweat.

Compounds	Concentration
Sodium Chloride (NaCl)	20 g/L
Ammonium Chloride (NH4Cl)	17.5 g/L
Acetic acid	5 g/L
Lactic acid	15 g/L
L(+)-Ascorbic acid	10 µM
Uric acid	59 µM
Pyruvic acid	0.18 mM
L-Glutamic acid	0.37 mM
Urea	10 mM

To confirm the detection of the device, the glucose was combined in the artificial sweat at different concentrations. In this experiment, 77, 125, 196, 317, 384, and 495 mg/dL were chosen as examples of six different glucose concentrations in artificial sweat. Figure 66 is the captured operating signals of the device in four seconds period. The result shows that the device works as expected. The LED correctly emits light related to the glucose concentration. The

lighting pulse width is longer at lower concentrations and shorter at higher concentrations. The average pulse width of each concentration is 0.15, 0.054, 0.045, 0.022, 0.013, and 0.01 second, respectively from low to high concentration. The operation and detection stop when stop emitting light to the photodiodes. Figure 67 shows the relationship between glucose concentration in artificial sweat and pulse width of the LED emitting pulse. Therefore, the designed device can detect glucose from artificial sweat using only optical power operation.
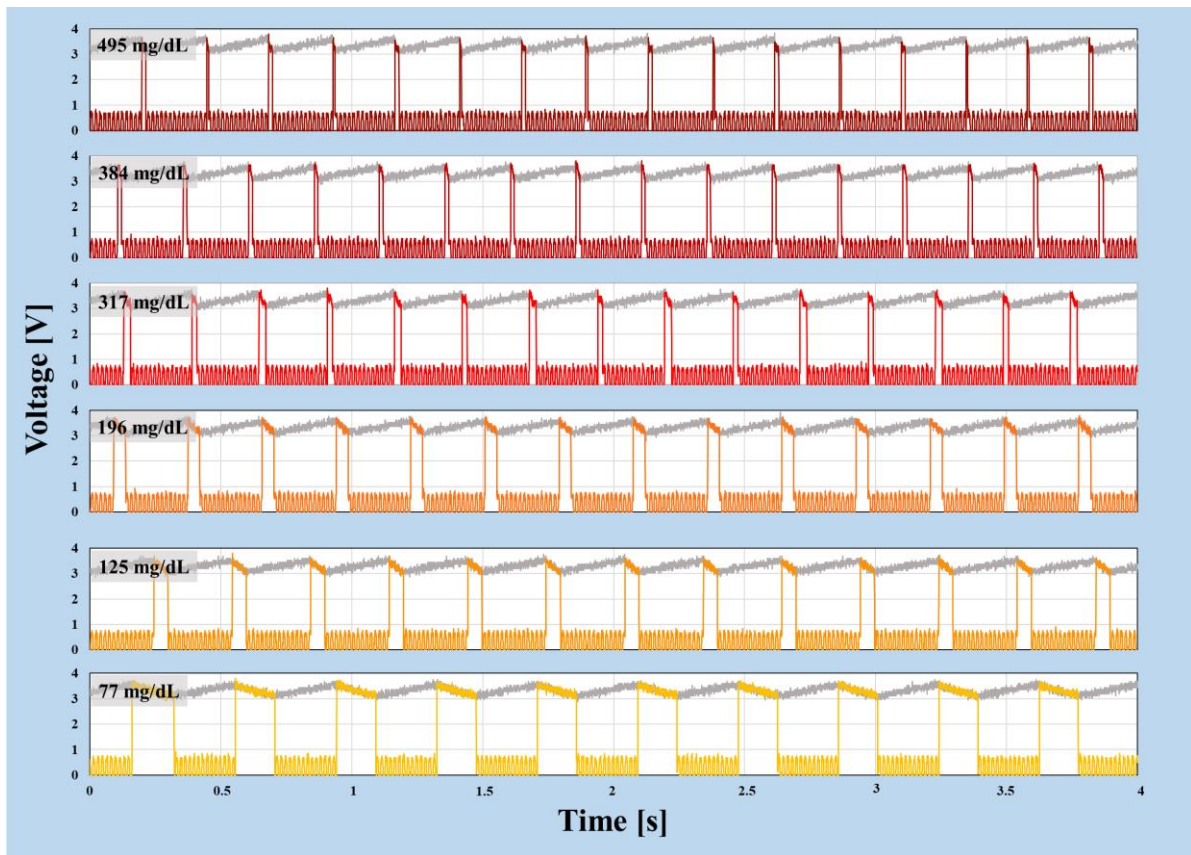
Figure 66 Oscilloscope signals in completely optically operation of voltage at LED of different glucose concentrations in artificial sweat. (Grey line is input voltage)
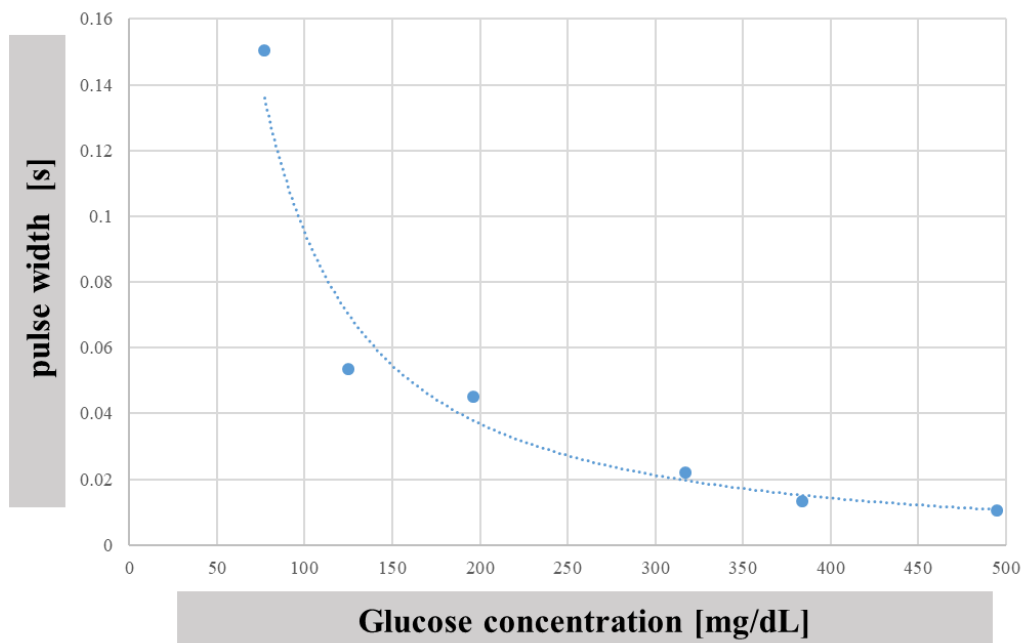
Figure 67 Relationship between the pulse width of the LED emitting pulse

and the glucose concentration in artificial sweat.

Comparing between the result of the pure glucose solution and the glucose in the artificial sweat experiment in Fig. 65 and Fig. 67, the graph trends of both experiments are similar. However, the result with the pure glucose solution is more sensitive than the result from the artificial sweat due to the sensor characteristic and the artificial sweat's compounds. The fact that the commercial glucose strip sensor in these experiments was designed for blood-based glucose detector and one time used purpose means the sensor is not durable for the sweat detection. Moreover, the acid compounds in the sweat might prevent the glucose oxidation reaction on the WE surface. This occurrence decreases the sensitivity of the device. Therefore, the design of the electrochemical sensor affects the detection performance of this design device.

According to the performance and sensitivity of the commercial glucose strip, the commercial glucose strip cannot detect glucose concentration lower than 20 mg/dL and the faraday current from the sensor will be too low to operate the LED. The chosen glucose

concentration ranges in this experiment bases on the glucose level in blood. However, the actual glucose concentration in sweat is approximately 0.36 to 10.8 mg/dL for healthy people [86], which is much lower than the blood glucose concentration. The main focus of this work is to design the optical power supply system for health monitoring applications and minimize the amperometric measurement circuit. This is a promising result confirming that the proposed battery-free attachable health monitoring device can noninvasively detect glucose in sweat using only optical power for device operation. Thus, the proposed attachable health monitoring device can easily improve the sensitivity by changing the ration between Mn6:Mn7 in the current mirror circuit (Fig. 44). So, the LED current becomes much larger even the faraday current is still low. In case the LED current is still low, choosing a low current consumption LED can improve the device performance. The low current consumption LED allows the device to display the glucose concertation even the LED current is low. The other way to improve the sensitivity of this device and apply for sweat detection only is by replacing the commercial glucose strip sensor with the higher sensitivity glucose sensor and specifically designed for sweat detection.

5.5 Summary & Discussion

The new concept of a battery-free attachable health monitoring device operated by optical power transfer was proposed with perspective to noninvasively detect the target metabolite and display the data on a smartphone. This device offers an alternative device for personalized healthcare and fulfills the limitation of the commercial health-monitoring device. The designed device accumulates power from light to operate an amperometric measurement circuit and detect target metabolites from sweat. Glucose was chosen as an example of the target metabolite in this work. The device was demonstrated and evaluated, and the results

indicate that it operates as an expectation. The results also reveal the device's ability to completely operate by optical power and differentiate the glucose concentration. The device requires 2.5 seconds for an initial time before start detection. For a more realistic demonstration, the device was evaluated with the artificial sweat solution. The device can detect the difference of 70 to 500 mg/dL glucose concentration and work as designed. Even the concentration used in the experiment is higher than the actual glucose concentration in sweat. The detection sensitivity can be improved by using higher sensitivity electrochemical glucose sensor for sweat detection.

For the next step, Figure 68 shows the goal design and function of the battery-free attachable health monitoring device. To reach the goal, the flexible PCB with sensing electrodes will be designed and fabricated for minimizing the size and giving flexibility of the device. After that, the data transmission between the designed device and smartphone, including an application for analyzing and user interface, will be developed.
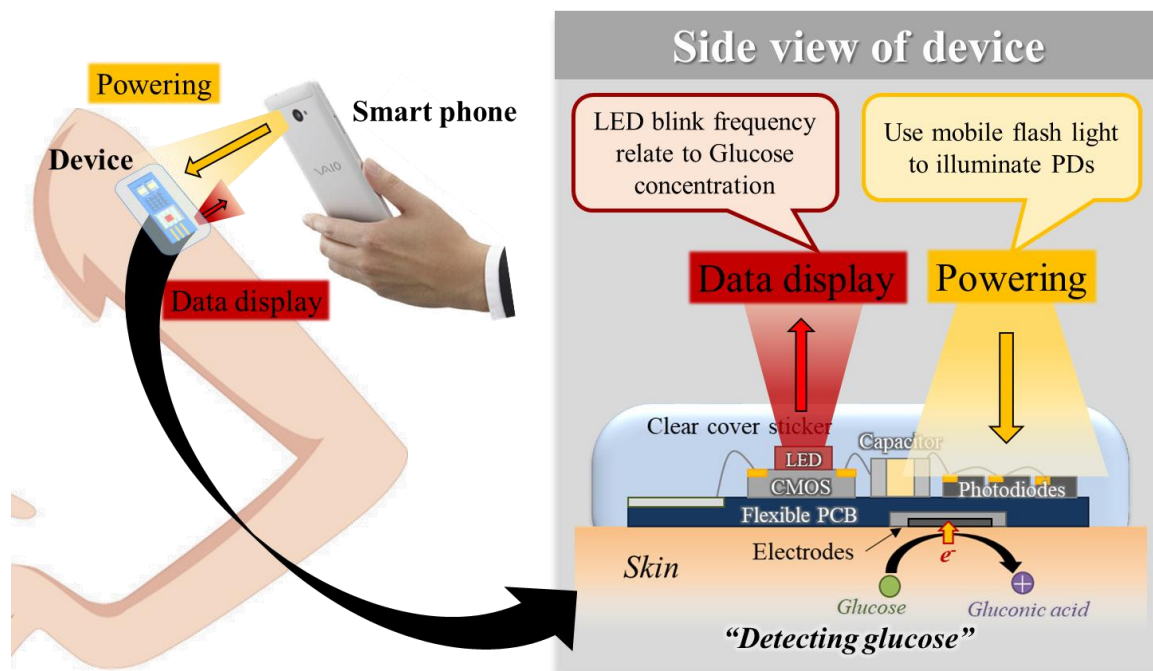
Figure 68 Concept design of CMOS-based battery-free attachable health monitoring device.

The detection of the proposed device is not limited to glucose. Moreover, the proposed device is also the capability to detect other biological/metabolic substances by simply changing the type of the electrochemical sensor and adjusting the oxidation voltage value (V_{oxi}) to match with the target substances. In the future, we plan to fabricate a complete package of the battery-free attachable health monitoring device and apply the device with other metabolites.

Chapter 6

Conclusion

6.1 Summary and Discussion

Wireless wearable or portable electronic devices have been developed and widely used in many applications. The fact that most of these devices power by batteries limits their design. Using the battery as the main power system of the device effects system lifetime, increases system volume, high risk of chemical hazards, and unhandy maintenance. Due to the limitations, a CMOS-based optical power-transfer system was proposed. The proposed system utilizes energy harvesting technology and CMOS technology for minimizing size, maximizing device lifetime, user and environmentally friendly, and remaining the portable/wearable ability for power supply in small electronic devices. The system was designed to accumulate energy from a serially connected, ultra-small photodiodes, and delivers the power intermittently to a target circuit. The results show that the system can wirelessly supply sufficient power for a small-size device using completely optical power. To demonstrate the optical power-transfer system, two devices for medical applications were designed and applied to the proposed system as their only power system.

The first device is for bio-implantable and IoT applications. From the viewpoint of the implantable device, the size and maintenance process of the device must be considered. This implantable device requires a clock signal and a continuous power supply. In order to continuously supply power, a dual-stage power-transfer circuit was developed by serially connecting two optical power-transfer circuits with a different set of bias voltages. The first stage provides a clock signal, and the second stage provides a continuous supply voltage. Then,

the optical ID circuit is included to generate the ID of the device and use it as a target load circuit.

The second application is a non-invasive wearable health monitoring device. As the structural advantages of wearable devices, such as their lightweight, flexibility, and disposability, it is reasonable to take a battery-free approach. The device was designed for noninvasively measuring glucose concentration using an amperometric measurement. Then, it transfers the measured data to display via a LED. Using the advantage of the "charge and operate" of the optical power-transfer circuit, the LED emitting period depends on the glucose due to the pulse width of the data signal.

In both applications, the proposed optical-power-transfer system effectively supplies sufficient power in both continuous and periodic form. The benefit of the pulse generating was also utilized as a clock signal for a digital circuit and a pulse width modulation (PWM) signal for data transmission. Even though the limitation of light accessibility and intensity might be a downside of the system, the demonstrated devices show that using the appropriate light wavelength and available light source can broaden the installation location and applications. Therefore, it is possible to use the proposed system in various applications as batteries and not limited to the only medical field.

Table 12 shows a comparison between the designed optical power-transfer system with other energy harvesting devices that also aim for small-size applications [13, 19, 87]. Comparing the designed system with other existed energy harvesting devices, the drawback of this designed system is low efficiency and unstable supply voltage. The supply voltage level from the system is between V_{TL} to V_{TH} depends on the bias setting, which means the supply voltage level is not constant but still in a useable range. However, the key design of the optical power-transfer system is a very simple circuit design and operation within a very small size.

Table 12 Comparison of different energy harvesting systems.

System	Power	Cost	Advantage	Disadvantage
Piezoelectric	40 - 80 µW	High	• high output voltage • no resonant	• expensive materials • coupling coefficient linked to material properties
Thermoelectric	1- 30 µW	-	• simple maintenance • low cost	• low efficiency
Fuel cells	2.2 - 430 µW/ cm^2	Low	• high power density	• short lifetime • not suitable for implantable application
Electromagnetic	1.8 mW/cm^2	High	• high output current • long lifetime • robustness	• expensive materials • low efficiency in small sizes
Low frequency magnetic field	Up to 3.1 W	-	• high power	• large dimension
Inductive links	0.4 -250 mW	-	• small dimension	• high transmitted power • low efficiency
Electrostatic	50 - 100 µW/cm^3	Low	• high output voltage • low cost	• high impact of parasitic capacitances
Optical power-transfer (This thesis)	0.8 µW	-	• small dimension • simple design and operation • suitable for medical application • easy to integrate with target load	• low efficiency • supply voltage level not constant

6.2 Opportunities for Future Research

I believe that this thesis makes a promising contribution toward the goal of providing an alternative power system for a battery-less wireless small electronic device. Besides the mentioned future plan for each device and the related medical applications, there are many open opportunities for future research. The following shows some of the possibilities of future research.

A smart house is an upcoming trend for smart life society. As mentioned in Chapter 4, the developed optical ID with optical power transfer system can be used as an IoT node for sensors and systems in the house. For example, a lighting system, security system, and temperature sensing. Due to the low maintenance requirement and fewer wires, it will be more convenient and more safety for users.

A remote monitoring system provides a variety of information and warnings. However, the location of this system is mostly in hard-to-reach or remote areas. That makes maintenance becomes harder and more dangerous. By introducing the optical power-transfer system, it enables the installation of standalone sensors with low maintenance requirement. Moreover, these standalone sensors can remotely control, monitor, and warn in a human risk situation, such as air pollution, worn out bearings, bridge stresses, and forest fires.

Last but not least, besides the standalone power system using only the optical power-transfer. The proposed system is also able to associate with the battery. These allow to increase battery life, decrease the dimension of the system, and power consumption. This combination is suitable for the systems or devices that need to optimize the size and decrease power consumption but still requires a higher level and very stable power.

References

[1]   V. Pop, H.J. Bergveld, P.H.L. Notten, and P.P.L. Regtien, "State-of-the-art of battery state-of-charge determination," in Meas. Sci. Technol., vol. 16, no. 12, Oct. 2015.

[2]   I. Buchmann, "Batteries in a Portable World, 2nd ed." British Columbia, Canada, Cadex Electronics Inc., 2001.

[3]   T.R. Crompton, and T.P.J. Crompton, "Battery Performance Eveluation," in Battery Reference Book (3rd edition), Newnes, Oxford, UK, 2000.

[4]   E. Odunlade, "Different Types of Batteries and their Applications," in Circuit Digest, Jul. 2018, Accessed on: May 20, 2020. [Online]. Available: https://circuitdigest.com/article/different-types-of-batteries

[5]   C. Harvey, "Lithium-ion Batteries and Recall Challenges for Medical Devices," in Medical Device and Diagnostic Industry, Mar. 2015, Accessed on: May 20, 2020. [Online]. Available: https://www.mddionline.com/lithium-ion-batteries-and-recall-challenges-medical-devices

[6]   C. Walker, "Surpassing The Limits of Battery Technology," in Elsevier, Nov. 2016, Accessed on: May 20, 2020. [Online]. Available: https://chemicalmaterials.elsevier.com/chemical-manufacturing-excellence/surpassing-limits-battery-technology

[7]   A. M. Dennis, D. Lancon, and J. L. Bear, "Implantable Battery Monitoring Means and Method," 1982.

[8]   R. D. Dell, C. Country, A. E. Mann, and B. Hills, "Implantable Device with Improved Battery Recharging and Powering Configuration," 2000.

[9]   M. Gasulla, M. T. Penella, and O. López-Lapena, "Powering Autonomous Sensors," Springer Link, Dordrecht, 2014.

[10] S. Roundy, D. Steingart, L. Frechette, P. K. Wright, and J. M. Rabaey, "Power Sources for Wireless Sensor Networks," in Wirel. Sens. Networks, pp. 1–17, 2004.

[11] M. a Hannan, S. Mutashar, S. a Samad, and A. Hussain, "Energy Harvesting for the Implantable Biomedical Devices: Issues and Challenges," in Biomed. Eng. OnLine, vol. 13, no. 79, Jun. 2014.

[12] A. Kansal and M. B. Srivastava, "An Environmental Energy Harvesting Framework for Sensor Networks," in Proc. ISLPED, Seoul, South Korea, 2003, p. 481-486.

[13] B. Pozo, J.I. Garate, J.A. Araujo, and S. Ferreiro, "Energy Harvesting Technologies and Equivalent Electronic Structural Models—Review," in Electronics, vol. 8, no. 5, Apr. 2019.

[14] S. Priya and D. J. Inman, "Energy Harvesting Technologies," Springer US, Boston, MA, 2009.

[15] S. W. Arms, C. P. Townsend, D. L. Churchill, J. H. Galbreath, and S. W. Mundell, "Power Management for Energy Harvesting Wireless Sensors," in Proc. SPIE, San Diego, CA, US, vol. 5762, no. 1, p. 267-275, 2005.

[16] S. Chalasani and J. M. Conrad, "A Survey of Energy Harvesting Source for Embedded Systems," in IEEE Southeast Conf., Huntsville, AL, USA, 2008, p. 442-447.

[17] A. Kansal and M. B. Srivastava, "An Environmental Energy Harvesting Framework for Sensor Networks," in Proc. Int. Symp. on Low Power Electronics and Design - ISLPED '03, 2003, p. 481.

[18] C. Ó. Mathúna, T. O'Donnell, R. V. Martinez-Catala, J. Rohan, and B. O'Flynn, "Energy Scavenging for Long-Term Deployable Wireless Sensor Networks," in Talanta, vol. 75, no. 3, p. 613-623, May 2008.

[19] J. Olivo, S. Carrara, and G. De Micheli, "Energy Harvesting and Remote Powering for Implantable Biosensors," in IEEE Sens. J., vol. 11, no.7, p. 1287-1302, Jul. 2011.

[20] J. Paulo and P. D. Gaspar, "Review and Future Trend of Energy Harvesting Methods for Portable Medical Devices," in Proc. World Congr. Engineering (WCE 2010), London, UK, 2010.

[21] J. Paulo and P. D. Gaspar, "Review and Future Trend of Energy Harvesting Methods for Portable Medical Devices," in Lect. Notes Eng. Comput. Sci., vol. 2184, no. 1, p. 909-914, Jun. 2010.

[22] H.-P. Tan, P. W. Q. Lee, W. K. G. Seah, and Z. A. Eu, "Impact of Power Control in Wireless Sensor Networks Powered by Ambient Energy Harvesting (WSN-HEAP) for Railroad Health Monitoring," in Int. Conf. Advanced Information Networking and Applications Workshops, Bradford, UK, 2009.

[23] A. Harb, "Energy Harvesting: State-of-the-Art," in Renewable Energy, vol. 36, no. 10, p. 2641-2654, Oct. 2011.

[24] S. Kuppusami and R. H. Oskouei, "Parylene Coating in Medical Devices and Implants: A Review," in Univers. J. Biomed. Eng., vol. 3, p. 9-14, 2015.

[25] R. R. Selmic, V. V. Phoha, and A. Serwadda, "Wireless Sensor Networks" Springer, Cham, Switzerland, 2016.

[26] A. Hogg, S. Uhl, F. Feuvrier, Y. Girardet, B. Graf, T. Aellen, H. Keppner, Y. Tardy, and J. Burger, "Protective Multilayer Packaging for Long-Term Implantable Medical Devices," in Sur. Coatings Technol., vol. 255, p. 124-129, 2014.

[27] Implantable device with improved battery recharging and powering configuration, by R. D. Dell, C. Country, A. E. Mann, and B. Hills. (May 2000) U.S. Patent 6067474.

[28] Implantable battery monitoring means and method, by J. H. Schulman. (Aug. 1982) U.S. Patent US4345603.

[29] S. Roundy, D. Steingart, L. Frechette, P. Wright, and J. Rabaey, "Wireless Sensor Networks," Springer, Berlin, Germany, 2004.

[30] A. Kobayashi, K. Ikeda, Y. Ogawa, H. Kai, M. Nishizawa, K. Nakazato, and K. Niitsu, "Design and Experimental Verification of a 0.19 V 53 µW 65 nm CMOS Integrated Supply-Sensing Sensor with a Supply-Insensitive Temperature Sensor and an Inductive-Coupling Transmitter for a Self-Powered Bio-Sensing System Using a Biofuel Cell," in IEEE Trans. on Biomed. Circuits Syst., vol. 11, no.6, p. 1313-1323, Dec. 2017.

[31] M. Douthwaite, E. Koutsos, D. C. Yates, P. D. Mitcheson, and P. Georgiou, "A Thermally Powered ISFET Array for On-Body pH Measurement," in IEEE Trans. Biomed. Circuits Syst., vol. 11, no. 6, p. 1324-1334, Aug. 2017.

[32] P. Visconti, P. Primiceri, R. Ferri, M. Pucciarelli, and E. Venere, "An Overview on State-of-art Energy Harvesting Techniques and Choice Criteria: a WSN Node for Goods Transport and Storage Powered by a Smart Solar-Based EH System," in Int. J. Energ. Res., vol. 7, no. 3, Sep. 2017.

[33] M. H. Alsharif, S. Kim, and N. Kuruoglu, "Energy Harvesting Techniques for Wireless Sensor Networks/Radio-Frequency Identification: A Review," in Symmetry, vol. 11, no. 865, Jul. 2019.

[34] T. Tokuda, I. Takaaki, N. Wuthibenjaphonchai, M. Haruta, T. Noda, K. Sasagawa, T. Tokuda, M. Sawan, and J. Ohta, "1 mm-Sized Optical Neural Stimulator Based on CMOS Integrated Photovoltaic Power Receiver," in AIP Adv., vol. 8, Apr. 2018.

[35] A.S. Chauvin and M. Grätzel, "Solar Energy Harvesting," in Chimia, vol. 67, no. 3, pp. 113, Jan. 2013.

[36] N. J. Guilar, T. J. Kleeburg, A. Chen, D. R. Yankelevich, and R. Amirtharajah, "Integrated Solar Energy Harvesting and Storage," in IEEE T. VLSI. Syst., vol. 17, no.5 pp. 627-637, May. 2009.

[37] A. Haeberlin, A. Zurbuchen, J. Schaerer, J. Wagner, S. Walpen, C. Huber, H. Haeberlin, J. Fuhrer, and R. Vogel, "Successful Pacing Using a Batteryless Sunlight-Powered Pacemaker," in Europace, vol. 16, no. 10, pp. 1534-1539, Oct. 2014.

[38] A. Haeberlin, A. Zurbuchen, S. Walpen, J. Schaerer, T. Niederhauser, C. Huber, H. Tanner, H. Servatius, J. Seiler, H. Haeberlin, J. Fuhrer, and R.Vogel, "The First Batteryless, Solar-powered Cardiac Pacemaker," in Heart Rhythm, vol. 12, no. 6, pp. 1317-1323, Jun. 2015.

[39] M. Mujeeb-U-Rahman, D. Adalian, C.F. Chang, and A. Scherer, "Optical Power Transfer and Communication Methods for Wireless Implantable Sensing Platforms," in J. Biomed. Opt., vol. 20, no. 9, Sep. 2015.

[40] V. Raghunathan, A. Kansal, J. Hsu, J. Friedman, and M. Srivastava, "Design Considerations for Solar Energy Harvesting Wireless Embedded Systems," in Proc. IPSN, Los Angeles, CA, USA, 2005, pp. 457-462.

[41] K. Song, J. H. Han, H. C. Yang, K. I. Nam, and J. Lee, "Generation of Electrical Power under Human Skin by Subdermal Solar Cell Arrays for Implantable Bioelectronic Devices," in Biosens. Bioelectron., vol. 92, pp. 364-371, Nov. 2016.

[42] G. Liu, R. Fuentes, H. Koser, and T. Kaya, "A self-powered power conditioning circuit for battery-free energy scavenging applications," in Analog Integr. Circ. S., vol. 83, no. 2, pp. 203-207, Apr. 2015.

[43] D. Newell and M. Duffy, "Improved Energy Management System for Low-Voltage, Low-Power Energy Harvesting Sources," in J. Phys.: Conf. Ser., vol. 773, no. 1, Nov. 2016.

[44] H. Kim, Y. J. Min, C. H. Jeong, K.-Y. Y. Kim, C. Kim, and S. W. Kim, "1-mW Solar-Energy-Harvesting Circuit Using an Adaptive MPPT with a AR and a Counter" in IEEE Trans. Circuits Syst. II, vol. 60, no. 6, p. 331-335, Jun. 2013.

[45] N. Wuthibenjaphonchai, T. Ishizu, M. Haruta, T. Noda, K. Sasagawa, T. Tokuda, M. Sawan, and J. Ohta, "CMOS-based optical energy harvesting circuit for biomedical and Internet of Things devices," in Jpn. J. Appl. Phys., vol. 57, no. 4S, Mar. 2018.

[46] N. Wuthibenjaphonchai, M. Haruta, T. Noda, K. Sasagawa, T. Tokuda, M. Sawan, S. Carrara, and J. Ohta, "Battery-free, sticker-like, device for health monitoring, operated by optical power transfer," in Proc. BIOCAS, Cleveland, OH, USA, 2018.

[47] R. Topics, K. Takakubo, and H. Takakubo, "Wide Range CMOS Voltage Detector with Low Current Consumption and Low Temperature Variation," in IEICE Trans. Fundam. Electron. Commun. and Comput. Sci. E92–A, no. 2, p. 443-450, Feb. 2009.

[48] M. Billinghurst, and T. Starner, "Wearable Devices: New Ways to Manage Information," in IEEE Computer 32, p. 57-64, 1999.

[49] N. Bui, and M. Zorzi, "Health care applications: a solution based on the internet of things," in Proc. 4th Int. Symp. Applied Sciences in Biomedical and Communication Technologies (ISABEL '11), p.131-136, Oct. 2011.

[50] Y.-H. Chen, B. Ng, W. K. G. Seah, and A.-C. Pang, "Modeling and Analysis: Energy Harvesting in the Internet of Things," in Proc. 19th Inter. Conf. on Modeling, Analysis and Simulation of Wireless and Mobile Systems (MSWiM), Malta, Nov. 2016.

[51] J. Gubbi, R. Buyya, S. Marusic, and M. Palaniswami, "Internet of Things (IoT): A vision, architectural elements, and future directions," in Future Gener. Comput. Syst., vol. 29, no. 7, p. 1645-1660, Sep. 2013.

[52] X. Li, R. Lu, X. Liang, X. Shen, J. Chen, and X. Lin, "Smart Community: an Internet of Things Application," in IEEE Commun. Maga., vol.49, no. 11, p. 68-75, Nov. 2011.

[53] J. R. Jagdeo, L. E. Adams, N. I. Brody, and D. M. Siegel, "Transcranial Red and Near Infrared Light Transmission in a Cadaveric Model," in PLOS ONE, vol.7, no. 10, Oct. 2012.

[54] Kingbright, "3.2x1.6mm SMD Chip LED lamp (KP-3216PBC-A, Blue)," 2010. [Online]. Available: http://docs-asia.electrocomponents.com/webdocs/032f/0900766b8032fa99.pdf.

[55] Kingbright, "3.2x1.6mm SMD Chip LED lamp (KP-3216SGC, Super bright green)," 2012. [Online]. Available: http://docs-asia.electrocomponents.com/webdocs/0330/0900766b803305ae.pdf.

[56] TDK, "MULTILAYER CERAMIC CHIP CAPACITORS C Series Commercial Grade General (Up to 50V) MULTILAYER CERAMIC CHIP CAPACITORS," 2014. [Online]. Available: http://docs-asia.electrocomponents.com/webdocs/1532/0900766b81532cd0.pdf.

[57] P. Lalanne and J. C. Rodier, "CMOS photodiodes based on vertical pnp junctions," *Work. Opt. Comput. Sci. Proc. 11th Int. Parallel Process. Symp., Geneva, Switz.*, no. January 1997, pp. 1–8, 1997.

[58] J. Ohta, "Smart CMOS Image Sensors and Applications,", CRC Press, FL, US, 2008.

[59] A.J. Bandodkar and J. Wang, "Non-invasive wearable electrochemical sensors: a review," in Trends. Biotechnol., vol. 32, no. 7, pp. 363-371, Jul. 2014.

[60] F. Faridbod, V.K. Gupta, and H.A. Zamani, "Electrochemical Sensors and Biosensors," in Int. J. Electrochem., vol. 2011, Dec. 2011.

[61] S. Carrara, "Bio/CMOS Interfaces and Co-Design," Springer, 2012.

[62] H. Li, X. Liu, L. Li, X. Mu, R. Genov, and A. J. Mason, "CMOS Electrochemical Instrumentation for Biosensor Microsystems: a review," in Sensors-Basel, vol. 17, no. 1, Dec. 2016.

[63] M. A. Mohammad, and J. Graham, "Current mirror Based Potentiostats for three electrode amperometric electrochemical sensors," in IEEE T. Circuits-I, vol. 56, no. 7, pp. 1339-1348, Aug. 2009.

[64] T. Kilic, V. Brunner, L. Audoly, and S. Carrara, "Smart e-patch for drugs monitoring in Schizophrenia," in Proc. ICECS, Monte Carlo, Monaco, 2016.

[65] W. Jia, A.J. Bandodkar, G. Valdés-Ramírez, J.R. Windmiller, Z. Yang, J. Ramírez, G. Chan, and J. Wang, "Electrochemical tattoo biosensors for real-time noninvasive Lactate monitoring in human perspiration," in Anal. Chem., vol. 85, no.14, pp. 6553-6560, Jul. 2013.

[66] Y. T. Liao, H. Yao, A. Lingley, B. Parviz, and B. P. Otis, "A 3- µW CMOS glucose sensor for wireless contact-lens tear glucose monitoring," in IEEE J. Solid-St. Circ., vol. 47, no. 1, pp. 335-344, Jan. 2012.

[67] American Diabetes Association, "Diagnosis and classification of diabetes mellitus: new criteria," in Diabetes Care, vol. 35, no. 1, pp. 64-71, Jan. 2012.

[68] "*Diabetes*," U.S. National Library of Medicine, Apr. 22, 2020. Accessed on: May. 19, 2020. [Online]. Available: https://medlineplus.gov/diabetes.html

[69] "*Type 1 Diabetes*," The global diabetes community, Jan. 15, 2019. Accessed on: May. 19, 2020. [Online]. Available: https://www. diabetes.co.uk/type1-diabetes.html

[70] "*Diabetes Type 1*," U.S. National Library of Medicine, Apr. 22, 2020. Accessed on: May. 19, 2020. [Online]. Available: https://medlineplus.gov/diabetestype1.html

[71] "*Type 2 Diabetes*," The global diabetes community, Jan. 15, 2019. Accessed on: May. 19, 2020. [Online]. Available: https://www. diabetes.co.uk/type2-diabetes.html

[72] "*Diabetes Type 2*," U.S. National Library of Medicine, Apr. 22, 2020. Accessed on: May. 19, 2020. [Online]. Available: https://medlineplus.gov/diabetestype2.html

[73] Type 2 diabetes: prevention in people at high risk, National Institute for health and care excellence (NICE), London, UK, Sep. 2019.

[74] A. Heller, and B. Feldman, "Electrochemical glucose sensors and their applications in diabetes management," in Chem. Rev., vol. 108, no. 7, pp. 2482-2505, May. 2008.

[75] D. Rodbard, "Continuous glucose monitoring: a review of successes, challenges, and opportunities," in Diabetes Technol. The., vol. 18, no.2, pp. 3-13, Feb. 2016.

[76] G. Cappon, G. Acciaroli, M. Vettoretti, A. Facchinetti, and G. Sparacino, "Wearable continuous glucose monitoring sensors: a revolution in diabetes treatment," in Electronics-Switz, vol. 6, no. 65, Sep. 2017

[77] S. K. Vashist, "Non-invasive glucose monitoring technology in diabetes management: a review," in Anal. Chim. Acta., vol. 750, pp. 16-27, Oct. 2012

[78] H. Chuang, M. Trieu, J. Hurley, E. J. Taylor, M. R. England, and S. A. Nasraway, "Pilot studies of transdermal continuous glucose measurement during and after cardiac surgery," in J. Diabetes Sci. Technol., vol. 2, no. 4, pp. 595–602, Jul. 2008.

[79] American Diabetes Association, "Implications of the diabetes control and complications trial," in Diabetes Care, vol. 26, no. 1, pp. 25–27, Jan. 2003.

[80] T.J. Roussel, D.J. Jackson, R.P. Baldwin, and R.S. Keynton, "Amperometric Techniques," in Encyclopedia of Microfluidics and Nanofluidics, Springer, Boston, MA, 2008.

[81] X.J. Zhang, and K. Hoshino, "Electrical Transducers: Electrochemical Sensors and Semiconductor Molecular Sensors," in Molecular Sensors and Nonodevices (2nd edition), p. 181-230, Academic Press, Cambridge, MA, US, 2019.

[82] M. M. Ahmadi, G. A. Jullien, and L. Fellow, "Current-mirror-based potentiostats for three-electrode amperometric electrochemical sensors," IEEE Trans. IEEE Trans. Circuits Syst., vol. 56, no. 7, pp. 1339–1348, 2008.

[83] "An Equivalent Circuit for Zimmer and Peacock Glucose Senors," Zimmer and Peacock, Accessed on: May. 19, 2020. [Online]. Available: https://www.zimmerpeacocktech.com/knowledge-base/faq/equivalent-circuit-to-zap-glucose-sensor/

[84] I. Taurino, G. Sanzo, F. Mazzei, G.D. Micheil, and S. Carrara, "Fast synthesis of platinum nanopetals and nanospheres for highly-sensitive non-enzymatic detection of glucose and selective sensing of ions," in Sci. Rep., vol. 5, no. 15277, Oct. 2015.

[85] F. Stradolini, et al., "Wireless Monitoring of Endogenous and Exogenous Biomolecules on an Android™ Interface," in IEEE Sens. J., vol. 16, no. 9, May 2016.

[86] N. E. Witkowska, M. Kundys, P. S. Jeleń, and M. Jönsson-Niedziółka, "Electrochemical Glucose Sensing: Is There Still Room for Improvement?" in Anal. Chem., vol. 88, no. 23, pp. 11271-11282, Dec. 2016.

[87] B. Shi, Z. Li, and Y. Fan. "Implantable Energy-Harvesting Devices," in Adv. Mater., vol. 30, no. 44, Jul. 2018

Appendix

Movie 1: The fully wireless optical operation under flashlight of the first version CMOS-based optical power-transfer circuit for bio-implantable and Internet of Things (IoT) device.

URL:https://www.dropbox.com/s/qqtfmvqs6vlhzzc/Movie%201_Deveice%20ver1%20Opertation.mp4?dl=0

Movie 2: The fully wireless optical operation under IR light of the third version CMOS-based optical power-transfer circuit for bio-implantable and Internet of Things (IoT) devices.

URL:https://www.dropbox.com/s/enxvrvso7v18gx3/Movie%202_Device%20ver3%20Operation.mp4?dl=0

Note that, these two movie files are in the dropbox account which belongs to Photonic Device Science Laboratory. These movie files can be found in the following folder "pdsl_student/Fon/PhD Thesis/Appendix".

List of Publications

- **Journals:**

[1]   T. Tokuda, I. Takaaki, **N. Wuthibenjaphonchai**, M. Haruta, T. Noda, K. Sasagawa, M. Sawan, and J. Ohta, "Design Optimization of CMOS Control Circuit for Integrated Photovoltaic Power Transfer" Sensors and Materials, Vol. 30(10), pp. 2343-2357, Oct. 2018. doi:10.18494/SAM.2018.1945

[2]   T. Tokuda, I. Takaaki, **N. Wuthibenjaphonchai**, M. Haruta, T. Noda, K. Sasagawa, M. Sawan, and J. Ohta, "1 mm-sized optical neural stimulator based on CMOS integrated photovoltaic power receiver," AIP Advance, Vol. 8(4), pp. 045018, Apr. 2018. doi:10.1063/1.5024243

[3]   **N. Wuthibenjaphonchai**, M. Haruta, T. Noda, K. Sasagawa, T. Tokuda, M. Sawan, and J. Ohta, "CMOS-based optical energy harvesting circuit for biomedical and Internet of Things devices" Japanese Journal of Applied Physics, Vol. 57(4S), pp. 04FM05, Mar. 2018. doi:10.7567/JJAP.57.04FM05

- **International conferences:**

[1]   T. Pakpuwadon, **N. Wuthibenjaphonchai**, M. Haruta, K. Sasagawa, T. Tokuda, and J. Ohta, "A battery-less, ultra-small wireless optical stimulator," Neuroscience Annual Meeting 2019 (SfN2019), McCormick Place, Chicago, Illinois, USA – Oct. 2019

[2]   **N. Wuthibenjaphonchai**, M. Haruta, K. Sasagawa, T. Tokuda, S. Carrara, and J. Ohta, "Proposal of an Optically-operated, Sticker-Like Device Platform for Health Monitoring,"

Engineering in Medicine and Biology Conference (EMBC2019), CityCube, Berlin, Germany – Jul. 2019

[3]   T. Tokuda, T. Pakpuwadon, **N. Wuthibenjaphonchai**, M. Haruta, T. Noda, K. Sasagawa, and J. Ohta, "CMOS-based, optically-powered implantable optogenetic stimulator*(invited)*" IEEE Life Sciences Conference (LSC2018), La Plaza, Quebec, Canada – Oct. 2018

[4]   **N. Wuthibenjaphonchai**, M. Haruta, T. Noda, K. Sasagawa, T. Tokuda, M. Sawan, S. Carrara, and J. Ohta, "Battery-Free Sticker-Like Device for Health Monitoring Operated by Optical Power Transfer," IEEE Biomedical Circuits and Systems Conference (BioCAS2018), Cleveland Marriott Downtown at Key Center, Ohio, USA – Oct. 2018

[5]   T. Pakpuwadon, **N. Wuthibenjaphonchai**, M. Haruta, T. Noda, K. Sasagawa, T. Tokuda, M. Sawan, and J. Ohta, "CMOS-integrated optical power transfer for an ultra small wireless implantable devices," 2018 International Conference on Solid State Devices and Materials (SSDM2018), The University of Tokyo, Tokyo, Japan – Sep. 2018

[6]   T. Tokuda, **N. Wuthibenjaphonchai**, I. Takaaki, M. Haruta, T. Noda, K. Sasagawa, T. Tokuda, M. Sawan, and J. Ohta, "Live Demonstration: IoT micronode with optical ID transmission capability operated by optical energy harvesting," IEEE International Symposium on Circuits and Systems(ISCAS2018), Firenze Fiera Congress and Exhibition Center, Florence, Italy – May 2018

[7]   **N. Wuthibenjaphonchai**, M. Haruta, T. Noda, K. Sasagawa, T. Tokuda, M. Sawan, and J. Ohta, "CMOS-based Optical Energy Harvesting Circuit for Implantable and IoT Devices," 2017 International Conference on Solid State Devices and Materials (SSDM2017), Sendai International Center, Sendai, Japan – Sep. 2017

[8]   **N. Wuthibenjaphonchai**, M. Haruta, T. Noda, K. Sasagawa, T. Tokuda, M. Sawan, and J. Ohta, "CMOS-based Optical Energy Harvesting Circuit for Medical and IoT Devices," Engineering in Medicine and Biology Conference 2017 (EMBC2017), International Convention Center, Jeju Island, Korea – Jul. 2017

[9]   **N. Wuthibenjaphonchai**, H. Takehara, H. Takehara, T. Noda, K. Sasagawa, T. Tokuda, and J. Ohta, "CMOS-based Implantable Glucose Sensor," KJF International Conference on Organic Materials for Electronics and Photonics 2016 (KJF-ICOMEP2016), ACROS, Fukuoka – Sep. 2016

● **Domestic conferences:**

[1]   **N. Wuthibenjaphonchai**, "Wireless Wearable Device for Non-invasive Health Monitoring, Operated by Optical Power Transfer," VDEC Design Forum 2019, Takinoyu hotel, Yamagata – Sep. 2019

[2]   T. Tokuda, T. Pakpuwadon, **N. Wuthibenjaphonchai**, M. Haruta, T. Noda, K. Sasagawa, and J. Ohta, "Batteryless ultra-small implantable optical stimulator," The 57th Annual Meeting of the Biophysical Society of Japan (BSJ2019), Seagaia Convention Center, Miyazaki – Sep. 2019

[3]   T. Tokuda, T. Pakpuwadon, **N. Wuthibenjaphonchai**, M. Haruta, T. Noda, K. Sasagawa, and J. Ohta, "CMOS-controlled optical power transfer for bioelectronic Devices," IEEJ Workshop Management System, Tokyo Institute of Technology, Suzukakedai Campus, Kanagawa – Jul. 2019

[4]   T. Pakpuwadon, **N. Wuthibenjaphonchai**, M. Haruta, K. Sasagawa, T. Tokuda, and J. Ohta, "Optical power transfer platform for ultra-small implantable device with alternative current limitations," LSI and System Workshop 2018, The University of Tokyo, Komaba Campus, Tokyo – May 2019

[5]   **N. Wuthibenjaphonchai**, M. Haruta, T. Noda, K. Sasagawa, T. Tokuda, and J. Ohta, "Wireless Sticker-like Health-monitoring Devices Operated by Optical Power Transfer," Institute of Electrical Engineers of Japan Conference 2019 (IEEJ2019), Hokkaido University of Science, Hokkaido – Mar. 2019

[6]   T. Pakpuwadon, **N. Wuthibenjaphonchai**, M. Haruta, K. Sasagawa, T. Tokuda, and J. Ohta, "CMOS Optical Power Receiver for Ultra-small Wireless Implantable device," International Workshop by the 174th Committee JSPS (IWSBN2019), Kyoto Terrsa, Kyoto – Jan. 2019

[7]   **N. Wuthibenjaphonchai**, M. Haruta, T. Noda, K. Sasagawa, T. Tokuda, S. Carrara, and J. Ohta, "Wireless Attachable Health Monitoring Device Operated by Optical Power," International Workshop by the 174th Committee JSPS (IWSBN2019), Kyoto Terrsa, Kyoto – Jan. 2019

[8]   T. Pakpuwadon, **N. Wuthibenjaphonchai**, M. Haruta, T. Noda, K. Sasagawa, T. Tokuda, M. Sawan, and J. Ohta, "Ultra-Small Optogenetic Simulator Powered by CMOS-Integrated Optical Power Receiver," Japan Society of Applied Physics Autumn Meeting 2018 (JSAP Autumn 2018), Nagoya Congress Center, Nagoya – Sep. 2018

[9]   T. Pakpuwadon, T. Ishizu, **N. Wuthibenjaphonchai**, M. Haruta, T. Noda, K. Sasagawa, T. Tokuda, M. Sawan, and J. Ohta, "CMOS integrated optical power transfer

platform for ultra-small implantable devices," LSI and System Workshop 2018, The University of Tokyo, Komaba Campus, Tokyo – May 2018

[10]   **N. Wuthibenjaphonchai**, M. Haruta, T. Noda, K. Sasagawa, T. Tokuda, and J. Ohta, "CMOS-based Optical Energy Harvesting for Biomedical and IoT Devices," Optics & Photonics Japan 2017 (OPJ2017), University of Tsukuba, Tokyo Campus, Tokyo – Nov. 2017

[11]   T. Ishizu, **N. Wuthibenjaphonchai**, M. Haruta, T. Noda, K. Sasagawa, T. Tokuda, and J. Ohta, "Optical Energy Harvesting for Implantable Optogenetic Stimulation Device," Japan Society of Applied Physics Autumn Meeting 2017 (JSAP Autumn 2017), Fukuoka Convention Center, Fukuoka – Sep. 2017

[12]   **N. Wuthibenjaphonchai**, M. Haruta, T. Noda, K. Sasagawa, T. Tokuda, and J. Ohta, "CMOS-based Optical Energy Harvesting for Bio-implantable Device," LSI and System Workshop 2017, The University of Tokyo, Komaba Campus, Tokyo – May 2017

[13]   **N. Wuthibenjaphonchai**, M. Haruta, T. Noda, K. Sasagawa, T. Tokuda, and J. Ohta, "CMOS-based Optical Energy Harvesting Circuit for Bio-implantable and IoT Devices," Japan Society of Applied Physics Spring Meeting 2017 (JSAP Spring 2017), Pacifico, Yokohama – Mar. 2017

[14]   **N. Wuthibenjaphonchai**, "CMOS-based Optical Energy Harvesting Circuit for Bio-implantable and IoT Devices," VDEC Design Forum 2016, The University of Tokyo, Hongochiku Campus, Tokyo – Aug. 2016

- **Presentations (Invitation):**

[1]　"CMOS-based Optical Energy Harvesting Circuit for Implantable and IoT Devices," IEEE Kansai Colloquium workshop (Ryukoku University, Osaka) – Jan. 2019

[2]　"IoT micronode with optical ID transmission powered by optical power transfer," Keihanna Research Complex (Doshisha University, Kyoto) – Jul. 2018

[3]　"CMOS-based Optical Energy Harvesting for Biomedical and IoT Devices," NAIST and Thai Universities for Research and Education Collaboration Symposium 2017 (Centara Grand at Central Plaza Ladprao, Bangkok, Thailand) – Sep. 2017

[4]　"Optical energy harvesting technology for intelligent light wavelength conversion and IoT node," Japan Science and Technology fair (Telecom Center Building, Tokyo) –Aug. 2017

- **Awards & Grants:**

[1]　VDEC design award for idea contest in VDEC Design Forum 2019

[2]　Charles Desoer Grant from IEEE Biomedical Circuits and Systems Conference 2018

[3]　VDEC design award for idea contest in VDEC Design Forum 2016

[4]　Japanese government scholarship (MEXT) by University recommendation
for studying Master degree: 144,000 yen per month for two years, 2015-2017

[5]　Japanese government scholarship (MEXT) by University recommendation
for studying Doctoral degree: 145,000 yen per month for three years, 2017-2020